

https://dspace.org/

Development of in vitro transcribed RNA interference activators for the therapeutic inhibition of the hepatitis B virus

Shrilall, Creanne Jizell

2024
University of the Witwatersrand, Johannesburg
https://hdl.handle.net/10539/42963
Shrilall, Creanne Jizell. (2024). Development of in vitro transcribed RNA interference activators for the therapeutic inhibition of the hepatitis B virus [Master's dissertation, University of the Witwatersrand, Johannesburg]. WireDSApace.

Downloaded from a DSpace repository. https://dspace.org/

DEVELOPMENT OF IN VITRO TRANSCRIBED RNA INTERFERENCE ACTIVATORS FOR THE THERAPEUTIC INHIBITION OF THE HEPATITIS B VIRUS

Creanne Jizell Shrilall

A dissertation submitted to the Faculty of Health Sciences, University of the Witwatersrand, in fulfilment of the requirements for the degree of

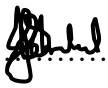
Master of Science in Medicine

Johannesburg, 2024

DECLARATION

I, Creanne Jizell Shrilall (student number: 1363661) declare that this dissertation is my own work. It is being submitted for the degree of Master of Science in Medicine in the University of the Witwatersrand, Johannesburg. It has not been submitted before for any degree or examination at this or any other university.

Signature



……...

Date

28 February 2024……...

DEDICATION

This work is dedicated to my parents Sharon Shrilall and Sanjay Shrilall, brother Kreesan Shrilall, partner Kashveer Ramgulam and my departed grandmother Dhukie Pillay for their unconditional love and support.

PUBLICATIONS AND PRESENTATIONS

Publications:

1. Samudh, N., Shrilall, C., Arbuthnot, P., Bloom, K., Ely, A., 2022. Diversity of Dysregulated Long Non-Coding RNAs in HBV-Related Hepatocellular Carcinoma. Frontiers in Immunology 13.

Presentations:

1. Shrilall, C., Arbuthnot, P., Ely, A, 2023. In vitro transcribed primary microRNA for the suppression of hepatitis B virus replication. International HBV Meeting; Kobe, Japan; 19th – 23rd Sep; the abstract has been accepted.

ABSTRACT

The current mainstream treatments available for patients who are chronically infected with the hepatitis B virus (HBV) are capable of suppressing viral replication, however these therapeutic strategies cannot eradicate the virus. Thus, the development of novel therapeutic strategies capable of eradicating the virus are urgently needed. The RNA interference (RNAi) pathway can be exploited by introducing RNAi activators such as primary microRNA (pri-miRNA) mimics into cells to silence genes of interest. The exploitation of the RNAi pathway by employing DNA expression cassettes that endogenously express pri-miRNA mimics which target the *hepatitis B x protein (HBx)* sequence has demonstrated to be efficient in inhibiting HBV replication. However, achieving safe, efficient, and cost-effective delivery remains a major challenge. The delivery of RNA therapeutics using non-viral vectors is safer and more cost-effective than the delivery of DNA therapeutics using viral vectors, and the use of chemically synthesised small interfering RNAs (siRNA) is expensive whereas in vitro transcription offers a cheaper alternative. Therefore, the purpose of this study was to in vitro transcribe pri-miRNA mimics that target the *HBx* sequence which is common to each of the viral transcripts. The rationale was that simultaneously targeting the viral transcripts may reduce viral protein production, thereby removing their immunosuppressive effects, which can potentially reactivate the host's natural defences to clear the virus. In this study, several pri-miR-31 mimics were successfully in vitro transcribed and assessed in cultured mammalian cells. The results obtained demonstrated the mimics to modestly inhibit viral replication, however these constructs were also shown to induce non-specific silencing, activate the interferon response, and were inefficiently processed into the expected guide sequences. Nevertheless, improvements can be made to the system to promote safe and efficient gene silencing. The modest inhibition demonstrated could have been attributed to inefficient processing due to the activation of the interferon response and limited trafficking of the pri-miR-31 mimics into the nucleus. The use of chemically modified nucleotides and employing precursor miRNA (pre-miRNA) may improve the safety and efficacy of these constructs. Therefore, this study demonstrated the potential of the in vitro transcribed miRNA mimics in inhibiting HBV, however improvements to the system could increase viral replication inhibition and reduce the immunogenicity of these constructs.

ACKNOWLEDGEMENTS

1. I would sincerely like to thank my supervisors Prof. Abdullah Ely and Prof. Patrick Arbuthnot for their continuous support, assistance, and patience throughout my studies, as without them the completion of this project would not be possible.

2. I would like to thank the members of the Antiviral Gene Therapy Research Unit (AGTRU) for their encouragement and companionship.

3. I am thankful to Dr Feng Zhang for supplying me with the pAAV-minCMV-mCherry plasmid.

4. I would like to thank Dr Ruben Hernandez Alcoceba for proving me with the pUCAsc-ISRE×3 plasmid.

5. I would like to thank my family and friends for their endless compassion and support.

6. I greatly appreciate the funding that I had received from AGTRU and the Poliomyelitis Research Foundation (PRF).

7. I am grateful to God for bestowing his blessings upon me.

TABLE OF CONTENTS

DECLARATION ..... **i**

DEDICATION ..... **ii**

PUBLICATIONS AND PRESENTATIONS ..... **iii**

ABSTRACT ..... **iv**

ACKNOWLEDGEMENTS ..... **v**

TABLE OF CONTENTS ..... **vi**

LIST OF FIGURES ..... **x**

LIST OF TABLES ..... **xiii**

LIST OF ABBREVIATIONS ..... **xiv**

CHAPTER 1 ..... **1**

1. INTRODUCTION **1**

1.1. Epidemiology and transmission **1**

1.2. Viral biology and genome organisation **2**

1.3. Viral replication cycle **4**

1.4. Current vaccines and treatments **6**

1.5. The microRNA biogenesis pathway **8**

1.6. Exploiting the RNAi pathway **9**

1.7. Pri-miRNA mimics **10**

1.8. In vitro transcribed RNAs **11**

1.9. Aim **13**

1.10. Objectives **13**

CHAPTER 2 ..... **15**

2. METHODS **15**

2.1. Design of the pT7-pri-miR-31 expression vectors **17**

2.2. Construction of the pT7-pri-miR-31 expression vectors **19**

2.2.1. Generation of the double-stranded insert 22

2.2.2. Isolation of the double-stranded insert 25

2.2.3. Isolation of the pmRNA-CMV-pA plasmid backbone 25
2.2.4. Ligation of the isolated insert into the pmRNA-CMV-pA plasmid backbone 26
2.2.5. Identification of the pCMV-pri-miR-31 plasmids and isolation of the pri-miR-31 encoding sequences 26
2.2.6. Ligation of the pri-miR-31 sequences into the pmRNA-CMV-T7-pA plasmid 27
2.3. RNA synthesis, purification, and analysis 27
2.3.1. In vitro transcription 27
2.3.2. Capping of in vitro transcribed RNA 28
2.3.3. Cellulose purification of in vitro transcribed RNA 28
2.3.4. Capillary gel electrophoresis 29
2.4. Tissue culture 29
2.4.1. Culturing conditions for mammalian cells 29
2.5. Transfection assays and expression analysis 29
2.5.1. Transfection of mammalian cell lines 29
2.5.2. Enzyme-linked immunosorbent assay (ELISA) 30
2.5.3. Dual-luciferase assay 30
2.5.4. Trizol RNA extraction 31
2.5.5. Collagen coating culture plates 31
2.6. Assessment of the constructed pT7-pri-miR-31 expression vectors 31
2.6.1. Assessment of HBV inhibition by the pT7-pri-miR-31 expression vectors 31
2.7. Assessment of the in vitro transcribed pri-miR-31 mimics 32
2.7.1. Assessment of HBV inhibition by the pri-miR-31 mimics 32
2.7.2. Investigation of cellular cytotoxicity by the pri-miR-31 mimics 33
2.7.3. Evaluation of interferon response by the pri-miR-31 mimics 34
2.8. Assessment of pri-miR-31 processing 35
2.8.1. Transfection and total RNA extraction 35
2.8.2. Radioactive labelling 35
2.8.3. Polyacrylamide gel electrophoresis (PAGE) 36

2.8.4. Staining, blotting and UV crosslinking 36
2.8.5. Hybridisation, stringency washing and visualisation 36
CHAPTER 3 38
3. RESULTS 38
3.1. Successful construction of the pT7-pri-miR-31 expression vectors 38
3.1.1. Generation of the double-stranded insert 38
3.1.2. PCR cloning of the double-stranded insert 39
3.1.3. Preparation of the pmRNA-CMV-pA plasmid backbone 40
3.1.4. Ligation of the isolated insert into the pmRNA-CMV-pA plasmid backbone 42
3.1.5. Identification of the pCMV-pri-miR-31 plasmids and isolation of the pri-miR-31 encoding sequences 43
3.1.6. Ligation of the pri-miR-31 sequences into the pmRNA-CMV-T7-pA plasmid 44
3.2. Assessment of the pT7-pri-miR-31 expression vectors 46
3.2.1. pT7-pri-miR-31 expression vectors inhibit HBV replication 46
3.3. Assessment of the pri-miR-31 mimics 48
3.3.1. pri-miR-31 mimics induce non-specific silencing and modestly inhibit HBV replication 48
3.3.2. Cellulose purified pri-miR-31/5 and pri-miR-31/8 mimics moderately induce specific HBV replication inhibition 55
3.3.3. Cellulose purified pri-miR-31 mimics do not affect cellular viability 58
3.3.4. Cellulose purified pri-miR-31 mimics induce interferon response 59
3.3.5. Cellulose purified pri-miR-31 mimics were inefficiently processed 64
CHAPTER 4 69
4. DISCUSSION 69
4.1. Construction and assessment of the pT7-pri-miR-31 expression vectors 69
4.2. Efficiency of the in vitro transcribed pri-miR-31 mimics 70
4.3. Processing of the in vitro transcribed pri-miR-31 mimics 70
4.4. Safety of the in vitro transcribed pri-miR-31 mimics 71
4.5. Chemical modifications 73

4.6. Delivery **74**

4.7. Off-target effects **76**

4.8. Conclusion **77**

CHAPTER 5 ..... **78**

5. APPENDIX **78**

5.1. Preparation, transformation, and propagation of chemically competent *E. coli* **78**

5.2. DNA purification and analysis **79**

5.2.1. Large scale plasmid DNA purification 80

5.2.2. Small scale plasmid DNA purification 81

5.2.3. Small scale high yield plasmid DNA purification 81

5.2.4. Restriction enzyme digestion 82

5.2.5. Agarose gel electrophoresis 82

5.2.6. DNA fragment purification 82

5.2.7. Ethanol precipitation 83

5.3. RNA synthesis, purification, and analysis **83**

5.3.1. Lithium chloride precipitation 83

5.4. Tissue culture **83**

5.5. Northern blot hybridisation **85**

5.6. Supplementary figures **86**

6. REFERENCES **118**

LIST OF FIGURES

Figure 1.1: Schematic representation of the HBV genome. 4
Figure 1.2: Schematic representation of the hepatitis B viral replication cycle. 6
Figure 1.3: Schematic representation of the miRNA biogenesis pathway. 9
Figure 1.4: Schematic representation of in vitro transcribed mRNAs and the in vitro transcribed anti-HBV pri-miR-31 mimics. 13
Figure 2.1: Design of the pT7-pri-miR-31 expression vectors. 18
Figure 2.2: Construction of the pmRNA-CMV-T7-pA expression vector. 20
Figure 2.3: Construction of the pT7-pri-miR-31 expression vectors. 21
Figure 2.4: Generation of the complete double-stranded insert. 24
Figure 3.1: Double-stranded insert after generation and purification. 39
Figure 3.2: Purified insert with *Sac*I and *Apa*I overhangs. 40
Figure 3.3: Preparation of the pmRNA-CMV-pA plasmid backbone. 41
Figure 3.4: Purified pmRNA-CMV-T7-pA plasmid with *Nhe*I and *Sal*I overhangs. 42
Figure 3.5: Isolated pri-miR-31 encoding sequences. 43
Figure 3.6: Identification of the generated pT7-pri-miR-31 expression vectors. 45
Figure 3.7: Assessment of HBV replication inhibition by the pCMV-pri-miR-31 and pT7-pri-miR-31 expression vectors by performing an ELISA. 47
Figure 3.8: In vitro transcribed RNA before and after capping. 49
Figure 3.9: Cellulose purified in vitro transcribed RNA before and after capping. 50
Figure 3.10: Assessment of HBV replication inhibition by the pri-miR-31 mimics prior to cellulose purification. 52
Figure 3.11: Assessment of HBV inhibition by the cellulose purified pri-miR-31 mimics by performing an ELISA. 54
Figure 3.12: Assessment of HBV inhibition by the cellulose purified pri-miR-31 mimics by performing dual-luciferase assays. 57
Figure 3.13: Assessment of cellular viability by the cellulose purified pri-miR-31 mimics using an MTT assay. 59
Figure 3.14: Evaluation of interferon response by the cellulose purified pri-miR-31 mimics by performing a dual luciferase assay. 60
Figure 3.15: Assessment of immune stimulation by the cellulose purified pri-miR-31 mimics by performing RT-qPCR assays. 63
Figure 3.16: In vitro transcribed RNA after LiCl precipitation, cellulose purification and capping. 65

Figure 3.17: Expression and processing of the pri-miR-31/5 mimics by Northern blot hybridisation analysis. 68
Figure S1: pmRNA-CMV-pA plasmid map. 86
Figure S2: Generation of the double-stranded insert. 87
Figure S3: pG-insert plasmid maps. 88
Figure S4: Screening for pG-insert positive clones after the purified insert was ligated into pGEM®-T Easy vector. 89
Figure S5: Sequencing analysis of the insert region of clone 5 and 6. 90
Figure S6: Screening of clone 5 and clone 6 using *Apa*I and *Pst*I to ensure recognition of the *Apa*I cleavage site after propagation and purification. 91
Figure S7: Restriction enzyme digestion of clone 5 using *Apa*I and *Sac*I to separate the insert from the pG-insert-R vector. 92
Figure S8: pmRNA-CMV-T7-pA plasmid map. 93
Figure S9: pmRNA-CMV-T7-pA clones screened with *Bsh*NI. 94
Figure S10: pmRNA-CMV-T7-pA clones digested with *Sal*I and *Nhe*I. 95
Figure S11: pmRNA-CMV-T7-pA clones screened with *Bsh*NI and *Bgl*I separately and *Sac*I and *Apa*I simultaneously. 96
Figure S12: pmRNA-CMV-T7-pA clones screened with *Sal*I and *Nhe*I separately. 97
Figure S13: Identification of the pCMV-pri-miR-31 plasmids. 98
Figure S14: Sequencing analysis of the pri-miR-31 encoding region of the monomeric pCMV-pri-miR-31 expression vectors. 99
Figure S15: Sequencing analysis of the pri-miR-31 encoding region of the trimeric pCMV-pri-miR-31 expression vectors 100
Figure S16: pmRNA-CMV-T7-pA and pCMV-pri-miR-31 plasmids digested with *Nhe*I. 101
Figure S17: pCMV-pri-miR-31 monomeric expression vectors after digestion with *Nhe*I and *Sal*I. 102
Figure S18: pCMV-pri-miR-31 trimeric expression vectors and pmRNA-CMV-T7-pA plasmid after digestion with *Nhe*I and *Sal*I. 103
Figure S19: Schematic representation of the pT7-pri-miR-31 expression vectors. 104
Figure S20: pT7-pri-miR-31 clones screened with *Nsb*I. 105
Figure S21: pT7-pri-miR-31 clones screened with *Bsh*NI. 106
Figure S22: pT7-pri-miR-31 plasmids after propagation and purification. 107
Figure S23: Fluorescence observed in the assay to assess HBV inhibition of the pT7-pri-miR-31 expression vectors. 108
Figure S24: Linearised pT7-pri-miR-31 plasmids before and after purification. 109

Figure S25: Fluorescence observed in the assay to assess HBV inhibition of the pri-miR-31 mimics prior to cellulose purification. 110
Figure S26: Fluorescence observed in the assay to assess HBV inhibition of the pri-miR-31 mimics after cellulose purification. 112
Figure S27: Schematic representation of the psiCHECK-HBx plasmid. 113
Figure S28: Fluorescence observed in the assay to assess specific HBV inhibition of the pri-miR-31 mimics after cellulose purification. 115
Figure S29: Fluorescence observed in the assay to assess cytotoxicity of the pri-miRNA-31 mimics. 116
Figure S30: Fluorescence observed in the assays to assess immunogenicity of the pri-miRNA-31 mimics. 116
Figure S31: Fluorescence observed in the analysis to assess processing efficiency of the pri-miRNA-31 mimics. 117

LIST OF TABLES

Table 2.1: Description of the plasmids used in this study. 15
Table 2.2: Description of the RNA used in this study. 17
Table 2.3: Primer sequences used to generate the double-stranded insert. 23
Table 2.4: Transfection mixes using the Lipofectamine™ 3000 kit. 30
Table 2.5: Transfection mixes using the Lipofectamine™ MessengerMAX™ Reagent. 30
Table 2.6: Primer sequences used to amplify the genes of interest. 35

LIST OF ABBREVIATIONS

1. AGO - argonaute
2. Cas - CRISPR-associated
3. cccDNA - covalently closed circular DNA
4. CMV IE - cytomegalovirus immediate-early
5. CMV - cytomegalovirus
6. CRISPR - clustered regularly interspaced short palindromic repeats
7. DMEM - Dulbecco's Modified Eagle Medium
8. DMEM/F12 - Dulbecco′s Modified Eagle′s Medium/F-12
9. DNA - deoxyribonucleic acid
10. DODAP - 1,2-dioleoyl-3-dimethylammoniumpropane
11. DODMA - 1,2-dioleyloxy-N,N-dimethyl-3-aminopropane
12. DOPE - 1,2-dioleoyl-sn-glycero-3-phosphoethanolamine
13. DOTAP - 1,2-dioleoyl-3-trimethylammonium propane
14. DOTMA - N-[1-(2,3-dioleyloxy)propyl]-N,N,N-trimethylammonium chloride
15. DR1 - direct repeat 1
16. DR2 - direct repeat 2
17. dsRNA - double stranded RNA
18. eGFP - enhanced green fluorescent protein
19. EGFR - epidermal growth factor receptor
20. eIF2α - eukaryotic translation initiation factor 2α
21. ELISA - enzyme-linked immunosorbent assay
22. ER - endoplasmic reticulum
23. HA - haemagglutinin
24. HBcAg - hepatitis B core antigen
25. HBeAg - hepatitis B e antigen
26. HBsAg - hepatitis B surface antigen
27. HBV - hepatitis B virus
28. HBx - hepatitis B X protein
29. HCC - hepatocellular carcinoma
30. HDR - homology-directed repair
31. HPLC - high performance liquid chromatography
32. HSPG - heparan sulphate proteoglycan
33. IFN - interferons

34. IPTG - isopropyl-β-D-thiogalactopyranosid
35. ISG - IFN stimulated gene
36. m1Ψ - *N1*-methylpseudouridine
37. m5C - 5-methylcytidine
38. m6A - *N6*-methyladenosine
39. MCS - multiple cloning site
40. MDA5 - melanoma differentiation associated protein 5
41. miR/miRNA - micro RNA
42. mRNA - messenger RNA
43. MTT - 3-(4,5-dimethylthiazol-2-yl)-2,5-diphenyltetrazolium
44. NA - nucleoside/nucleotide analogue
45. NO - nitric oxide
46. NTCP - sodium taurocholate co-transporting polypeptide
47. OAS - 2'-5'-oligoadenylate synthetase
48. ORF - open reading frame
49. PCR - polymerase chain reaction
50. PEG - polyethylene glycol
51. PEG-IFN-α - pegylated interferon alpha
52. PKR - protein kinase
53. pre-miRNA - precursor miRNA
54. pri-miRNA - primary miRNA
55. PRR - pattern recognition receptor
56. rcDNA - relaxed circular DNA
57. RFP - red fluorescent protein
58. RIG-I - retinoic acid inducible gene I
59. RISC - RNA induced silencing complex
60. RLR - retinoic acid inducible gene I like receptor
61. RNA - ribonucleic acid
62. RNAi - RNA interference
63. RNase L - ribonuclease L
64. ROS - reactive oxygen species
65. RT-qPCR -reverse transcription quantitative PCR
66. s2U - 2-thiouridine
67. shRNA - short hairpin RNA
68. siRNA - small interfering RNA

69. ssRNA - single stranded RNA
70. TALEN - transcription activator-like effector nuclease
71. TLR - toll-like receptor
72. UTR - untranslated region
73. X-gal - 5-bromo-4-chloro-3-indolyl-βD-galactopyranoside
74. ZFN - zinc finger nuclease
75. Ψ - pseudouridine

CHAPTER 1

1. INTRODUCTION

1.1. Epidemiology and transmission

Hepatitis B is an inflammatory disease of the liver that is caused by the hepatitis B virus (HBV). The disease has been found to greatly contribute to morbidity and mortality throughout the world, with the acute and chronic form of the disease accounting for approximately 90 000 and 800 000 deaths each year, respectively (World Health Organization, 2017). These incident rates occur as acute infections are more likely to be cleared by the immune system as opposed to chronic infections, which are able to persist and may eventually lead to cirrhosis, hepatocellular carcinoma (HCC), or liver failure [reviewed in (Liang, 2009)].

The chronic form of the disease affects over 257 million people worldwide, with the highest prevalence in the Western Pacific and African regions (World Health Organization, 2017). Infection with acute HBV may present as asymptomatic, or symptomatic which can range from fatigue to jaundice, or in rare cases, liver failure [reviewed in (Liang, 2009)]. The risk of acute infection developing into chronicity decreases with age of infection (Hyams, 1995; Edmunds et al., 1993). Thus, progression from acute to chronic disease occurs in approximately 90% of perinatally infected infants and less than 5% of infected adults (Hyams, 1995; Edmunds et al., 1993). Chronically infected patients may present with symptoms similar to those associated with the acute form of the disease or more severe symptoms such as palmar erythema, spider telangiectasia, fetor hepaticus and splenomegaly [reviewed in (Liang, 2009)]. Exposure to infected blood or other bodily fluids allows the virus to be transmitted from one individual to another [reviewed in (Papastergiou et al., 2015)]. In areas of low prevalence most infections are acquired through horizontal transmission from engaging in high-risk behaviours [reviewed in (Hwang and Cheung, 2011)]. However, in areas of high prevalence, infections are predominantly acquired through horizontal transmission or through vertical transmission from mother to child [reviewed in (Hwang and Cheung, 2011)].

There are ten HBV genotypes (A to J) that have been identified and many of these can be further categorised into various subgenotypes [reviewed in (Tong and Revill, 2016)]. It is estimated that most chronic infections worldwide are caused by genotypes A to E (Velkov et al., 2018) . HBV genotypes are geographically distributed with genotypes A and E predominantly occurring in sub-Saharan Africa, genotypes B and C mainly presenting in east and southeast Asia, and genotype D primarily arising in Central Asia, southern Asia, western

Asia, and northern Africa (Velkov et al., 2018). Each genotype differs in nucleotide sequence by at least 8% [reviewed in (Sunbul, 2014)]. The development of disease and response to treatment varies between each group, thus it is crucial to be able to differentiate between these genotypes [reviewed in (Sunbul, 2014)].

1.2. Viral biology and genome organisation

The hepatitis B virus is classified as a member of the Hepadnaviridae family [reviewed in (Gust et al., 1986)]. The virion is approximately 42 nm in diameter and consists of an outer lipid envelope embedded with large (L), middle (M) and small (S) surface proteins (Sonveaux et al., 1995; Ueda et al., 1991; Dane et al., 1970). The envelope surrounds an icosahedral nucleocapsid core which encloses the viral genome and polymerase (Böttcher et al., 1997; Robinson, 1975). The viral genome is approximately 3.2 kb in length and exists as partially double-stranded relaxed circular DNA (rcDNA) [reviewed in (Karayiannis, 2017)] (Figure 1.1). The rcDNA consists of a complete negative strand and an incomplete positive strand and encodes four overlapping open reading frames (ORFs) namely *core* (*C*), *polymerase* (*P*), *surface* (*S*) and *X* [reviewed in (Tsukuda and Watashi, 2020)] (Figure 1.1). During replication the rcDNA is converted into covalently closed circular DNA (cccDNA) which serves as a template for the transcription of five viral transcripts specifically pre-genomic RNA (3.5 kb), pre-core mRNA (3.5 kb), preS1 mRNA (2.4 kb), preS2/S mRNA (2.1 kb) and X mRNA (0.7 kb) [reviewed in (Zhao et al., 2021)] (Figure 1.1). The transcripts each have a 5' cap and a 3' polyadenylated tail. The length of each transcript is dependent on the location of its relevant promoter as transcription terminates at a single polyadenylation signal [reviewed in (Lamontagne et al., 2016)]. This results in the transcripts having a common 3' end which is identical to the shortest mRNA specifically the X mRNA.

The X mRNA is transcribed from the *X* ORF and translates into the regulatory hepatitis B x protein (HBx) which serves to maintain cccDNA expression (Lucifora et al., 2011). The SMC5/6 complex which normally functions to limit expression from episomal DNA can bind to cccDNA and inhibit its transcription (Decorsière et al., 2016; Murphy et al., 2016). However, after infection with HBV the HBx directs the SMC5/6 complex to the E3 ubiquitin ligase proteasome for degradation which prevents it from inhibiting transcription of the cccDNA (Decorsière et al., 2016; Murphy et al., 2016). The HBx also promotes binding of the parvulin 14 and 17 proteins to the cccDNA which enhances cccDNA formation by escalating viral RNA transcription (Saeed et al., 2019).

The preS1 mRNA and preS2/S mRNA are transcribed from the *S* ORF and translates into the hepatitis B surface antigen (HBsAg) proteins [reviewed in (Zhao et al., 2021)]. The preS1

mRNA translates into the L-HBsAg protein and the preS2/S mRNA translates into the M-HBsAg and S-HBsAg proteins [reviewed in (Zhao et al., 2021)]. These proteins are responsible for attachment and entry into the hepatocyte as well as nucleocapsid envelopment and viral particle secretion (Yan et al., 2012; Bruss and Ganem, 1991). They also contribute to viral persistence by deregulating the immune system [reviewed in (Zhao et al., 2021)]. The pre-core mRNA is transcribed from the *C* ORF and translates into the hepatitis B e antigen (HBeAg) protein which is suspected to suppress the immune response and prevent viral clearance [(Chen et al., 2005) and reviewed in (Zhao et al., 2021)].

The pre-genomic RNA serves as a template for the translation of the hepatitis B core antigen (HBcAg) and the DNA polymerase protein [reviewed in (Lamontagne et al., 2016)]. HBcAg is encoded within the *C* ORF and is responsible for co-ordinating and self-assembling to form the nucleocapsid core which encapsulates the pre-genomic RNA and DNA polymerase protein [reviewed in (Zlotnick et al., 2015)]. The carboxy-terminal domain of HBcAg is required for pre-genomic encapsidation and contributes to genome replication pleiotropically (Lewellyn and Loeb, 2011; Nassal, 1992). Furthermore, HBcAg plays a role in regulating viral transcription by binding to the cccDNA and regulating its epigenetics [reviewed in (Diab et al., 2018)]. These proteins are also associated with T cell exhaustion which contributes to immune escape [reviewed in (Zhao et al., 2021)]. The polymerase protein is encoded within the *P* ORF and is responsible for synthesising the rcDNA by reverse transcription [reviewed in (Seeger and Mason, 2000). It also has roles in encapsidation and may contribute to innate immune evasion [(Bartenschlager et al., 1990) and reviewed in (Zhao et al., 2021)].

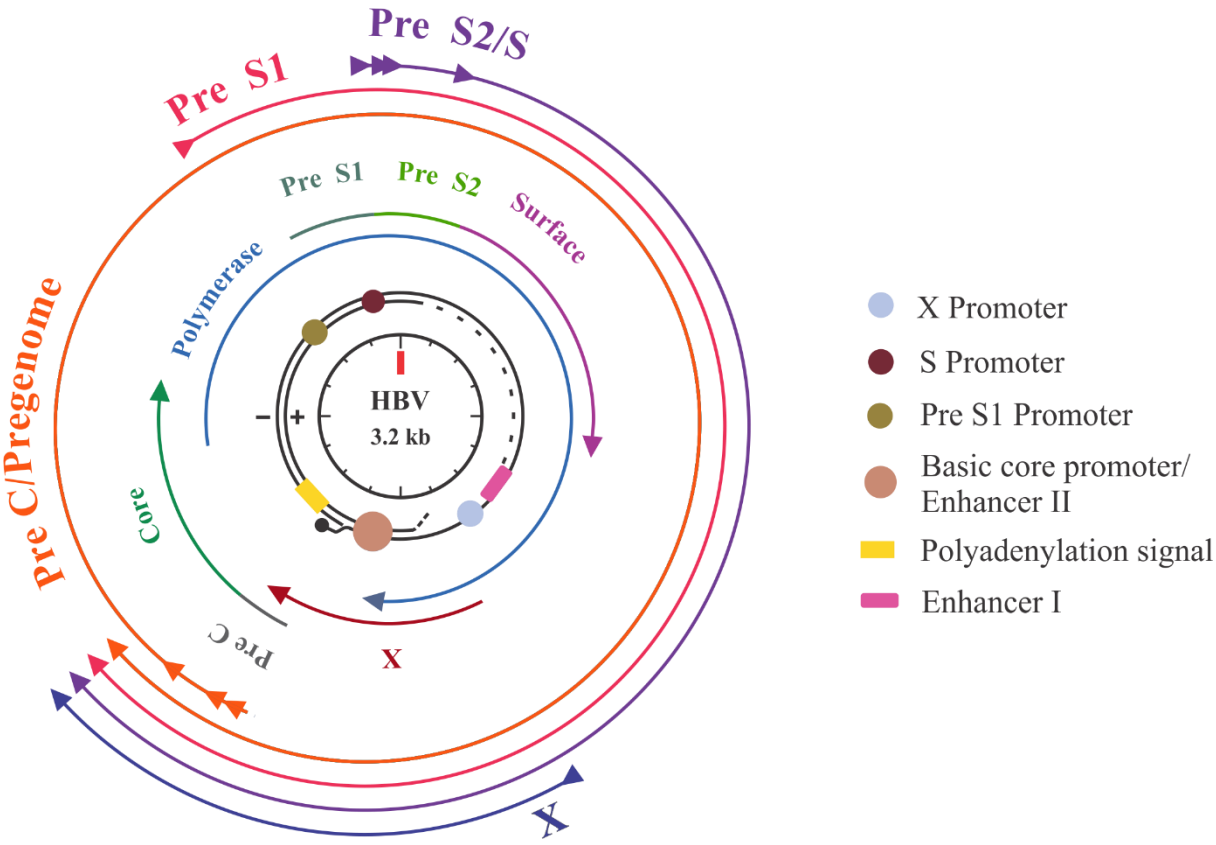


Figure 1.1: Schematic representation of the HBV genome. The inner circle represents the HBV genome which consists of a complete negative strand and an incomplete positive strand. The four inner arrows surrounding the genome represents the four ORFs. The four outer arrows surrounding the ORFs represents the five viral transcripts. The rectangular and circular symbols represent the transcriptional regulatory elements. [Adapted from (Moolla et al., 2002)].

1.3. Viral replication cycle

The hepatitis B viral replication cycle involves several steps which include viral attachment, entry, replication, and secretion (Figure 1.2). Entry is first initiated through low-affinity binding of the virus to heparan sulphate proteoglycan (HSPG) receptors present on the surface of the hepatocyte (Leistner et al., 2008; Schulze et al., 2007). This is followed by high-affinity binding of the preS1 domain of the large envelope protein to the hepatocyte-associated sodium taurocholate co-transporting polypeptide (NTCP) receptor (Yan et al., 2012). The subsequent interaction of NTCP to the host epidermal growth factor receptor (EGFR) then triggers the endocytotic entry of the virus into the hepatocyte (Iwamoto et al., 2020, 2019). The internalised virus is then guided through the endosomal network by the activated EGFR and assisting host molecules (Iwamoto et al., 2020). The mechanism in which the nucleocapsid is released into the cytoplasm remains unclear however it is presumed that the release occurs after the viral envelope fuses with the endosomal membrane [reviewed in

(Tsukuda and Watashi, 2020)]. The nucleocapsid is then transported to the nuclear pore complex where it disassembles and releases the rcDNA into the nucleus (Rabe et al., 2003). The rcDNA is modified by host-derived cellular enzymes to remove the polymerase protein from the 5' end of the negative strand and the RNA primer from the 5' end of the positive strand [reviewed in (Prifti et al., 2021)]. The positive and negative strands are then repaired, ligated and modified to generate a stable double-stranded cccDNA minichromosome [reviewed in (Xia and Guo, 2020)]. The cccDNA minichromosome serves as a template for the transcription of the five viral transcripts using the host derived RNA polymerase II [reviewed in (Zhao et al., 2021)].

Following translation of the viral polymerase it attaches to the epsilon structure on the 5' end of the pre-genomic RNA and forms a complex which triggers its encapsulation by the core proteins (Knaus and Nassal, 1993; Junker-Niepmann et al., 1990). Once encapsulated, the polymerase attaches the first nucleotide of the negative strand directly to itself to initiate polymerisation and then uses the bulge region of epsilon as a template to synthesise the next few nucleotides of the negative strand (Nassal and Rieger, 1996; Rieger and Nassal, 1996). It is then translocated with the attached sequence to the direct repeat 1 (DR1) located at the 3' end of the pre-genomic RNA (Nassal and Rieger, 1996; Rieger and Nassal, 1996). The polymerase uses the attached sequence as a primer to extend the negative strand while degrading the majority of the pre-genomic RNA template (Loeb et al., 1991). The extreme 5' end of the pre-genomic RNA that remains undegraded is then translocated to the direct repeat 2 (DR2) located towards the 5' end of the negative strand where it serves as an RNA primer (Loeb et al., 1991). The primer is used to synthesise the positive strand until it reaches the 5' end of the negative strand (Loeb et al., 1991). Circularisation then occurs when the 3' extending end of the positive strand is translocated to the corresponding 3' end of the negative strand [reviewed in (Chen et al., 2015)]. This conformation allows for further elongation of the positive strand before it randomly terminates, leaving the polymerase still attached to the 5' end of the negative strand [reviewed in (Chen et al., 2015)]. The mature nucleocapsid which contains the newly formed rcDNA with the attached polymerase can then either enter the endoplasmic reticulum (ER) or the nucleus. If it enters the ER, it will acquire a membrane with surface antigen proteins, and be released from the hepatocyte as a new virion through the use of the host's multivesicular body system (Watanabe et al., 2007). If it enters the nucleus it will function to replenish the supply of cccDNA to allow the virus to establish persistent infections in the hepatocyte and cause chronic HBV (Tuttleman et al., 1986).

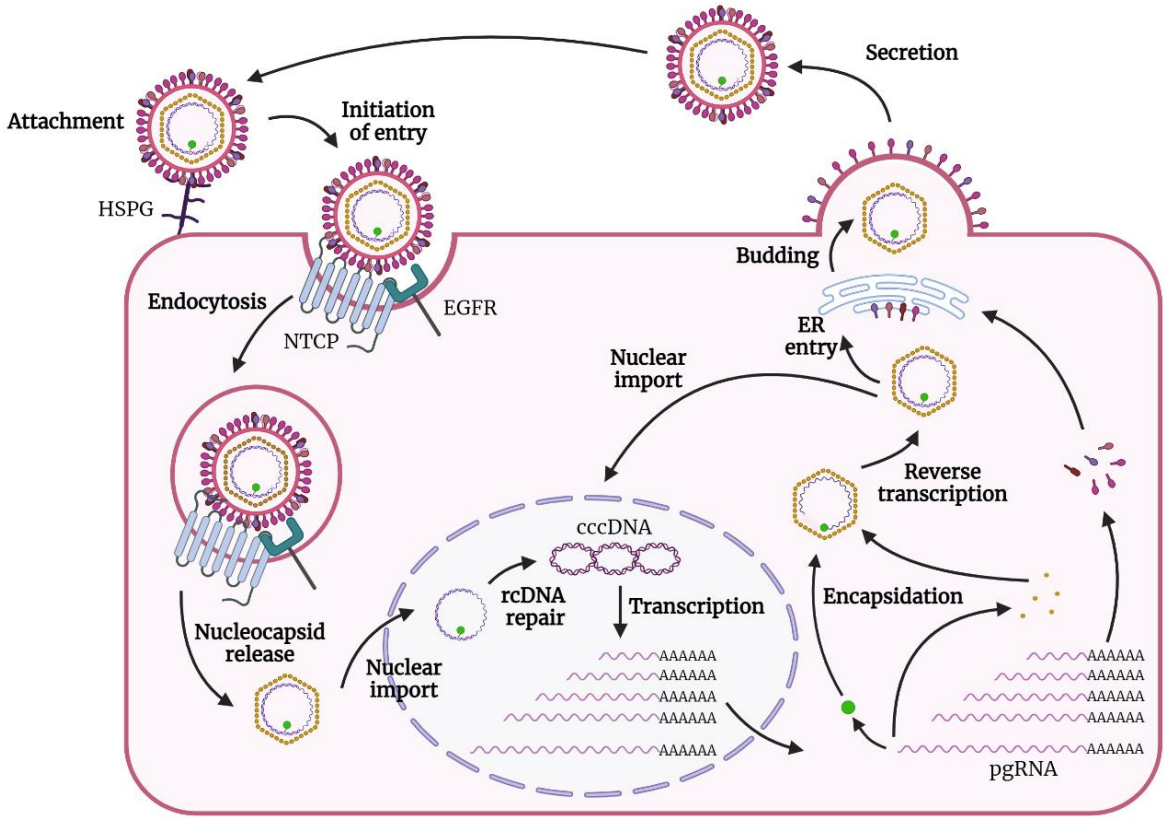


Figure 1.2: Schematic representation of the hepatitis B viral replication cycle. The virus first binds to HSPG receptors present on the surface of the hepatocyte which facilitates the attachment of the virus to adjacent NTCP receptors. The subsequent interaction of NTCP to EGFR triggers endocytosis and internalisation of the virus. The internalised virus travels through the endosomal network towards the nucleus where it releases the nucleocapsid. The nucleocapsid is then transported to the nuclear pore where it disassembles and releases the rcDNA into the nucleus. The rcDNA is converted to cccDNA which serves as a template for the transcription of the viral transcripts. The pre-genomic RNA and viral mRNAs are translated into the viral proteins. The polymerase protein attaches to the pre-genomic RNA which triggers encapsidation by the core proteins. The pre-genomic RNA is then used as a template by the polymerase protein to synthesise the rcDNA. The mature nucleocapsid containing the newly formed rcDNA and polymerase can then either enter the ER or nucleus. If it enters the ER, it will acquire an outer lipid envelope with embedded surface proteins and be secreted to infect other hepatocytes. If it enters the nucleus it will function to replenish the supply of cccDNA thus allowing viral persistence. This figure was created with BioRender.com.

1.4. Current vaccines and treatments

The HBsAg vaccine has been proven to be effective in inducing a long-lasting protective antibody response against new HBV infections in approximately 95% of healthy individuals who have completed their vaccine series [reviewed in (Poland and Jacobson, 2004)]. The remaining 5% of healthy individuals who do not respond to the HBsAg vaccine and those individuals who are immunocompromised can also acquire protective immunity through the

use of other existing vaccine interventions (Krawczyk et al., 2014; McDermott et al., 1998). Although these vaccines are effective in preventing new HBV infections from occurring, the overall vaccination coverage remains low, especially in developing countries, such as South Africa (Subaiya et al., 2015). This occurs as it is recommended that the vaccine be administered within 24 hours after birth, and developing countries experience challenges which may hinder timely delivery (World Health Organization, 2017). Furthermore, since more than one dose is recommended, this may become challenging to achieve in regions with limited resources (World Health Organization, 2017). Therefore, infants born in these countries are at a high risk of contracting HBV and developing chronic infection.

The current mainstream treatments for people with chronic HBV are pegylated interferon alpha (PEG-IFN-α) and nucleoside/nucleotide analogue (NA) therapy. IFN-α is a therapeutic cytokine which inhibits viral genome transcription, promotes viral nucleocapsid decay, induces cccDNA degradation and accelerates natural killer cell proliferation, activation, and antiviral activity (Lucifora et al., 2014; Micco et al., 2013; Belloni et al., 2012; Xu et al., 2010). Conventional IFN-α was the first agent approved to treat chronic HBV infections, however due to its adverse pharmacokinetic properties and short half-life it was gradually replaced with its pegylated counterpart PEG-IFN-α [reviewed in (Tsai, 2021)]. A major limitation with PEG-IFN-α therapy is that only approximately 30% of chronically infected patients who receive treatment achieve HBeAg seroconversion and reduction of viral DNA (Lau et al., 2005; Cooksley et al., 2003). PEG-IFN-α also requires weekly subcutaneous administration and is associated with a considerable number of adverse events which may include flu-like symptoms, fatigue, depression, irritability, neutropenia, and thrombocytopenia [reviewed in (Rijckborst et al., 2011)]. On the other hand, treatment with PEG-IFN-α can sustain the rate of HBeAg seroconversion for up to 5 years post-treatment (Chuang et al., 2018).

NAs mainly function to reduce HBV DNA replication by directly targeting the HBV polymerase and inhibiting its reverse transcriptase activity [reviewed in (Menéndez-Arias et al., 2014)]. The NAs approved for the treatment of chronic hepatitis B include lamivudine, adefovir, entecavir, telbivudine and tenofovir. They are administered orally once a day and are generally safe with minimal adverse events (de Fraga et al., 2020). A major disadvantage with earlier NAs such as lamivudine is that they are associated with increased risk of antiviral resistance, however newer drugs in particular entecavir and tenofovir have a high resistance barrier (Tenney et al., 2009; Yuen et al., 2007). Thus, entecavir, tenofovir disoproxil fumarate and tenofovir alafenamide are currently recommended as the first line NA treatment for

chronic hepatitis B infections [reviewed in (Terrault et al., 2018)]. The majority of patients who receive treatment with these high resistance drugs are able to achieve reduction in serum HBV DNA and normal alanine aminotransferase concentrations [reviewed in (Tsai, 2021)]. Furthermore, long-term treatment can increase overall survival and decrease the rate of HCC progression (Papatheodoridis et al., 2018; Idilman et al., 2015). NA therapy can also markedly reduce the amount of intrahepatic cccDNA and decrease the risk of mother to child transmission of HBV (Funk et al., 2021; Jia et al., 2020; Lai et al., 2017). Although viral suppression can be achieved with NA monotherapy, HBeAg and HBsAg seroclearance is relatively low in long-term treatment (Seto et al., 2013). While both treatment strategies are able to suppress viral replication, neither are capable of eradicating cccDNA from infected patients. Therefore, novel therapeutics capable of eradicating cccDNA are urgently needed.

1.5. The microRNA biogenesis pathway

The microRNA (miRNA) biogenesis pathway or RNA interference (RNAi) pathway is an innate gene silencing mechanism present in most eukaryotic systems in which targeted mRNA molecules are inhibited to control gene expression [reviewed in (Ha and Kim, 2014)] (Figure 1.3). miRNA genes are located within the genome as single genes or groups of genes [reviewed in (Treiber et al., 2019)]. These genes are expressed under the control of RNA polymerase II promoters to produce single stranded primary miRNA (pri-miRNA) sequences (Lee et al., 2004). The pri-miRNA sequences may contain single or multiple hairpin loops with a 5’ cap and poly(A) tail, and are processed by the microprocessor complex (Lee et al., 2004). The microprocessor complex is a heterotrimeric complex, comprised of two molecules of a double-stranded RNA binding protein, DGCR8 and one molecule of a ribonuclease III enzyme, Drosha (Nguyen et al., 2015). DGCR8 binds and stabilises Drosha and Drosha recognises the basal junction of the hairpin loops and cleave the 5′ and 3′ strands 11 bp away from the recognition site at the lower stem of the pri-miRNA to produce individual hairpin loops of approximately 70 nucleotides in length (Nguyen et al., 2015; Han et al., 2004). The individual hairpin loops are known as a precursor miRNA (pre-miRNA) and are exported to the cytoplasm via Exportin-5 (Lund et al., 2004). In the cytoplasm, Dicer which is a ribonuclease III enzyme, processes the pre-miRNA to form a ~22 bp miRNA duplex with 2 nucleotide 3’ overhangs (Zhang et al., 2004; Bernstein et al., 2001). The miRNA duplex enters the RNA induced silencing complex (RISC) where it assembles with argonaute (AGO) proteins [reviewed in (Kobayashi and Tomari, 2016)]. Thereafter, the two strands are separated, and the passenger strand is removed while the guide strand remains. The guide strand or mature miRNA leads the complex to complementary mRNA which is then silenced

either through degradation of the mRNA (perfect match) or inhibition of translation (imperfect match) [reviewed in (Jonas and Izaurralde, 2015)].

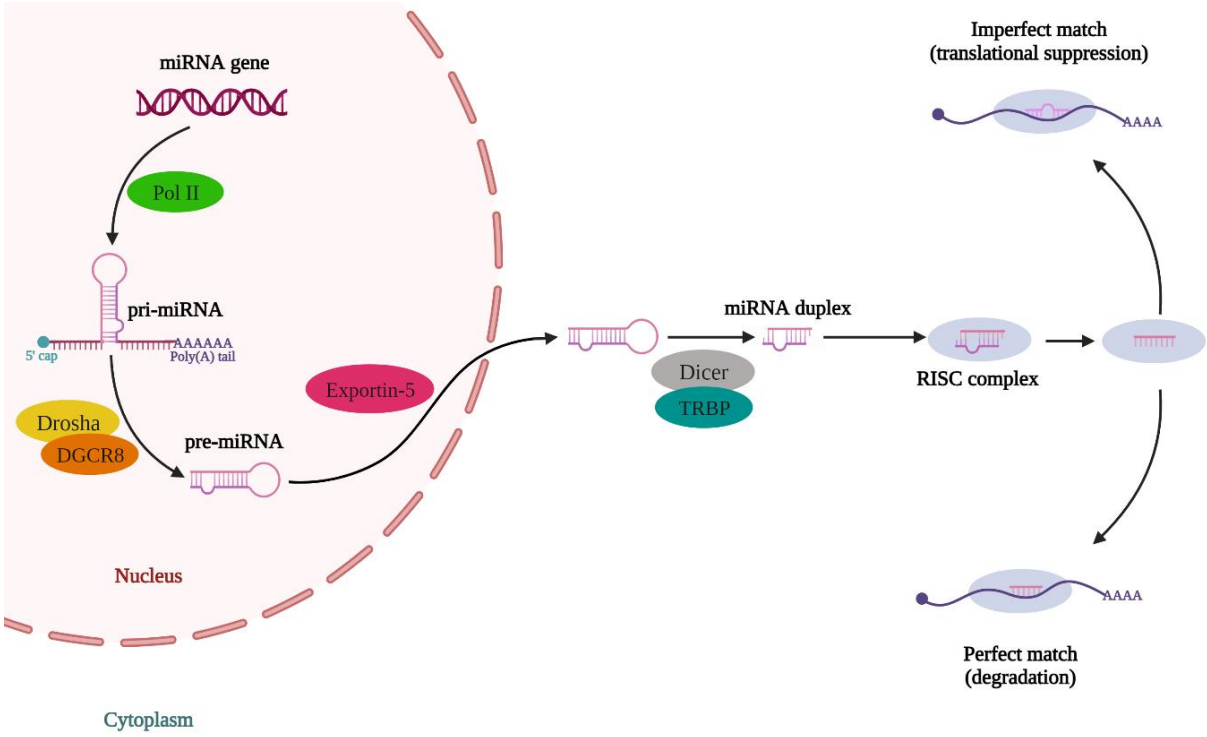


Figure 1.3: Schematic representation of the miRNA biogenesis pathway. miRNA genes are expressed under the control of RNA polymerase II promoters to produce single stranded pri-miRNA sequences. These sequences are then cleaved by the microprocessor complex to produce pre-miRNA. The pre-miRNA sequences are exported to the cytoplasm via Exportin-5 where it is processed by Dicer to form the miRNA duplex. The miRNA duplex then enters RISC where the passenger strand is removed while the guide strand remains. The guide strand leads the complex to complementary mRNA which is silenced either through degradation of the mRNA (perfect match) or inhibition of translation (imperfect match). This figure was created with BioRender.com.

1.6. Exploiting the RNAi pathway

The RNAi pathway can be exploited by introducing RNAi activators into cells to silence genes of interest for various applications [reviewed in (Ambesajir et al., 2012)]. These activators are generally designed to mimic intermediates of the miRNA biogenesis pathway, thus efficient gene silencing is dependent on the structure and sequence of the miRNA mimics produced. RNAi activators such as short hairpin RNAs (shRNAs) resemble the structure of naturally occurring pre-miRNA sequences, artificial pri-miRNAs (pri-miRNA mimics) simulate pri-miRNA sequences, and synthetic small interfering RNAs (siRNAs) imitate miRNA duplexes [reviewed in (Maepa et al., 2015)]. shRNAs and pri-miRNA mimics are generally expressed endogenously from expression cassettes that have been delivered into

target cells whereas siRNAs are usually generated exogenously [reviewed in (Maepa et al., 2015)]. These activators have all been previously shown to efficiently inhibit HBV replication in vitro and in vivo, however there are several challenges associated with the use of these constructs (Ely et al., 2009; Carmona et al., 2006; Giladi et al., 2003).

The challenge with the use of expression cassettes that endogenously express shRNAs or pri-miRNA mimics is that these constructs may remain within the host cells for several years and as a consequence may cause undesirable effects. Furthermore, these expression cassettes are commonly delivered using viral vectors which has the potential to integrate into the host genome and cause mutagenesis that could lead to severe adverse events [(Raper et al., 2003) and reviewed in (Poletti and Mavilio, 2018)]. Moreover, the viral vectors used to deliver these expression cassettes are expensive and difficult to produce at large scale and are limited in their packaging capacity [(Wu et al., 2010) and reviewed in (Naso et al., 2017)]. The use of exogenously expressed RNAs on the other hand bypasses these challenges as the delivery of RNA sequences using non-viral vectors have been shown to be safer and are significantly more cost effective than the delivery of DNA sequences using viral vectors.

The challenge with the use of chemically synthesised siRNAs is that these constructs are still costly to manufacture [reviewed in (Levanova and Poranen, 2018)]. Therefore, since RNA constructs are transiently expressed, the repeat dosing required to treat chronic infections will become challenging. The use of in vitro transcribed siRNAs offers a significant cost advantage over chemically synthesised siRNAs as in vitro transcription is less expensive [reviewed in (De Paula et al., 2007)]. However, the production yield of in vitro transcribed siRNAs due to their duplex structure may be hindered by the formation of imperfect strands during the in vitro transcription process which may prevent complementary sequences from annealing during hybridisation [(reviewed in (Levanova and Poranen, 2018)].

1.7. Pri-miRNA mimics

Pri-miRNA mimics are advantageous over shRNAs and siRNAs as these constructs require additional processing by the RNAi machinery, thus the products produced are more likely to be recognised and produce the intended guide sequences. Several studies assessing pri-miRNA mimics expressed from expression cassettes were performed in vitro and in vivo. In a study performed by Ely and colleagues, various expression cassettes were generated to produce anti-HBV pri-miR-31/5 and pri-miR-122/5 mimics from either a Pol II (CMV) or Pol III (U6) promoter (Ely et al., 2008). These constructs were designed to target regions within the *HBx* sequence and were demonstrated effective at inhibiting HBV replication both in vitro and in vivo. The effectiveness observed by the miR-31/5 and miR-122/5 expression cassettes

were similar to that demonstrated by their shRNA counterparts, however, the miR-31/5 and miR-122/5 expression cassettes exhibited improved transcriptional control. In addition, the miR-31/5 and miR-122/5 expression cassettes had minimal to no effect on independent RNAi-mediated gene silencing and were non-toxic when tested in vitro and in vivo. Furthermore, processing of the pri-miRNA mimics into mature miRNA guide sequences were shown to be more efficient for the Pol II (CMV) generated transcripts compared to the Pol III (U6) systems.

In another study performed by Ely and colleagues, several trimeric expression cassettes were generated to produce anti-HBV pri-miR-31/5-8-9, pri-miR-31/5-9-8, pri-miR-31/8-5-9, pri-miR-31/8-9-5, pri-miR-31/9-5-8 and pri-miR-31/9-8-5 mimics from a Pol II (CMV) promoter (Ely et al., 2009). These constructs were designed to target specific regions within the *HBx* sequence and were demonstrated to effectively inhibit HBV replication in vitro. However, processing efficiency into individual guide strands and silencing of the specific target sequences were different for each of the pri-miR-31 mimics, depending on the position of the monomers within the trimeric expression cassettes. The pri-miR-31/5-9-8 and pri-miR-31/9-8-5 mimics were not able to produce mature guide 8 strands, which was possibly due to the pri-miR-31/8 sequence downstream of the pri-miR-31/9 sequence. Furthermore, each of the pri-miR-31 trimeric expression cassettes did not induce toxicity or disrupt the endogenous miRNA pathway in vitro. The pri-miR-31/5-8-9 and pri-miR-31/8-5-9 mimics were also tested in mice and were shown to significantly reduce HBsAg without evidence of toxicity or disruption from the promoter, thus indicating the silencing capabilities of trimeric pri-miR-31 mimics in vivo. The advantage of trimeric expression cassettes is that simultaneous silencing of multiple targets can be achieved using a single vector. The results from the study demonstrated, each of the pri-miR-31 mimics, except for pri-miR-31/5-9-8 and pri-miR-31/9-8-5 were able to inhibit their respective targets, irrespective of an introduced mutation within target 5 of the viral genome, indicating that this multitargeting attribute may assist in overcoming mutational escape that may occur during chronic infection. Therefore, these studies together demonstrated the efficiency of the pri-miR-31 expression cassettes in combatting HBV, however the use of in vitro transcribed pri-miR-31 mimics could possibly be a safer and more cost-effective novel therapeutic approach against the virus.

1.8. In vitro transcribed RNAs

The use of in vitro transcribed mRNAs has recently gained the interest of many researchers in the field of gene therapeutics due to its promising applications in immunotherapy, protein replacement therapy, and regenerative medicine. These constructs are generated through a

process of in vitro transcription and are subsequently delivered into target cells where the in vitro transcribed mRNAs are translated into desired proteins. In vitro transcription is a commonly used method for producing RNA molecules from DNA templates [reviewed in (Ryczek et al., 2022)]. This method relies on the specificity of a particular RNA polymerase to recognise its promoter sequence within the provided DNA template and subsequently produce complementary RNA molecules under the transcriptional control of the recognised promoter [reviewed in (Ho and Yu, 2016)]. The incorporation of certain elements within the DNA template determines the durability and immunogenicity of the constructs that will be produced [reviewed in (Kuhn et al., 2012)]. In vitro transcribed mRNAs are usually designed to resemble and function as naturally occurring mRNAs to prevent these constructs from activating the innate immune response and inducing severe adverse effects (Figure 1.4). In vitro transcribed RNAs that contain a 5' cap, modified nucleotides, a terminal 5' UTR, and a terminal 3' UTR with a poly(A) sequence have been shown to be more durable and less immunogenic than those that do not contain these elements [reviewed in (Steinle et al., 2017)]. The 5' cap can be added to the transcripts during or after in vitro transcription, serving to prevent RNA degradation and reduce immune stimulation, whereas the other elements can be incorporated within the DNA template [reviewed in (Kwon et al., 2022) and (Wadhwa et al., 2020)]. The modified nucleotides, terminal 5' and 3' UTRs, and poly(A) tail are responsible for inhibiting immune activation, enhancing RNA stability, and preventing RNA degradation respectively [(Karikó et al., 2005) and reviewed in (Steinle et al., 2017)]. The purification of the in vitro transcribed RNAs by high-performance liquid chromatography or cellulose based methods can also reduce immunogenicity by facilitating the removal of contaminating products that may be produced during the in vitro transcription process (Baiersdörfer et al., 2019; Karikó et al., 2011). In vitro transcribed mRNAs are more cost-effective to produce than chemically synthesised RNAs and the delivery of these constructs using non-viral vectors is safer than the delivery of expression cassettes using viral vectors. In addition, pri-miR-31 mimics have been shown to be effective at inhibiting HBV replication through targeting of the *HBx* sequence. Therefore, the purpose of this study was to adapt the technology used to generate in vitro transcribed mRNAs and use it to produce in vitro transcribed pri-miR-31 mimics which target the *HBx* region that is common to each of the viral transcripts. Since viral antigens, especially HBsAg and HBeAg, are produced in considerable quantities during chronic HBV infection, this can lead to an immunosuppressive effect on the host antiviral response where it will be unable to eradicate the virus [reviewed in (Khanam et al., 2021)]. Therefore, the rationale was that simultaneously targeting the viral mRNAs may reduce viral protein production and subsequently remove the suppressive effect

that these proteins have on the immune system which has the potential to reactivate the host's natural defences to clear the virus.

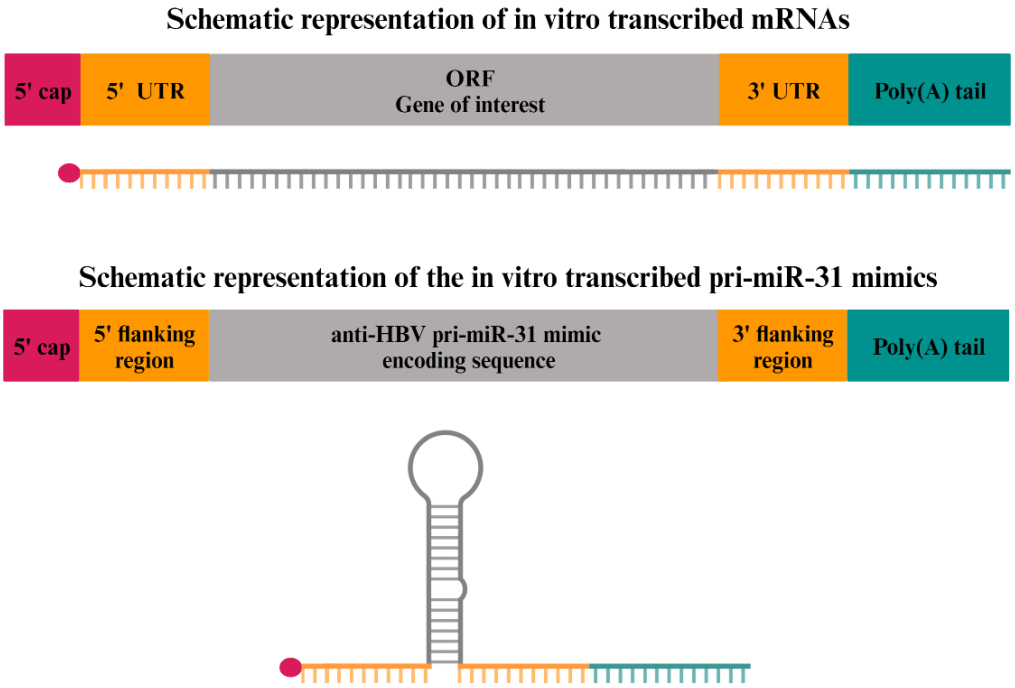


Figure 1.4: Schematic representation of in vitro transcribed mRNAs and the in vitro transcribed anti-HBV pri-miR-31 mimics. In vitro transcribed mRNAs and the in vitro transcribed pri-miR-31 mimics contain a 5' cap, a terminal 5' region, an encoding sequence, and a terminal 3' region with a poly(A) sequence. In vitro transcribed mRNAs are designed to express a desired protein whereas the in vitro transcribed pri-miR-31 mimics are designed to simultaneously silence the HBV transcripts. This figure was created with BioRender.com.

1.9. Aim

The aim of this project was to in vitro transcribe therapeutic anti-HBV pri-miRNA mimics capable of targeting the *HBx* region common to all of the viral transcripts thereby simultaneously silencing the viral mRNAs and consequently suppressing viral replication.

1.10. Objectives

1. Generate pT7-pri-miR-31 expression vectors capable of expressing anti-HBV pri-miR-31 mimics for in vitro transcription.
2. Assess HBV replication inhibition of the constructed pT7-pri-miR-31 expression vectors in cultured mammalian cells.
3. In vitro transcribe anti-HBV pri-miR-31 mimics using the pT7-pri-miR-31 expression vectors as templates.
4. Assess HBV replication inhibition of the in vitro transcribed pri-miR-31 mimics in cultured mammalian cells.

5. Evaluate immune stimulation and cytotoxicity of the in vitro transcribed pri-miR-31 mimics in cultured mammalian cells.
6. Assess pri-miR-31 mimic processing by performing Northern blot hybridisation analysis.

CHAPTER 2

2. METHODS

Several plasmids were used in this study, some of which were generated during the course of this study, while the others were procured from other sources. A complete list of all the plasmids used can be found in Table 2.1. Table 2.2 lists RNA from commercial sources used in this study.

Table 2.1: Description of the plasmids used in this study.

Cloning plasmids	
pmRNA-CMV-pA	The pmRNA-CMV-pA plasmid was initially developed to in vitro transcribe mRNA that will be translated to produce large amounts of a desired protein (unpublished data). The plasmid has a T7 promoter, a 5' UTR, a Kozak sequence, an HA (haemagglutinin) tag and a 3' UTR with a poly(A) sequence (Figure S1). The T7 promoter allows for high yield in vitro transcription, the Kozak sequence plays a role in initiating protein translation and the HA tag functions as an identifier of the translated protein.
pCMV-pri-miR-31/5 pCMV-pri-miR-31/8 pCMV-pri-miR-31/9 pCMV-pri-miR-31/589 pCMV-pri-miR-31/895	These pri-miR-31 encoding plasmids have been described previously by Ely and colleagues (Ely et al., 2009). The plasmids contain a monomeric or trimeric pri-miR-31 mimic encoding sequence downstream of the cytomegalovirus immediate-early (CMV IE) promoter enhancer. The mimics were designed to target specific sites within the *HBx* region, as this region is common to all of the viral transcripts.
pmRNA-CMV-eGFP-pA	The pmRNA-CMV-eGFP-pA plasmid was previously constructed to contain an enhanced green fluorescent protein (eGFP) sequence under the control of the T7 promoter. It also contains the same backbone as the pT7-pri-miR-31 plasmids and thus was used as a control in this study.
pTZ57R	The pTZ57R plasmid is a commercial plasmid that does not contain any eukaryotic expression elements. It was used as a control to check for transfection of an equal amount of DNA.
pCI-neo	The pCI-neo plasmid is a commercial mammalian expression

	vector that contains a CMV IE promoter.
Target plasmids	
pCH-9/3091	The pCH-9/3091 plasmid was previously developed by Nassal and colleagues (Nassal, 1992; Nassal et al., 1990). The plasmid contains a greater-than-genome length HBV sequence (genotype D) which allows it to stimulate HBV replication when transfected in vitro and in vivo. Transcription of the pCH-9/3091 plasmid is guided by the human CMV IE promoter to generate pre-genomic RNA which is then reverse transcribed to form cccDNA. The cccDNA serves as a template for the transcription of the viral transcripts and subsequent viral proteins which contribute to the replication process.
psiCHECK-HBx	The psiCHECK-HBx plasmid was previously generated by Weinberg and colleagues (Weinberg et al., 2007). The plasmid contains an independently located firefly luciferase reporter and an *HBx* sequence within the 3' UTR of a *Renilla* luciferase sequence, which makes *Renilla* a knockdown reporter for the *HBx* sequence.
Reporter plasmids	
pCI-neo-eGFP	The pCI-neo-eGFP plasmid was developed by Passman and colleagues (Passman et al., 2000). It contains an eGFP sequence under the control of the CMV IE promoter. In cultured cells the plasmid expresses eGFP protein which emits green fluorescence upon exposure to ultraviolet light. The pCI-neo-eGFP plasmid is a useful marker to assess transfection efficiencies.
mCherry (pAAV-minCMV-mCherry)	The pAAV-minCMV-mCherry plasmid was a gift from Feng Zhang (Addgene plasmid # 27970 ; http://n2t.net/addgene:27970 ; RRID:Addgene_27970). It contains a red fluorescent protein (RFP) sequence (Zhang et al., 2011). In cultured cells the plasmid produces RFP protein which emits red fluorescence upon exposure to ultraviolet light. The mCherry plasmid is a useful marker to assess transfection efficiencies.

pUCAsc-ISRE×3	The pUCAsc-ISRE×3 plasmid was a gift from Dr Ruben Hernandez Alcoceba (unpublished data). It has a firefly luciferase reporter sequence that is responsive to signalling from interferon proteins.
phRL-CMV	The phRL-CMV plasmid was purchased from Promega (Promega, WI, US). It has a *Renilla* luciferase reporter sequence that is constitutively expressed under the control of the CMV (cytomegalovirus) promoter.

Table 2.2: Description of the RNA used in this study.

CleanCap-eGFP	The CleanCap-eGFP mRNA was produced by TriLink Bio Technologies (TriLink Bio Technologies, CA, US). It was designed to mimic processed mature mRNA with a Cap1 structure and a poly(A) tail. The mRNA expresses an eGFP which makes it a useful marker to assess transfection efficiencies.
Poly I:C	Poly I:C is synthetic double-stranded RNA which consists of base pairs that induces immune stimulation.

2.1. Design of the pT7-pri-miR-31 expression vectors

The pT7-pri-miR-31 expression vectors were designed for use as templates to in vitro transcribe anti-HBV pri-miR-31 mimics that target the *HBx* region which is common to each of the viral transcripts. The pT7-pri-miR-31/5, pT7-pri-miR-31/8 and pT7-pri-miR-31/9 expression vectors were designed to generate monomeric pri-miR-31 mimics whereas the pT7-pri-miR-31/589 and pT7-pri-miR-31/895 expression vectors were designed to generate trimeric pri-miR-31 mimics (Figure 2.1). These expression vectors were designed to contain a CMV promoter, a T7 promoter, a 5' flanking region, a pri-miR-31 mimic encoding sequence, and a 3' flanking region with a poly(A) signal. The monomeric and trimeric pri-miR-31 mimic encoding sequences were obtained from pCMV-pri-miR-31 expression vectors and contain mature miRNA mimic regions flanked by naturally derived pri-miR-31 sequences. The pCMV-pri-miR-31 expression vectors were chosen specifically as they have previously demonstrated to be efficient at inhibiting HBV replication in vitro (Ely et al., 2009). These expression vectors contain a CMV promoter, a T7 promoter, a pri-miR-31 mimic encoding sequence and a poly(A) signal.

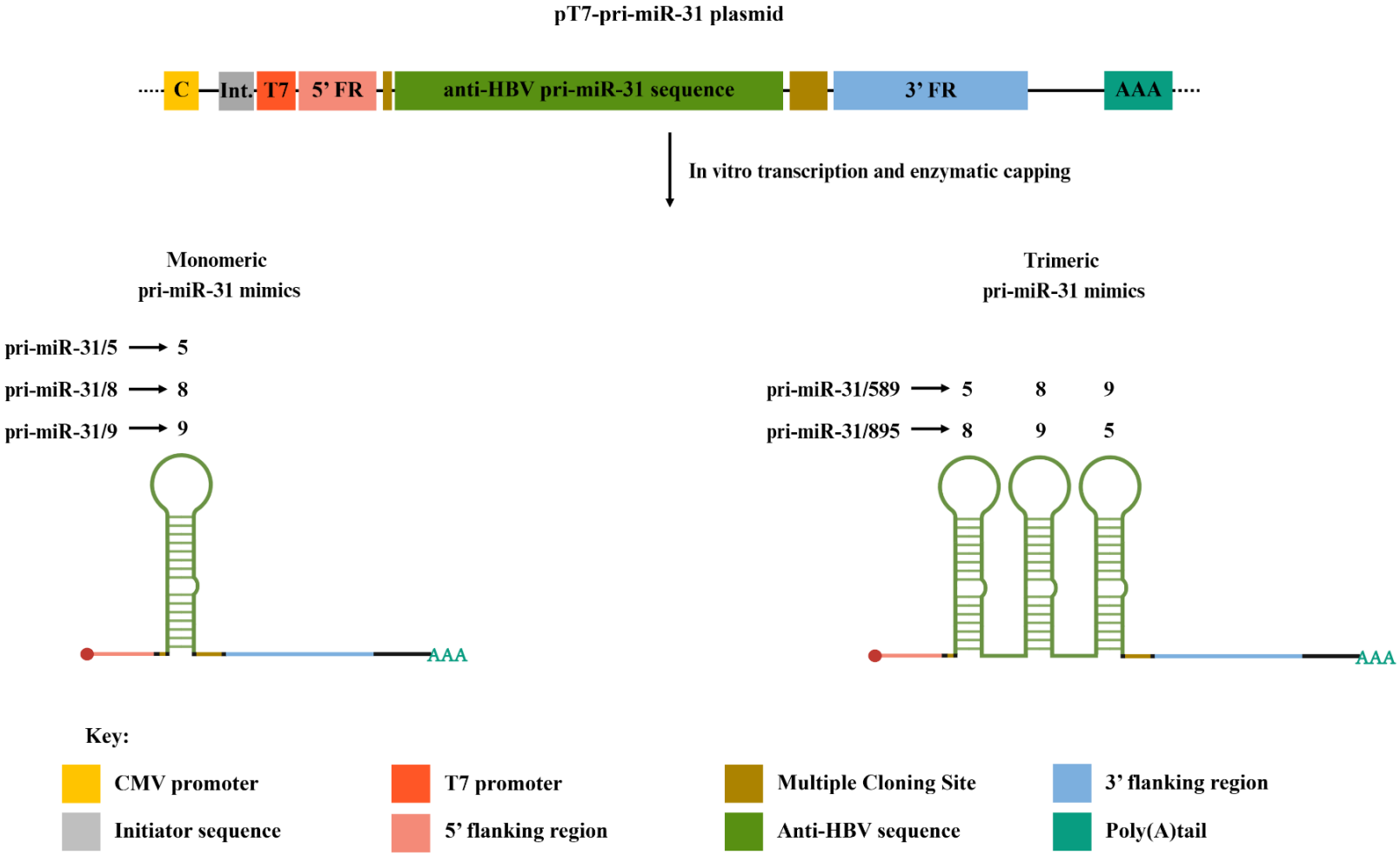


Figure 2.1: Design of the pT7-pri-miR-31 expression vectors. The pT7-pri-miR-31 expression vectors were designed for use as templates to in vitro transcribe anti-HBV pri-miR-31 mimics. The pT7-pri-miR-31/5, pT7-pri-miR-31/8 and pT7-pri-miR-31/9 expression vectors were designed to generate monomeric pri-miR-31 mimics whereas the pT7-pri-miR-31/589 and pT7-pri-miR-31/895 expression vectors were designed to generate trimeric pri-miR-31 mimics. These expression vectors were designed to contain a CMV promoter, a T7 promoter, a 5' flanking region (FR), a pri-miR-31 mimic encoding sequence, and a 3' flanking region with a poly(A) signal. This figure was created with BioRender.com.

2.2. Construction of the pT7-pri-miR-31 expression vectors

The pT7-pri-miR-31 expression vectors were constructed using conventional molecular cloning techniques (Figure 2.2 and 2.3). The pmRNA-CMV-pA plasmid backbone was ligated with a generated insert to create a pmRNA-CMV-T7-pA plasmid that was designed to in vitro transcribe mRNA. The pmRNA-CMV-T7-pA plasmid was constructed to function as a destination vector to allow a monomeric or trimeric pri-miR-31 mimic encoding sequence to be inserted. The monomeric and trimeric pri-miR-31 mimic encoding sequences were cleaved from pCMV-pri-miR-31 plasmids and were ligated into the pmRNA-CMV-T7-pA plasmid to generate the pT7-pri-miR-31 expression vectors.

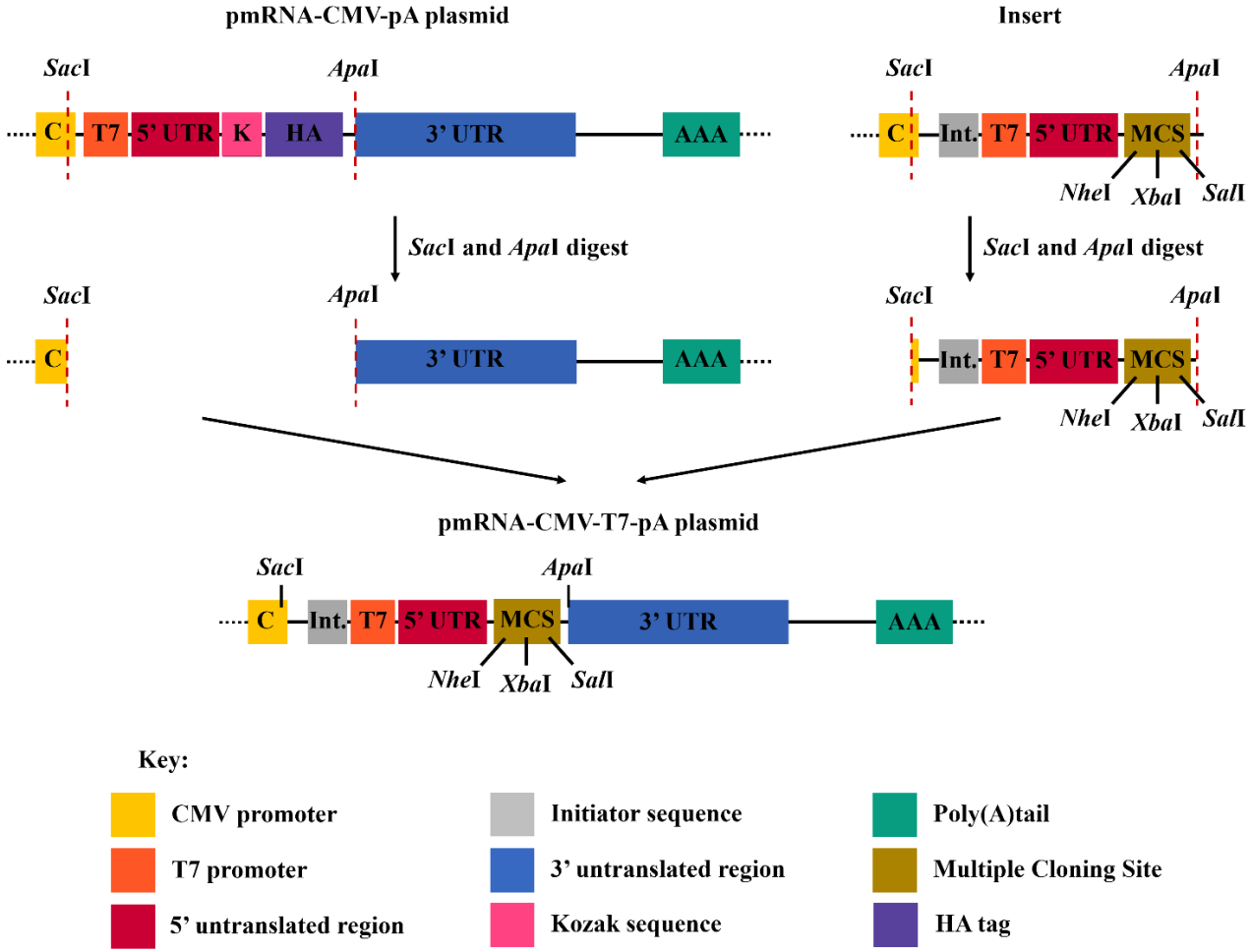


Figure 2.2: Construction of the pmRNA-CMV-T7-pA expression vector. The pmRNA-CMV-pA plasmid was digested with *Sac*I and *Apa*I restriction enzymes to remove the T7 promoter, 5' UTR, Kozak sequence and HA tag. A generated insert which consisted of a T7 promoter, 5' UTR and a multiple cloning site (MCS) containing *Nhe*I, *Xba*I and *Sal*I restriction sites was digested with *Sac*I and *Apa*I to create overhangs which are complementary to the overhangs of the pmRNA-CMV-pA plasmid backbone. The digested insert was ligated into the pmRNA-CMV-pA plasmid to create the pmRNA-CMV-T7-pA plasmid.

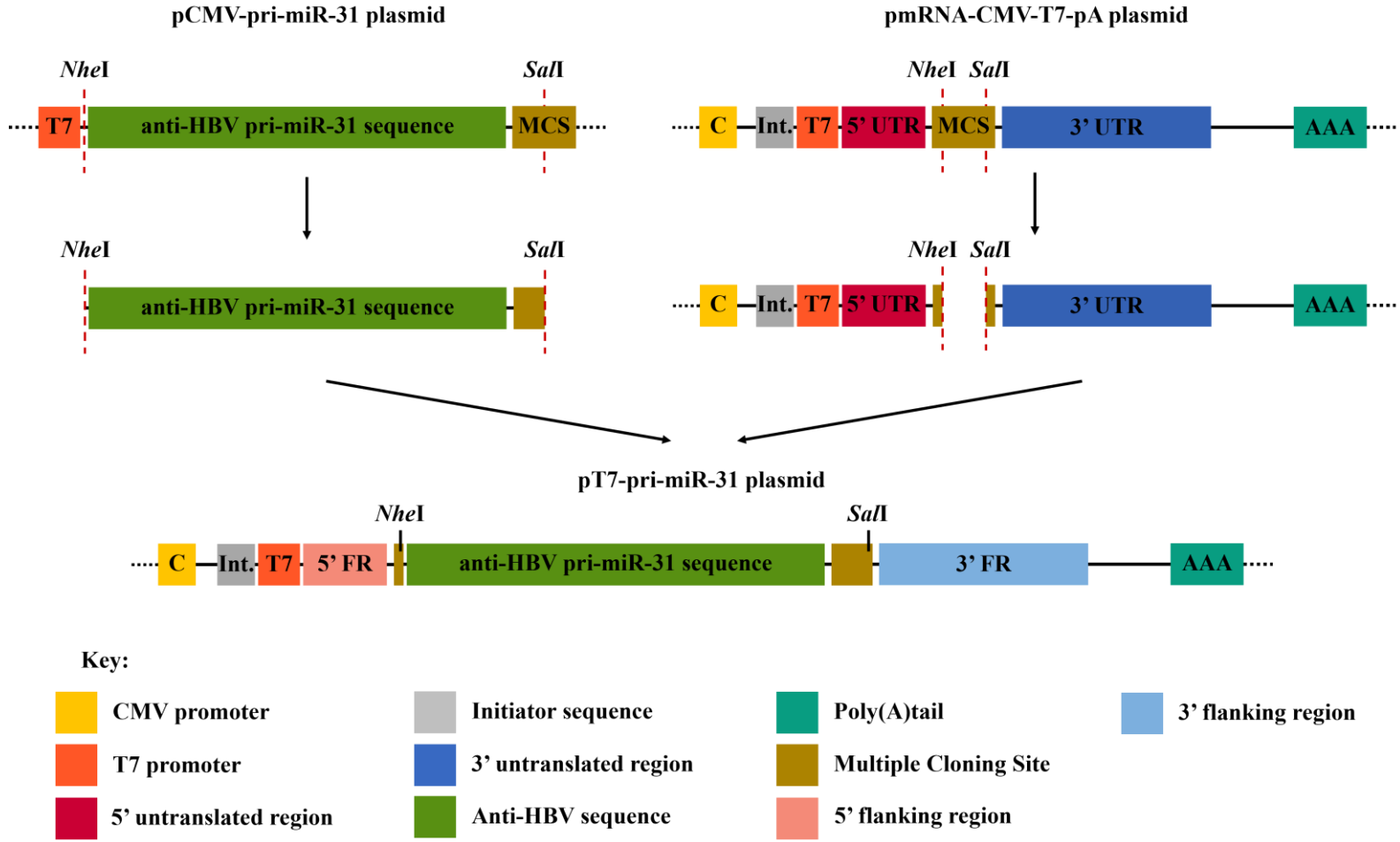


Figure 2.3: Construction of the pT7-pri-miR-31 expression vectors. The pCMV-pri-miR-31 plasmids were cleaved by *Nhe*I and *Sal*I restriction enzymes to release the pri-miR-31 mimic encoding region. The pmRNA-CMV-T7-pA plasmid was cleaved by *Nhe*I and *Sal*I restriction enzymes to create overhangs that are complementary to the overhangs of the pri-miR-31 encoding sequences. The mimic encoding sequences were inserted into the MCS of the pmRNA-CMV-T7-pA plasmid to generate the pT7-pri-miR-31 plasmids.

2.2.1. Generation of the double-stranded insert

Four oligonucleotides, F1, R1, F2 and R2 which were synthesised by phosphoramidite chemistry (Inqaba Biotechnology, South Africa) were used as primers to generate a double stranded insert in two separate PCRs (Figure 2.4 and Table 2.3). In the first PCR, the F1 and R1 primers which were designed to overlap at their 3' ends, were extended to synthesise the middle section of the insert. The reaction mix was prepared in duplicate by adding 500 pmol of F1, 500 pmol of R1, 25 µl of PCR Master Mix (2×) (Thermo Fisher Scientific, MA, US) and sterile water to a final volume of 50 µl, in each PCR tube. Two negative controls were included, one without R1 and the other without F1. Both controls were prepared by adding either 100 pmol of F1 or 100 pmol of R1, and 5 µl of PCR Master Mix (2×) (Thermo Fisher Scientific, MA, US) to a final volume of 10 µl with sterile water. The cycling conditions were set up according to the manufacturer's instructions with minor adjustments: initial denaturation at 95°C for 5 minutes, 34 cycles of denaturation at 95°C for 30 seconds, annealing at 48°C for 40 seconds, extension at 72°C for 30 seconds and a final extension at 72°C for 5 minutes. The PCR products were then resolved on a 2% agarose gel (Section 5.2.5). Thereafter, 45 µl of each product was added to 55 µl of sterile water and purified using the MinElute Gel Extraction kit (Qiagen, Germany) (Section 5.2.6). The purified PCR products were resolved on a 2% agarose gel (Section 5.2.5). In the second PCR, the F2 and R2 primers, which were designed to overlap the ends of the PCR product from the first PCR, were extended to create the complete insert. The reaction mix was prepared in duplicate by adding 50 ng of the purified PCR product, 10 pmol of F2, 10 pmol of R2, 25 µl of PCR Master Mix (2×) (Thermo Fisher Scientific, MA, US) and water to a final volume of 50 µl, in each PCR tube. A negative control was included without the PCR product. The cycling conditions were set up according to the manufacturer's instructions with minor adjustments: initial denaturation at 95°C for 5 minutes, 34 cycles of denaturation at 95°C for 30 seconds, annealing at 50°C for 40 seconds, extension at 72°C for 30 seconds and a final extension at 72°C for 5 minutes. The products from the second PCR were then resolved on a 2% agarose gel (Section 5.2.5). Thereafter, both reactions which contained the amplicons from the second PCR run were combined to a volume of 80 µl and purified using the MinElute Gel Extraction kit (Section 5.2.6). The resulting purified insert was resolved on a 2% agarose gel (Section 5.2.5).

Table 2.3: Primer sequences used to generate the double-stranded insert.

F1	5’- CAGATCTAATACGACTCACTATAGGGAAATAAGAGAGAAAAGAA -3’
F2	5’- GATCGAGCTCGTTTAGTGAACCGTCAGATCTAATACGACTCACT -3’
R1	5’- TCGCTAGCTATATTTCTTCTTACTCTTCTTTTCTCTCTTATTTC -3’
R2	5’- GATCGGGCCCGTCGACTCTAGAGATCGCTAGCTATATTTCTTCT -3’

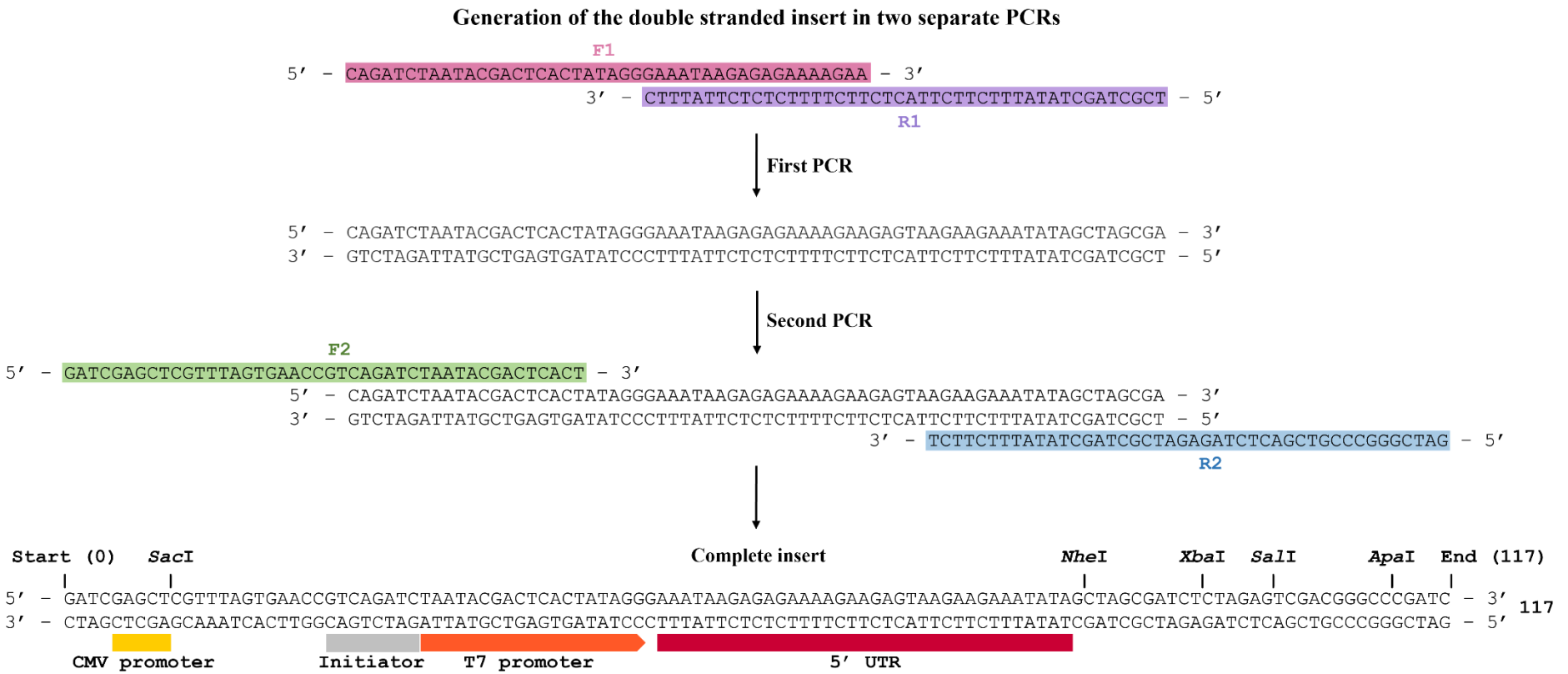


Figure 2.4: Generation of the complete double-stranded insert. The double-stranded insert was designed to contain a *Sac*I restriction site (located towards the start of the sequence), a T7 promoter, a 5' UTR, a MCS containing *Nhe*I, *Xba*I and *Sal*I restriction sites, and an *Apa*I restriction site (located towards the end of the sequence). The insert was generated in two separate PCR extension reactions. In the first PCR, the F1 and R1 primers which were designed to overlap at their 3' ends, were extended to synthesise the middle section of the insert. In the second PCR, the F2 and R2 primers, which were designed to overlap the ends of the PCR product from the first PCR, were extended to synthesise two strands with complementary 3' ends that were annealed and further extended to generate the complete insert.

2.2.2. Isolation of the double-stranded insert

The purified insert was ligated into the pGEM®-T Easy vector at a 1:3, 1:5 and 1:8 vector to insert molar ratio using the pGEM®-T Easy vector system according to the manufacturer's instructions (Promega, WI, US). Each ligation reaction was prepared by adding 5.82, 9.70 or 15.52 ng of the purified insert, 1 µl of pGEM®-T Easy Vector (50 ng), 5 µl of 2× Rapid ligation buffer, 1 µl of T4 DNA Ligase and sterile water to a final volume of 10 µl. A negative control was included which did not contain the purified insert. The ligation mixes were incubated at room temperature for 1 hour. Thereafter, 50 µl of chemically competent *E. coli* was transformed with 2 µl of each ligation mix and plated on a single ampicillin positive Luria Bertani agar plate supplemented with 8 µl of IPTG (100 mg/ml) and 40 µl of X-gal (20 mg/ml) (Section 5.1). Selected colonies were each inoculated into 4 ml of Luria Bertani medium supplemented with 4 µl of ampicillin (100 µg/ml) and incubated overnight at 37℃ with shaking at 150 rpm. Following incubation, the plasmids were isolated using the EconoSpin^{TM} All-in-One Mini Spin Columns (Epoch Life Science, TX, US) (Section 5.2.2). The plasmids were screened using *Pvu*II in a single digestion reaction and *Sac*I and *Apa*I in a double digestion reaction (Section 5.2.4 and 5.2.5). The clones which contained the correct sized insert were sequenced using the M13F(-20) primer (5'-GTAAAACGACGGCCAGT-3') (Inqaba Biotechnology, South Africa). Following sequencing analysis, the plasmids which possessed the correct insert sequence were digested with *Apa*I and *Pst*I simultaneously and resolved on a 2% agarose gel (Section 5.2.4 and 5.2.5). The plasmids were then propagated and purified at large scale (Section 5.1 and 5.2.1). Thereafter, the plasmids were screened, and a selected positive clone was digested with *Apa*I and *Sac*I and assessed by agarose gel electrophoresis (Section 5.2.4 and 5.2.5). The 103 bp fragments which denoted the insert were then isolated and resolved on an agarose gel (Section 5.2.6 and 5.2.5).

2.2.3. Isolation of the pmRNA-CMV-pA plasmid backbone

The pmRNA-CMV-pA plasmid was double digested with *Sac*I and *Apa*I to separate the T7 promoter, 5′ UTR region, Kozak sequence and HA tag from the plasmid backbone (Figure 2.2 and Section 5.2.4). The digested samples were then resolved on a 1% agarose gel and the 3 632 bp bands which indicated the pmRNA-CMV-pA plasmid backbone were excised from the gel and purified using the MinElute Gel Extraction Kit (Qiagen, Germany) (Section 5.2.5 and Section 5.2.6). Following purification, the plasmid backbone was quantified by spectrophotometry and visualised on a 0.8% agarose gel (Section 5.2.5).

2.2.4. Ligation of the isolated insert into the pmRNA-CMV-pA plasmid backbone

The purified insert was ligated into the pmRNA-CMV-pA backbone at a 1:3, 1:6 and 1:12 vector to insert molar ratio to create the pmRNA-CMV-T7-pA plasmid using the T4 DNA ligase kit according to the manufacturer's instructions (New England Biolabs, MA, US). Each ligation reaction was prepared by adding 5.11, 10.22 or 20.44 ng of the purified insert, 50 ng of the pmRNA-CMV-pA backbone, 2 µl of T4 DNA Ligase Buffer (10×), 1 µl of T4 DNA Ligase and sterile water to a final volume of 20 µl. A negative control was included which did not contain the purified insert. The reaction mixes were incubated at room temperature for 1 hour and heat inactivated at 65℃ for 10 minutes. Thereafter, 50 µl of chemically competent *E. coli* was transformed with 5 µl of each ligation mix and plated on a single ampicillin positive agar plate (Section 5.1). Selected transformed colonies were each inoculated into 4 ml of Luria Bertani medium supplemented with 4 µl of ampicillin (100 µg/ml) and incubated overnight at 37℃ with shaking at 150 rpm. Following incubation, the plasmids were isolated using the small-scale high yield plasmid prep protocol and visualised on a 1% agarose gel (Section 5.2.3 and 5.2.5). The isolated plasmids were then screened on a 1% agarose gel after digestion with *Bsh*NI (Section 5.2.4 and 5.2.5). The pmRNA-CMV-pA plasmid was also digested with *Bsh*NI and included as a control. The clones which produced the correct size bands were digested with *Sal*I and *NheI* and resolved on a 1% agarose gel to ensure that the enzymes were able to recognise these specific restriction sites (Section 5.2.4 and 5.2.5). Thereafter, the positive clones were propagated, purified at large scale, and visualised on an agarose gel (Section 5.1, 5.2.1 and 5.2.5). The plasmids were then screened, and a selected positive clone was digested with *NheI* and purified by ethanol precipitation before visualisation on an agarose gel (Section 5.2.5, 5.2.4 and 5.2.7). The clone was then digested with *Sal*I and resolved on an agarose gel before the 3719 bp band of interest was isolated and assessed by agarose gel electrophoresis (Section 5.2.4, 5.2.5 and 5.2.6).

2.2.5. Identification of the pCMV-pri-miR-31 plasmids and isolation of the pri-miR-31 encoding sequences

The pCMV-pri-miR-31 plasmids were propagated, purified at large scale, and screened by restriction enzyme digestion and sequencing analysis (Section 5.1, 5.2.1 and 5.2.4). The band of interest was isolated from the positive clones by digestion with *NheI* and *Sal*I and the purified sequences were assessed by agarose gel electrophoresis (Section 5.2.4, 5.2.7, 5.2.6 and 5.2.5).

2.2.6. Ligation of the pri-miR-31 sequences into the pmRNA-CMV-T7-pA plasmid

The isolated pri-miR-31 sequences were ligated into the pmRNA-CMV-T7-pA plasmid at a 1:3, 1:6 and 1:12 vector to insert molar ratio in a 20 µl reaction volume according to the manufacturer's instructions (New England Biolabs, MA, US). Each reaction was prepared by adding 15.08, 30.16 or 60.32 ng of the monomeric pri-miR-31 sequence, or 42.03, 84.06 or 168.12 ng of the trimeric pri-miR-31 sequence, 50 ng of the pmRNA-CMV-T7-pA plasmid, 2 µl of T4 DNA Ligase Buffer (10×), 1 µl of T4 DNA Ligase and sterile water to a final volume of 20 µl. A negative control was included without the insert. The reaction mixes were incubated at room temperature for 1 hour and heat inactivated at 65 ℃ for 10 minutes. Thereafter, 50 µl of chemically competent *E. coli* was transformed with 5 µl of each ligation mix and plated on a single ampicillin positive agar plate (Section 5.1). Selected transformed colonies were each inoculated into 10 ml of Luria Bertani medium supplemented with 10 µl of ampicillin (100 µg/ml) and incubated overnight at 37℃ with shaking at 150 rpm. The plasmids were then isolated using the EconoSpin™ All-in-One Mini Spin Columns (Epoch Life Science, TX, US) and visualised on a 1% agarose gel (Section 5.2.2 and 5.2.5). Thereafter, the plasmids were screened with *Nsb*I and *Bsh*NI separately on a 1% agarose gel (Section 5.2.4 and 5.2.5). The generated monomeric expression vectors with the correct size bands were sequenced using the T7 (5'-AATACGACTCACTATAG-3') and M13-R (5'-CAGGAAACAGCTATGAC-3') primers whereas the generated trimeric expression vectors with the correct size bands were sequenced using the T7 (5'-AATACGACTCACTATAG-3') primer (Inqaba Biotechnology, South Africa). Following sequencing analysis, the plasmids were propagated, purified at large scale, and screened by restriction enzyme digestion (Section 5.1, 5.2.1 and 5.2.4).

2.3. RNA synthesis, purification, and analysis

2.3.1. In vitro transcription

The pmRNA-CMV-eGFP-pA, pT7-pri-miR-31/5, pT7-pri-miR-31/8, pT7-pri-miR-31/9, pT7-pri-miR-31/589 and pT7-pri-miR-31/895 plasmids were digested with the *Bpi*I restriction enzyme and assessed by agarose gel electrophoresis to ensure linearisation (Section 5.2.4 and 5.2.5). The linearised plasmids were then purified by ethanol precipitation and resolved on an agarose gel to assess the integrity of the constructs after purification (Section 5.2.7 and 5.2.5). Thereafter, the linearised plasmids were used as templates to in vitro transcribe the eGFP, pri-miR-31/5, pri-miR-31/8, pri-miR-31/9, pri-miR-31/589 and pri-miR-31/895 RNA respectively. In vitro transcriptions were performed using the TranscriptAid T7 High Yield Transcription Kit (Thermo Fisher Scientific, MA, US) according to the manufacturer's

instructions. Each reaction was prepared by adding nuclease-free water, 4 µl of 5× TranscriptAid reaction buffer, 8 µl of ATP/CTP/GTP/UTP mix, 1 µg of template DNA and 2 µl of TranscriptAid enzyme mix in this specified order to a final volume of 20 µl with nuclease-free water. The mixture was briefly centrifuged then incubated at 37ºC for 2 hours. Thereafter, 1 µl of DNase was added and the mixture was incubated at 37ºC for a further 15 minutes. The in vitro transcribed RNA constructs were then purified with lithium chloride and resolved on a formaldehyde gel (Section 5.3.1).

2.3.2. Capping of in vitro transcribed RNA

In vitro transcribed RNA was capped using the Vaccinia Capping System (New England Biolabs, MA, US), according to the manufacturer's instructions. Briefly, 10 µg of RNA was combined with nuclease-free water to a final volume of 15 µl. The solution was heated at 65ºC for 5 minutes then transferred to ice for an additional 5 minutes. Thereafter, the RNA solution was mixed with 2 µl of 10× capping buffer, 1 µl of GTP (10 mM), 1 µl of SAM (2 mM) and 1 µl of vaccinia capping enzyme. The mixture was incubated at 37ºC for 30 minutes. The capped in vitro transcribed RNA constructs were then purified by lithium chloride and assessed on a formaldehyde gel to assess the integrity of the constructs (Section 5.3.1).

2.3.3. Cellulose purification of in vitro transcribed RNA

The study performed by Baiersdörfer and colleagues described a cellulose-based method to remove contaminating dsRNA from *in vitro* transcribed mRNA (Baiersdörfer et al., 2019). The method was followed according to the authors instructions with a few adjustments. Briefly, 1 ml of chromatography buffer was added to 0.2 g of cellulose powder (Sigma-Aldrich, MO, US) and incubated at room temperature with shaking at ~250 rpm for 10 minutes. Seven hundred microliters of the cellulose mixture was then added to an ultrafiltration spin column and centrifuged at 14 000 ×g for 1 minute. The flow-through was discarded and 500 µl of chromatography buffer was added to the column and incubated at room temperature with shaking at ~250 rpm for 5 minutes. Thereafter, the column was centrifuged at 14 000 ×g for 1 minute before the flow through was discarded and the column was transferred into a sterile microcentrifuge tube. One hundred micrograms of *in vitro* transcribed RNA was then added to chromatography buffer to a final volume of 500 µl. The mixture was added to the spin column and incubated at room temperature with shaking at ~250 rpm for 30 minutes. Thereafter, the tube was centrifuged at 14 000 ×g for 1 minute before the resulting flow through was added back into the spin column. The tube was then incubated at room temperature with shaking at ~250 rpm for 30 minutes before it was

centrifuged at 14 000 ×g for 1 minute. Following centrifugation, the RNA suspension was purified by lithium chloride precipitation (Section 5.3.1).

2.3.4. Capillary gel electrophoresis

RNA fragments were analysed using either the Agilent 2100 Bioanalyzer System (Agilent, CA, US) or the Agilent 5200 Fragment Analyzer System (Agilent, CA, US). The Agilent 2100 Bioanalyzer System (Agilent, CA, US) was used with the Agilent RNA 6000 Nano Kit (Agilent, CA, US) according to the manufacturer's instructions where 1 µl (100 ng/µl) of the prepared RNA samples were loaded. The Agilent 5200 Fragment Analyzer System (Agilent, CA, US) was used with the Agilent DNF-471 RNA Kit (15 nt) (Agilent, CA, US) according to the manufacturer's instructions where 2 µl (25 ng/µl) of the denatured RNA samples were loaded.

2.4. Tissue culture

2.4.1. Culturing conditions for mammalian cells

Liver-derived HepG2-hNTCP cells and kidney derived Hek293T cells were maintained in T-75 culture flasks (Thermo Fisher Scientific, MA, US) with 15 ml of growth medium. The flasks were left to incubate in a humidified incubator at 37ºC with 5% CO_2. HepG2-hNTCP cells were maintained in Dulbecco′s Modified Eagle′s Medium/F-12 (DMEM/F12) (Life Technologies, CA, US) supplemented with penicillin (200 U/ml), streptomycin (200 µg/ml), HEPES (10 mM), hydrocortisone (50 µM), insulin (5 µg/ml), G418 (400 µg/ml) and FBS (10%). Hek293T cells were maintained in high glucose Dulbecco's Modified Eagle Medium (DMEM) (Life Technologies, CA, US) supplemented with penicillin (100 U/ml), streptomycin (100 µg/ml) and FBS (10%). The confluency of the cell cultures was monitored regularly under a confocal light microscope (Olympus, Japan).

2.5. Transfection assays and expression analysis

2.5.1. Transfection of mammalian cell lines

HepG2-hNTCP cells and Hek293T cells were transfected using either the Lipofectamine™ 3000 Reagent kit (Thermo Fisher Scientific, MA, US) or the Lipofectamine™ MessengerMAX™ Reagent (Thermo Fisher Scientific, MA, US). The lipid and lipofectamine mix for either of the transfection reactions were prepared according to the size of the culture plate in which the cells were seeded. The prepared mixes were incubated at room temperature for 5 minutes then combined and incubated further at room temperature for 20 minutes. The combined mixture was added to the seeded cells and the plate was left to incubate in a humidified incubator at 37ºC with 5% CO_2. The tables below indicate the reagents and their respective volumes used per well to perform the transfection reactions.

Table 2.4: Transfection mixes using the Lipofectamine™ 3000 kit.

	DNA-lipid complex mix per well				Lipofectamine mix per well	
Culture plate	**DNA or RNA**	**P3000**	**Opti-MEM**	**sterile water**	**Lipofectamine 3000**	**Opti-MEM**
48-well	100-500 ng	0.5-1 µl	20 µl	to 25 µl	0.15-0.75 µl	to 25 µl
10 cm^2	10 µg	20 µl	450 µl	to 500 µl	30 µl	to 500 µl

Table 2.5: Transfection mixes using the Lipofectamine™ MessengerMAX™ Reagent.

	RNA-lipid complex mix per well			Lipofectamine mix per well	
Culture plate	**RNA**	**Opti-MEM**	**Nuclease-free water**	**Lipofectamine MessengerMAX**	**Opti-MEM**
48-well	100-500 ng	20 µl	to 25 µl	0.75 µl	to 25 µl
10 cm^2	10 µg	450 µl	to 500 µl	30 µl	to 500 µl

2.5.2. Enzyme-linked immunosorbent assay (ELISA)

The level of HBsAg in the harvested cell culture media was measured with an ELISA using the Monolisa™ HBs Ag ULTRA kit (Bio-Rad, CA, US), according to the manufacturer's instructions. Briefly, 100 µl of each sample was distributed into the wells of the pre-coated microplate. Thereafter, 50 µl of conjugate solution was added to the samples and gently mixed. The plate was covered with adhesive film and incubated at 37ºC for 1 hour and 30 minutes. Thereafter, the wells were washed four times with the diluted washing solution (1×) using the Immuno Wash™ 1575 Microplate Washer (Bio-Rad, CA, US). Next, 100 µl of enzyme development solution was added to each well and the plate was incubated in the dark for 30 minutes at room temperature. Following incubation, 100 µl of stopping solution was added to each well and mixed to stop the reaction. The plate was then incubated at room temperature for 4 minutes before the optical density of the samples were measured at 490 and 655 nm using the iMARK Microplate Reader (Bio-Rad, CA, US).

2.5.3. Dual-luciferase assay

The Dual-Luciferase® Reporter Assay System (Promega, WI, USA) was used to assess firefly and *Renilla* luciferase expression. Briefly, the culture medium was removed from the growing cells and 65 µl of 1× PLB was added to each well of the 48-well plate. Thereafter, the plate was gently rocked at room temperature for 15 minutes before 10 µl of each sample was distributed into a 96-well plate. Next, 50 µl of LAR II was added per well and the firefly

luciferase activity was measured using the GloMax® Explorer Multimode Microplate Reader (Promega, WI, USA). Thereafter, 50 µl of Stop & Glo® Reagent was added to each sample and the *Renilla* luciferase activity was measured.

2.5.4. Trizol RNA extraction

The total RNA was extracted from the cells using the TRIzol™ Reagent (Thermo Fisher Scientific, MA, US) according to the manufacturer's instructions. Briefly, the medium was removed from the culture plate and the appropriate volume of TRIzol™ Reagent (1 ml = 1 volume) was added and mixed until the solution was homogenised. The lysate was then incubated at room temperature for 5 minutes before 0.2 volumes of chloroform was added. The solution was mixed and incubated at room temperature for 3 minutes. Thereafter, the mixture was centrifuged at 12 000 ×g for 15 minutes at 4ºC before the upper aqueous phase was transferred to a sterile microcentrifuge tube and combined with 0.5 volumes of isopropanol. The mixture was then incubated at 4ºC for 10 minutes then centrifuged at 12 000 ×g for a further 10 minutes. The supernatant was discarded, and the pellet was resuspended in 1 volume of 75% ethanol before the resuspension was briefly mixed and centrifuged at 7500 ×g at 4ºC for 5 minutes. Following centrifugation, the supernatant was discarded, and the pellet was air-dried for 5 minutes. The pellet was resuspended in the appropriate volume of nuclease-free water before the suspension was heated at 60ºC for 15 minutes. The total extracted RNA was then stored at -80ºC.

2.5.5. Collagen coating culture plates

Tissue culture 48-well plates were coated using the Collagen I (Rat Tail) solution (Gibco, MT, USA). The thin coating procedure was followed according to the manufacturer's instructions. Briefly, the Collagen I solution (3 mg/ml) (Gibco, MT, USA) was diluted in 20 mM of acetic acid to a final concentration of 50 µg/ml. Thereafter, 125 µl of the solution was added to each well of the microwell plate. The plate was incubated in the dark at room temperature for 1 hour before the solution was removed, and the wells were washed three times with 125 µl of complete DMEM/F12.

2.6. Assessment of the constructed pT7-pri-miR-31 expression vectors

2.6.1. Assessment of HBV inhibition by the pT7-pri-miR-31 expression vectors

Two days prior to transfection, HepG2-hNTCP cells were seeded in a 48-well plate at a density of 60%. On the day of transfection, the growth medium from each well was replaced and the cells were transfected with 50 ng of pCH-9/3091 (target), 50 ng of pCI-neo-eGFP (marker) and 400 ng of pCI-neo (negative control), pCMV-pri-miR-31/5, pCMV-pri-miR-31/8, pCMV-pri-miR-31/9, pCMV-pri-miR-31/589, pCMV-pri-miR-31/895, pmRNA-CMV-

pA (negative control), pT7-pri-miR-31/5**,** pT7-pri-miR-31/8, pT7-pri-miR-31/9, pT7-pri-miR-31/589, T7-pri-miR-31/895 or pTZ57R (negative control). The pCMV-pri-miR-31 plasmids were chosen specifically as they have previously demonstrated to be effective at inhibiting HBV replication in vitro (Ely et al., 2009). The pCI-neo, pmRNA-CMV-pA and pTZ57R plasmids were used as negative controls as they were not expected to reduce HBsAg expression. pCI-neo and pmRNA-CMV-pA were chosen specifically as they contain the backbone of the pCMV-pri-miR-31 and pT7-pri-miR-31 plasmids respectively. pTZ57R was chosen as an additional negative control as it does not contain a backbone common to the other plasmids. The transfections were performed in triplicate using the Lipofectamine™ 3000 kit (Thermo Fisher Scientific, MA, US) where 0.75 µl of Lipofectamine™ 3000 Reagent and 1 µl of P3000 was used per well (Section 2.5.1). Three wells which were left untreated served as an untransfected control. Two days after transfection, the cells were analysed by fluorescence microscopy and the culture medium was harvested and assessed by performing an ELISA (Section 2.5.2).

2.7. Assessment of the in vitro transcribed pri-miR-31 mimics

2.7.1. Assessment of HBV inhibition by the pri-miR-31 mimics

The ability of the pri-miR-31 mimics to inhibit HBsAg prior to cellulose purification was assessed by performing an ELISA. One day prior to transfection, HepG2-hNTCP cells were seeded in a 48-well plate at a density of 70%. On the day of transfection, the growth medium from each well was replaced and the cells were transfected with 50 ng of pCH-9/3091 as the target, 50 ng of mCherry as the marker, and three wells that were left untreated served as the untransfected control. The transfections were performed using the Lipofectamine™ 3000 kit (Thermo Fisher Scientific, MA, US) where 0.15 µl of Lipofectamine™ 3000 Reagent and 1 µl of P3000 was used per well (Section 2.5.1). One day after transfection, the growth medium from each well was replaced and the cells were transfected with 500 ng of pri-miR-31/5, pri-miR-31/8, pri-miR-31/9, pri-miR-31/589, pri-miR-31/895, eGFP (negative control) or CleanCap-eGFP (negative control) RNA. The transfections were performed in triplicate using the Lipofectamine™ MessengerMAX™ Reagent (Thermo Fisher Scientific, MA, US) (Section 2.5.1). One day after RNA transfection, the cells were analysed by fluorescence microscopy, and the culture medium was harvested and assessed by performing an ELISA (Section 2.5.2).

The ability of the pri-miR-31 mimics to inhibit HBsAg following cellulose purification was assessed by performing an ELISA, as previously described, with the following adjustments. Two days prior to transfection, a collagen coated plate was seeded at a density of 60%. On the

day of transfection, the cells were transfected with pCH-9/3091 as the target and mCherry as the marker, and the cells that were only transfected with pCH-9/3091 and mCherry served as the mock control. One day after RNA transfection, the cells were analysed by fluorescence microscopy and the culture medium was harvested for assessment with an ELISA (Section 2.5.2). The growth medium from each well was replaced and the plate was incubated in a humidified incubator at 37ºC with 5% CO_2. Two days after RNA transfection, the cells were analysed by fluorescence microscopy and the culture medium was harvested and assessed by performing an ELISA (Section 2.5.2).

The evaluation of specific HBV inhibition by the pri-miR-31 mimics following cellulose purification was assessed by performing dual-luciferase assays. The transfection procedures were performed as previously described in this section, with the following adjustments. One day prior to transfection, two collagen coated plates were seeded at a density of 70%. On the day of transfection, the cells were transfected with psiCHECK-HBx as the target and mCherry as the marker, and the cells that were transfected with only psiCHECK-HBx and mCherry served as the mock control. One day after RNA transfection, the cells were analysed by fluorescence microscopy and one of the plates was assessed by a dual-luciferase assay (Section 2.5.3). Two days after RNA transfection, the remaining plate was analysed and assessed by a dual-luciferase assay (Section 2.5.3).

2.7.2. Investigation of cellular cytotoxicity by the pri-miR-31 mimics

An 3-(4,5-dimethylthiazol-2-yl)-2,5-diphenyltetrazolium (MTT) assay was performed to determine cytotoxicity of the pri-miR-31 mimics in Hek293T cells after transfection. Two days prior to transfection, Hek293T cells were seeded at a confluency of 40% in a 96-well plate. On the day of transfection, the cells were transfected with 100 ng of pri-miR-31/5, pri-miR-31/8, pri-miR-31/9, pri-miR-31/589, pri-miR-31/895, eGFP (negative control) or CleanCap-eGFP (negative control). The transfection reactions were performed in triplicate using the Lipofectamine™ MessengerMAX™ Reagent (Section 2.5.1). The cells that were treated with the transfection mixture alone served as the mock control. The cells that were treated with 125 µl of 1% Triton X-100 served as a positive control and cells that were left untreated served as the untransfected control. One day after transfection, the cells were analysed by fluorescence microscopy and 20 µl of MTT solution (5 mg/ml, in 1× PBS) was added into each well. The plate was gently mixed by shaking for 5 minutes and allowed to incubate at 37ºC with 5% CO_2 for 1 hour. Following incubation, the culture medium was removed, and the formazan product was resuspended in 200 µl of DMSO. Thereafter, 50 µl of

each sample was diluted in 50 µl of saline and the optical densities were measured at a ratio of 570 nm to 655 nm using the iMARK™ microplate absorbance reader (Bio-Rad, CA, US).

2.7.3. Evaluation of interferon response by the pri-miR-31 mimics

A dual-luciferase assay was performed to evaluate the immune response produced by Hek293T cells after transfection with the pri-miR-31 mimics. One day prior to transfection, Hek293T cells were seeded in a 48-well plate at a density of 45%. On the day of transfection, the cells were transfected with 50 ng of phRL-CMV, 50 ng of pUCAsc-ISRE×3 and 100 ng of pri-miR-31/5, pri-miR-31/8, pri-miR-31/9, pri-miR-31/589, pri-miR-31/895, eGFP (negative control), CleanCap-eGFP (negative control) or poly I:C (positive control). The transfections were performed in triplicate using the Lipofectamine™ 3000 kit (Thermo Fisher Scientific, MA, US) where 0.15 µl of Lipofectamine™ 3000 Reagent and 0.5 µl of P3000 was used per well (Section 2.5.1). The cells that were transfected with only phRL-CMV and pUCAsc-ISRE×3 served as the mock control. Two days after transfection, the cells were analysed by fluorescence microscopy and the ratio of firefly to *Renilla* expression was measured (Section 2.5.3).

Reverse transcription quantitative PCR (RT-qPCR) assays were performed to evaluate the immune response produced by Hek293T cells after transfection with the pri-miR-31 mimics. One day prior to transfection, Hek293T cells were seeded in a 24-well plate at a density of 45%. On the day of transfection, the cells were transfected with 500 ng of pri-miRNA-31/5, pri-miRNA-31/8, pri-miRNA-31/9, pri-miRNA-31/589, pri-miRNA-31/895, eGFP (mock control), CleanCap-eGFP (negative control) or poly I:C (positive control). The transfection reactions were performed in triplicate using the Lipofectamine™ MessengerMAX™ Reagent (Section 2.5.1). Three wells which were left untreated served as an untransfected control. One day after transfection, the cells were analysed by fluorescence microscopy and the total RNA was extracted from the cells using 300 µl of Trizol® Reagent (Thermo Fisher Scientific, MA, US) per well (Section 2.5.4). The extracted RNA was then used as templates in the following RT-qPCRs to quantify the amount of *GAPDH*, *IFN-β*, *OAS1* and *MxA* mRNA that was produced. The RT-qPCRs were performed using the Luna® Universal One-Step RT-qPCR Kit (New England Biolabs, MA, US) according to the manufacturer's instructions. Briefly, each reaction contained 5 µl of Luna Universal One-Step Reaction Mix (2×), 0.5 µl of Luna WarmStart® RT Enzyme Mix (20×), 0.4 µl of the relevant forward primer (10 µM), 0.4 µl of the relevant reverse primer (10 µM), 1 µl of undiluted template RNA (<500 ng) and nuclease-free water to a final volume of 10 µl. The cycling conditions were as follows: reverse transcription at 55°C for 10 minutes, initial denaturation at 95°C for 1 minute, 44 cycles of

denaturation at 95°C for 10 seconds, extension at 60°C for 30 seconds (plate read) and melting from 65°C to 95°C at increments of 0.5°C for 5 seconds (plate read at each temperature increment). These conditions were carried out by the CFX96 Touch™ Real-Time PCR Detection System (Bio-Rad, CA, US).

Table 2.6: Primer sequences used to amplify the genes of interest.

Primer name	**Primer sequence**
GAPDH forward	5'-GAAGGTGAAGGTCGGAGTC-3'
GAPDH reverse	5'-GAAGATGGTGATGGGATTTC-3'
IFN-β forward	5'-TCCAAATTGCTCTCCTGTTGTGCT-3'
IFN-β reverse	5'-CCACAGGAGCTTCTGACACTGAAAA-3'
OAS1 forward	5'-CGAGGGAGCATGAAAACACATTT-3'
OAS1 reverse	5'-GCAGAGTTGCTGGTAGTTTATGAC-3'
MxA forward	5'-CTGGTGCTGAAACTGAAGAAAC-3'
MxA reverse	5'-ATCTCAATCTCGTAGTCCTGGTA-3'

2.8. Assessment of pri-miR-31 processing

2.8.1. Transfection and total RNA extraction

One day prior to transfection, Hek293T cells were seeded in 10 cm^2 plates at a density of 45%. On the day of transfection, the cells were transfected with 10 µg of eGFP or pri-miR-31/5 using the Lipofectamine™ MessengerMAX™ Reagent (Thermo Fisher Scientific, MA, US), or 10 µg of pCMV-pri-miR-31/5 using the Lipofectamine™ 3000 kit (Thermo Fisher Scientific, MA, US) (Section 2.5.1). One day after transfection, the cells that were transfected with eGFP or pri-miR-31/5 were analysed by fluorescence microscopy and the total RNA was extracted using 1 ml of Trizol reagent per plate (Section 2.5.4). Two days after transfection, the cells that were transfected with pCMV-pri-miR-31/5 were analysed and the total RNA was extracted using the same procedure (Section 2.5.4).

2.8.2. Radioactive labelling

A DNA probe which was designed to bind the miR-31/5 sequence was radioactively labelled and purified in a single Sephadex column for use during hybridisation to detect the RNA of interest. Six DNA oligonucleotides of different lengths were radioactively labelled in separate reactions and purified in a single Sephadex column to generate a molecular weight ladder to estimate the size of the RNA produced after gel electrophoresis. The probe and oligonucleotides were radioactively labelled with T4 PNK according to the manufacturer's instructions (New England Biolabs, MA, US). Each reaction was prepared by adding 2.5 µl of

DNA (10 pmol), 2.5 µl of T4 PNK Reaction Buffer (10×), 0.5 µl of [γ-^{32}P] ATP (3000 Ci/mmol) (PerkinElmer, MA, US), 1 µl of T4 PNK and nuclease-free water to a final volume of 25 µl. The samples were then incubated at 37 ºC for 30 minutes. Sephadex columns were prepared to purify the labelled oligonucleotides from the unincorporated nucleotides. The radioactively labelled samples were added into the syringe and centrifuged at 2000 rpm for 2 minutes.

2.8.3. Polyacrylamide gel electrophoresis (PAGE)

A 20% denaturing polyacrylamide gel solution was prepared by mixing 15.2 g of acrylamide, 0.8 g of bisacrylamide, 40 g of urea and 8 ml of 10× TBE buffer to a final volume of 80 ml with sterile water. The solution was heated in a hot water bath until the urea completely dissolved. Thereafter, 30 µl of TEMED and 300 µl of 10% APS was added. The solution was then briefly mixed, poured into the gel casting system and allowed to solidify. The samples were prepared by combining 15 µl of RNA loading dye (2×) (New England Biolabs, MA, US), 40 µg of total RNA extracted from the cells that were transfected with either eGFP, pri-miR-31/5 or pCMV-pri-miR-31/5, and nuclease-free water to a final volume of 30 µl (Section 2.8.1). The ladder was prepared by adding 10 µl of RNA loading dye (2×) (New England Biolabs, MA, US), 6 µl of the radioactively labelled molecular ladder, and nuclease-free water to a final volume of 20 µl (Section 2.8.2). The mixes were then heated at 95ºC for 5 minutes and placed on ice. The prepared ladder and samples were loaded into the wells of the gel and left to run at 300 V until the bromophenol dye reached the bottom of the gel.

2.8.4. Staining, blotting and UV crosslinking

The gel was stained in 200 ml of 0.5× TBE buffer supplemented with 8 µl of ethidium bromide. Thereafter, electroblotting was performed and the system was left to run at 0.49 A for 30 minutes to allow the RNA to transfer from the gel onto the nylon membrane. The transferred RNA was then fixed onto the membrane using the Ultraviolet Crosslinker system (UVP, CA, US). Following crosslinking, the ladder was cut out and separated from the RNA samples.

2.8.5. Hybridisation, stringency washing and visualisation

The UV crosslinked membrane containing the ladder was enclosed in plastic film and placed in a cassette with an imaging plate. The cassette was stored at room temperature in the dark to expose for a day. The plate was then imaged using the FLA-7000 imaging system (Fujifilm, Tokyo, JP). The UV crosslinked membrane containing the RNA samples was inserted into a small glass hybridisation cylinder with 10 ml of PerfectHyb Plus buffer (Sigma-Aldrich, MO, US). The cylinder was then left to incubate at 45ºC for 5 minutes with rotation. Following

incubation, 1 ml of the buffer was removed and combined with 25 µl of the radioactively labelled probe. The entire volume was then added into the cylinder and left to incubate at 45 ºC overnight with rotation. Following overnight incubation, the buffer was discarded, and the membrane was washed twice with 25 ml of pre-warmed low stringency wash buffer. The membrane was then incubated twice with 25 ml of pre-warmed low stringency wash buffer at 25 ºC for 5 minutes with rotation. Thereafter, the membrane was washed twice with 25 ml of pre-warmed high stringency wash buffer at 42 ºC for 20 minutes with rotation. The membrane was then enclosed in plastic film and placed in a cassette with an imaging plate. The cassette was stored at room temperature in the dark to expose for a week. The plate was then imaged using the FLA-7000 imaging system (Fujifilm, Japan).

CHAPTER 3

3. RESULTS

3.1. Successful construction of the pT7-pri-miR-31 expression vectors

3.1.1. Generation of the double-stranded insert

The double-stranded insert was generated by four oligonucleotides in two separate PCRs (Figure 2.4). In the first PCR, the F1 and R1 primers were expected to anneal at their 3' ends and extend to synthesise the middle section of the insert. To determine whether the middle section of the insert was synthesised after the first PCR, the resulting PCR products were resolved on an agarose gel (Figure S2a). Following visualisation, the reactions which contained both the F1 and R1 primers resulted in a single band of 69 bp as expected. The negative control reactions both resulted in a faint band however this can be attributed to the large size of the primers as well as the considerable amount of primer that was added to each reaction. These results suggested that the middle section of the insert was successfully synthesised after the first PCR. Following synthesis, the products were purified, and resolved on an agarose gel to assess the integrity of the constructs. The purified products were visualised and a single band of 69 bp was shown, which indicated that the constructs remained intact after purification (Figure S2b).

In the second PCR, the F2 and R2 primers were expected to anneal to the ends of the PCR product from the first PCR and extend to create the complete insert. To confirm that the complete insert was synthesised after the second PCR, the PCR products were resolved on an agarose gel. The products produced bands of 117 bp as expected (Figure S2c). Thereafter, the products were combined and purified simultaneously, and resolved on an agarose gel to assess the integrity of the construct after purification. The purified product produced a single band of 117 bp as expected which confirmed the integrity of the synthesised insert after purification (Figure 3.1).

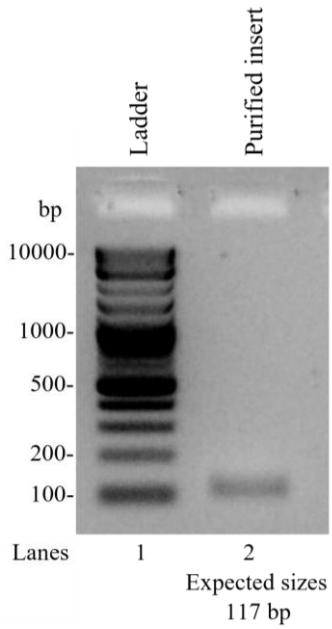


Figure 3.1: Double-stranded insert after generation and purification. The double-stranded insert was generated in two separate PCR extension reactions. The products from the second PCR were purified and resolved on a 2% agarose gel to assess the integrity of the construct after purification. Lane 1: 1 kb plus DNA ladder (New England Biolabs, MA, US). Lane 2: purified insert.

3.1.2. PCR cloning of the double-stranded insert

The purified insert was ligated into the pGEM®-T Easy vector to create the pG-insert and the subsequent clones were screened by restriction enzyme digestion and sequencing analysis to identify the plasmids with the correct insert sequence (Figure S3, S4 and S5). The clones were screened with *Pvu*II in a single digestion reaction and *Sac*I and *Apa*I in a double digestion reaction (Figure S4a and S4b). The results indicated that clones 2, 5, 6 and 7 contained the correct size insert. Thereafter, clones 5 and 6 were chosen and sequenced to confirm that the insert contained the correct sequence. The sequencing data obtained was aligned against the design sequence (Figure S5). The results revealed discrepancies within the *Apa*I site of both clones however this was a confirmatory screen. The results obtained previously from the *Sac*I and *Apa*I digestion reactions already demonstrated that the *Apa*I sites were intact (Figure S4b). The plasmids were then screened with *Apa*I and *Pst*I simultaneously to confirm whether the *Apa*I restriction enzyme was able to recognise the *Apa*I cleavage site (Figure S6a). These results demonstrated that clones 5 and 6 contained the correct sequence of interest from the *Apa*I site to the *Sac*I site. The clones were then propagated, purified, and screened before clone 5 was chosen and digested with *Apa*I and *Sac*I simultaneously to separate the insert from the vector and to create overhangs that were compatible with the overhangs of the pmRNA-CMV-pA plasmid backbone (Figure S6b and S7). The digestion reaction resulted in

two expected bands of 3031 and 103 bp, and one band which may have been as a result of co-migration of the expected 55 and 56 bp fragments (Figure S7). The 103 bp bands which denoted the insert were excised, purified, and resolved on an agarose gel to assess integrity. Following agarose gel electrophoresis, a single band of 103 bp was observed as expected which indicated that the insert remained intact after purification (Figure 3.2).

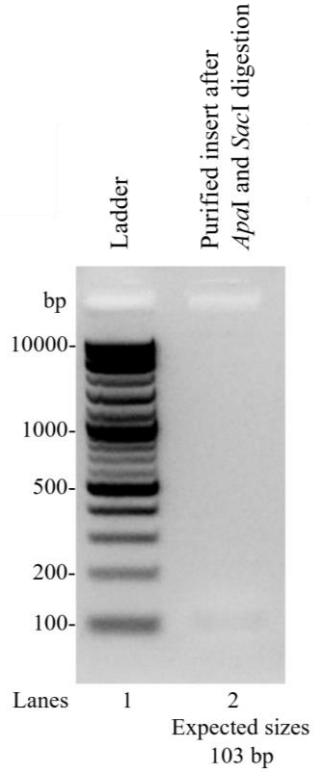


Figure 3.2: Purified insert with *Sac*I and *Apa*I overhangs. Clone 5 which contained the correct insert sequence was digested with *Apa*I and *Sac*I simultaneously. The 103 bp band which denoted the insert was extracted from the gel, purified, and resolved on an agarose gel to assess the integrity of the construct after purification. Lane 1: 1 kb plus DNA ladder (New England Biolabs, MA, US). Lane 2: purified insert with *Sac*I and *Apa*I overhangs.

3.1.3. Preparation of the pmRNA-CMV-pA plasmid backbone

The pmRNA-CMV-pA plasmid was double digested with *Sac*I and *Apa*I restriction enzymes and resolved across several lanes on an agarose gel to separate the 3632 bp plasmid backbone from the 124 bp unwanted sequence (Figure 3.3a). The correct size bands were observed and the 3632 bp bands that represented the plasmid backbone were extracted from the gel and purified. Following purification, the integrity of the pmRNA-CMV-pA backbone was assessed by agarose gel electrophoresis. As expected, a single band of 3632 bp was produced which confirmed that the pmRNA-CMV-pA plasmid backbone remained intact after purification (Figure 3.3b).

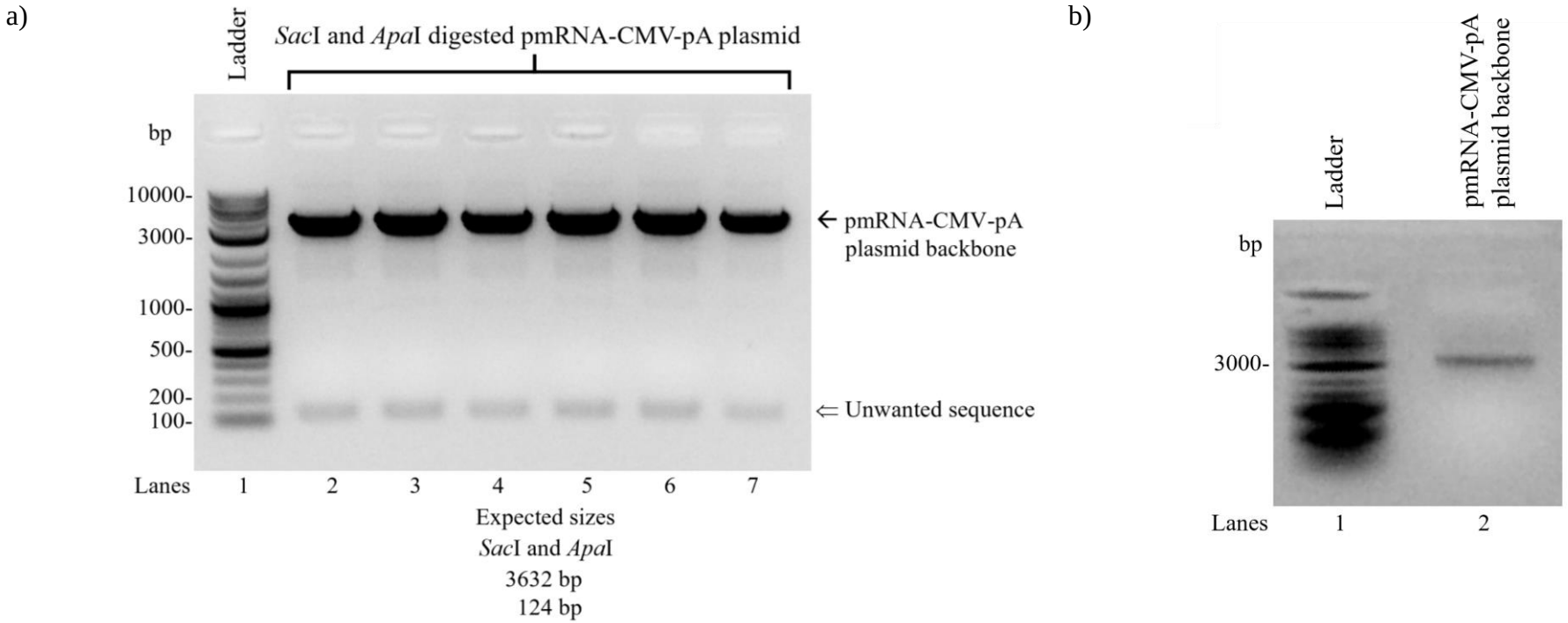


Figure 3.3: Preparation of the pmRNA-CMV-pA plasmid backbone. (a) The pmRNA-CMV-pA plasmid was double digested with *Sac*I and *Apa*I to separate the plasmid backbone from the unwanted sequence. Lane 1: 1 kb plus DNA ladder (New England Biolabs, MA, US). Lanes 2 to 7: *Sac*I and *Apa*I digested pmRNA-CMV-pA plasmid. The single lined arrow depicts the 3632 bp pmRNA-CMV-pA plasmid backbone and the double lined arrow shows the 124 bp unwanted sequence. The fragments were resolved on a 1% agarose gel and the bands depicting the pmRNA-CMV-pA plasmid backbone were excised from the agarose gel and purified. (b) The integrity of the purified pmRNA-CMV-pA plasmid backbone was assessed on a 0.8% agarose gel. Lane 1: 1 kb plus DNA ladder (New England Biolabs, MA, US). Lane 2: purified pmRNA-CMV-pA plasmid backbone.

3.1.4. Ligation of the isolated insert into the pmRNA-CMV-pA plasmid backbone

The isolated insert was ligated into the pmRNA-CMV-pA backbone to create the pmRNA-CMV-T7-pA plasmid and the subsequent clones were screened by restriction enzyme digestion to identify the positive clones (Figure 2.2 and Figure S8). The clones were screened with *Bsh*NI (Figure S9). Thereafter, the chosen plasmids were screened with *Sal*I and *Nhe*I separately to ensure that these enzymes were able to recognise these specific restriction sites (Figure S10). These clones were then screened after propagation and purification (Figure S11 and S12). The results obtained indicated that clones 3 and 6 were positive clones. Thereafter, clone 3 was chosen and sequentially digested with *NheI* and *Sal*I (Figure S16 and S18). The 3719 bp band of interest was excised from the gel, purified, and resolved on a gel to assess the integrity of the construct (Figure 3.4). Following agarose gel electrophoresis, a single band of 3719 bp was produced which indicated that the plasmid remained intact after purification.

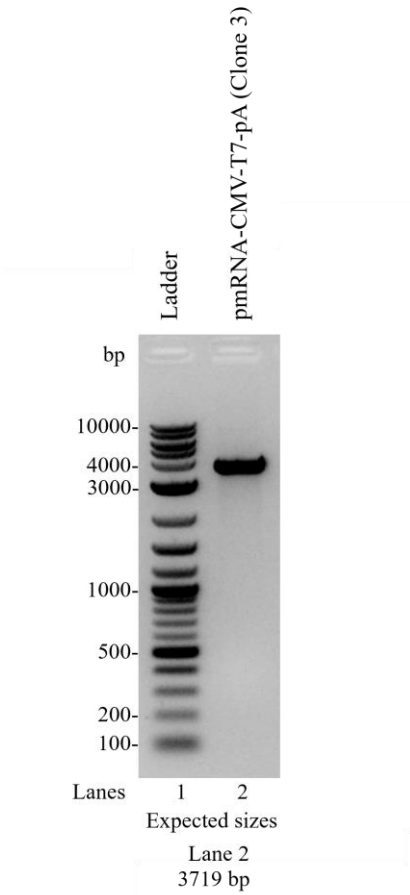


Figure 3.4: Purified pmRNA-CMV-T7-pA plasmid with *Nhe*I and *Sal*I overhangs. The pmRNA-CMV-T7-pA plasmid was digested with *NheI* and *Sal*I and the band of interest was excised, purified, and resolved on a 1% agarose gel to assess integrity. Lane 1: 1 kb plus DNA ladder (New England Biolabs, MA, US). Lane 2: pmRNA-CMV-T7-pA plasmid with *NheI* and *Sal*I overhangs.

3.1.5. Identification of the pCMV-pri-miR-31 plasmids and isolation of the pri-miR-31 encoding sequences

The identities of the pCMV-pri-miR-31 plasmids were confirmed by restriction enzyme digestion and sequencing analysis (Figure S13, S14 and S15). The confirmed plasmids were sequentially digested with *Nhe*I and *Sal*I to separate the pri-miR-31 encoding sequence from the rest of the plasmid (Figure S16, S17 and S18). The 187 bp bands produced by the monomeric expression vectors and 521 bp bands produced by the trimeric expression vectors which represented the pri-miR-31 encoding sequences, were excised from the gel, purified, and assessed by agarose gel electrophoresis (Figure S17 and S18). The results indicated that the pri-miR-31 encoding sequences were successfully isolated from the pCMV-pri-miR-31 expression vectors (Figure 3.5).

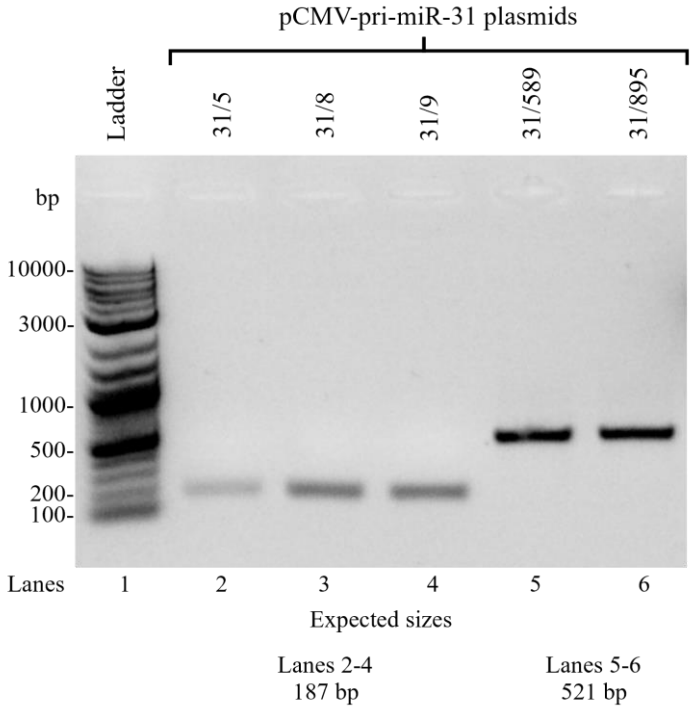


Figure 3.5: Isolated pri-miR-31 encoding sequences. The pri-miR-31 encoding sequences were isolated from the pCMV-pri-miR-31 expression vectors and resolved on a 1% agarose gel. Lane 1: 1 kb plus DNA ladder (New England Biolabs, MA, US). Lanes 2 to 6: isolated pri-miR-31 encoding sequences.

3.1.6. Ligation of the pri-miR-31 sequences into the pmRNA-CMV-T7-pA plasmid

The isolated pri-miR-31 sequences were ligated into the pmRNA-CMV-T7-pA plasmid to generate the pT7-pri-miR-31 plasmids (Figure S19). Thereafter, the plasmids were screened with *Nsb*I and *Bsh*NI separately to identify the positive clones (Figure S20 and S21). The results obtained confirmed that each of the clones contained the correct size insert. The clones were propagated, purified, and visualised on an agarose gel to assess integrity (Figure S22). The plasmids were then screened with *Bsh*NI and *Nsb*I separately to confirm the identity of the plasmids after propagation (Figure 3.6). Following agarose gel electrophoresis, the plasmids produced the correct band sizes as expected which confirmed the identity of the pT7-pri-miR-31 expression vectors.

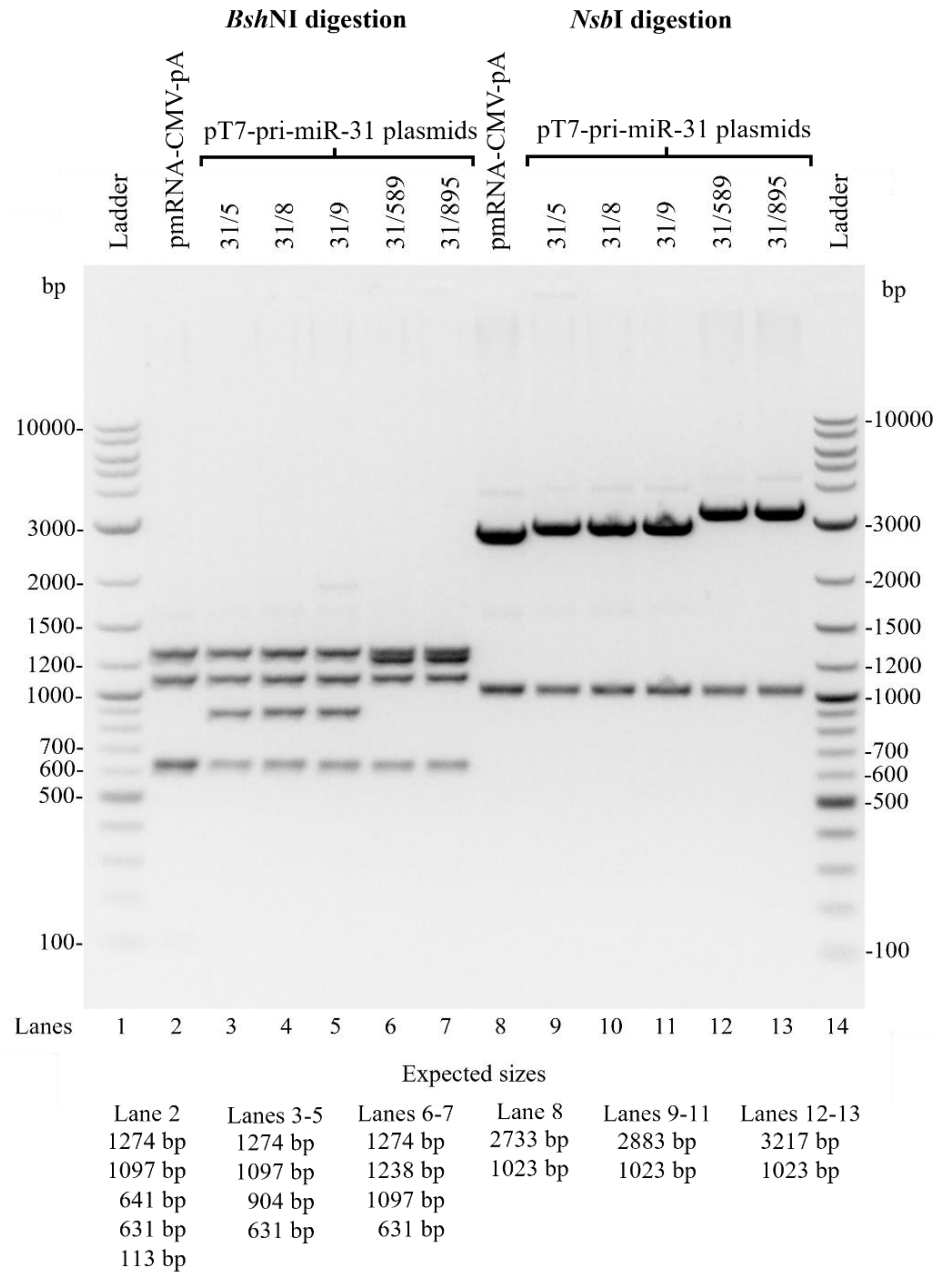


Figure 3.6: Identification of the generated pT7-pri-miR-31 expression vectors. The positive pT7-pri-miR-31 clones were screened with *Bsh*NI and *Nsb*I to confirm the identity of the plasmids after propagation. Lane 1 and 14: 1 kb plus DNA ladder (New England Biolabs, MA, US). Lane 2: pmRNA-CMV-pA plasmid digested with *Bsh*NI. Lanes 3 to 7: pT7-pri-miR-31 plasmids digested with *Bsh*NI. Lane 8: pmRNA-CMV-pA plasmid digested with *Nsb*I. Lanes 9 to 13: pT7-pri-miR-31 plasmids digested with *Nsb*I.

3.2. Assessment of the pT7-pri-miR-31 expression vectors

3.2.1. pT7-pri-miR-31 expression vectors inhibit HBV replication

To determine whether the constructed pT7-pri-miR-31 plasmids were able to inhibit HBV replication, the amount of HBsAg produced after transfection was measured by performing an ELISA (Figure 3.7). The cells were transfected with the pCH-9/3091 plasmid as the target and the pCI-neo-eGFP plasmid as the marker. GFP expression was consistent throughout each well transfected with the pCI-neo, pCMV-pri-miR-31 and pT7-pri-miR-31 plasmids, which indicated equivalent transfection efficiencies (Figure S23). The cells that were transfected with either of the pCMV-pri-miR-31 plasmids demonstrated a reduction in HBsAg when compared to the cells that were transfected with pCI-neo. The pCMV-pri-miR-31/5, pCMV-pri-miR-31/8, pCMV-pri-miR-31/9, pCMV-pri-miR-31/589 and pCMV-pri-miR-31/895 plasmids demonstrated a 79.1%, 50.9%, 55.0%, 83.8% and 84.9% knockdown respectively with p-values <0.01. The cells that were transfected with either of the pT7-pri-miR-31 plasmids demonstrated a reduction in HBsAg when compared to the cells that were transfected with pmRNA-CMV-pA. The pT7-pri-miR-31/5, pT7-pri-miR-31/8, pT7-pri-miR-31/9, pT7-pri-miR-31/589 and pT7-pri-miR-31/895 plasmids demonstrated a 63.1%, 42.8%, 23.2%, 70.7% and 70.7% knockdown respectively with p-values <0.01. These results indicated that the design of the pT7-pri-miR-31 plasmids were suitable to in vitro transcribe functional pri-miR-31 mimics.

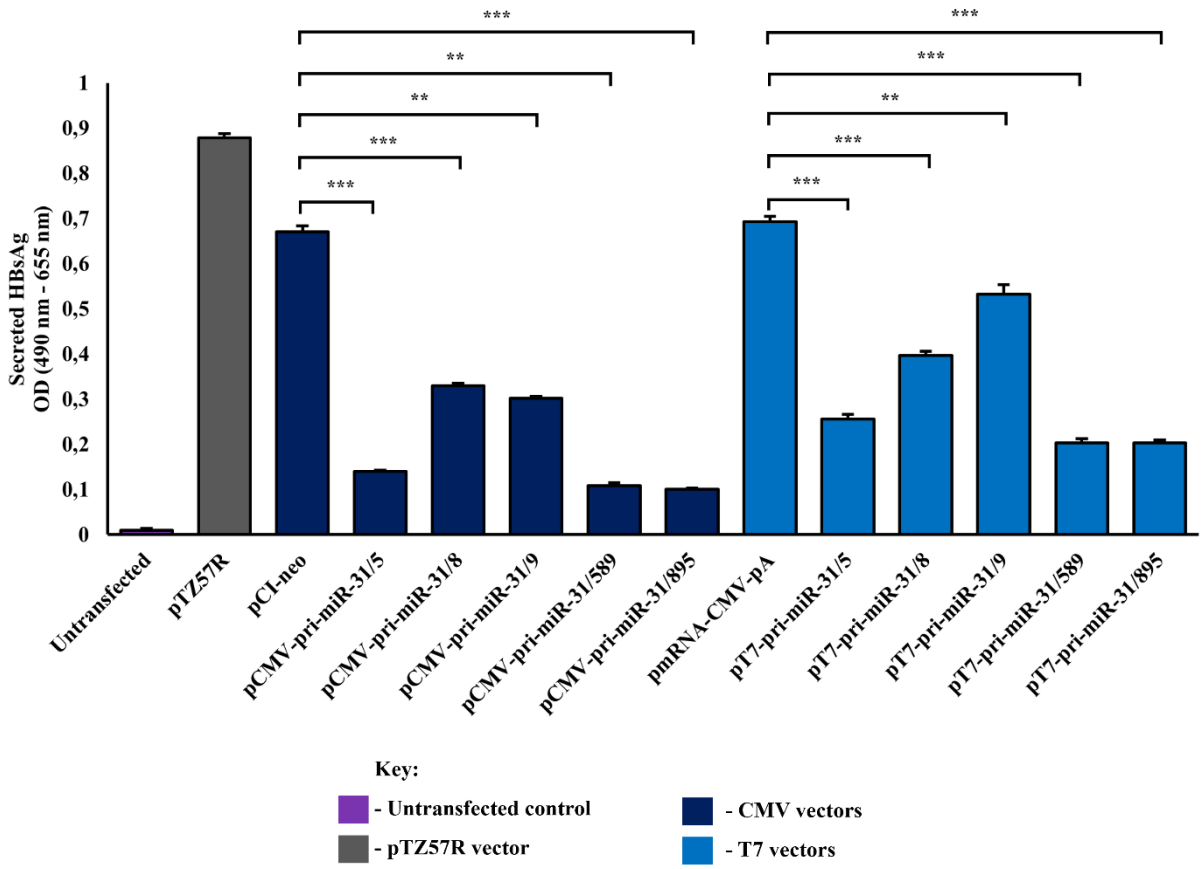


Figure 3.7: Assessment of HBV replication inhibition by the pCMV-pri-miR-31 and pT7-pri-miR-31 expression vectors by performing an ELISA. HepG2-hNTCP cells were transfected with pCH-9/3091 (target), pCI-neo-eGFP (marker) and an experimental plasmid which either contains the pri-miR-31 sequence (pCMV-pri-miR-31 plasmid or pT7-pri-miR-31 plasmid) or does not contain the pri-miR-31 sequence (pTZ57R, pCI-neo or pmRNA-CMV-pA). HBsAg expression was assessed two days after transfection by performing an ELISA. The graphs were plotted using the mean and the error bars indicate the standard error of the mean (SEM) (n=3). The statistical significance was calculated using the student's paired two-tailed t-test (*** indicates $p<0.001$ and ** indicates $p<0.01$).

3.3. Assessment of the pri-miR-31 mimics

3.3.1. pri-miR-31 mimics induce non-specific silencing and modestly inhibit HBV replication

The pmRNA-CMV-eGFP-pA and pT7-pri-miR-31 plasmids were digested with *Bpi*I and assessed by agarose gel electrophoresis to ensure linearisation (Figure S24a). The digested plasmids were then purified by ethanol precipitation and resolved on an agarose gel to analyse the integrity of these constructs after purification (Figure S24b). The linearised plasmids were then used as templates to in vitro transcribe the eGFP mRNA and pri-miR-31 mimics. The in vitro transcribed RNAs were purified with lithium chloride and resolved on a formaldehyde gel to assess the integrity of these constructs (Figure 3.8a). The RNAs were then either capped or cellulose purified prior to capping before these constructs were purified by LiCl precipitation, and assessed by formaldehyde gel electrophoresis (Figure 3.8b, 3.9a and 3.9b). The results obtained indicated that the in vitro transcribed eGFP mRNA and pri-miR-31 mimics were suitable for assessment in vitro.

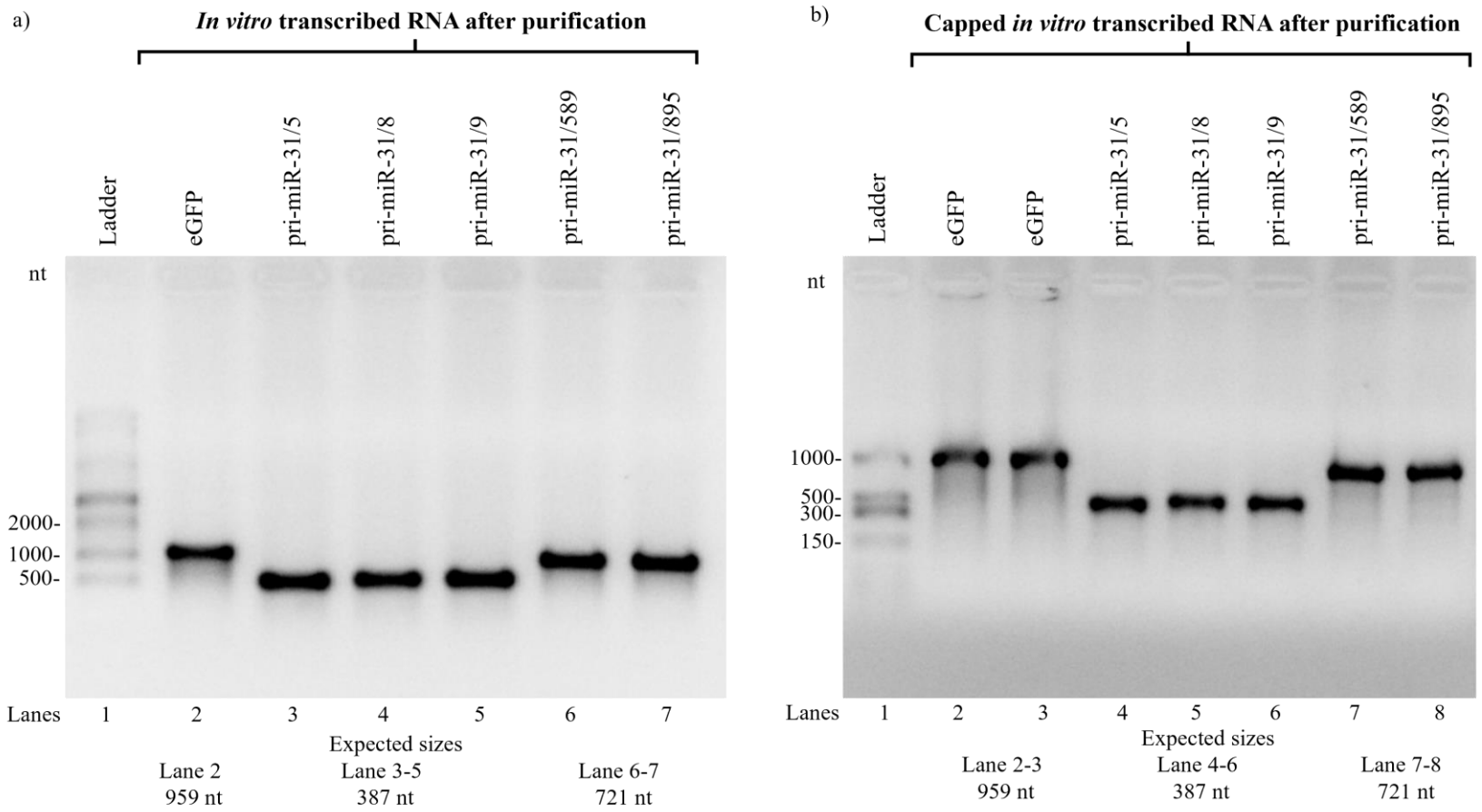


Figure 3.8: In vitro transcribed RNA before and after capping. (a) The linearised pmRNA-CMV-eGFP-pA and pT7-pri-miR-31 plasmids were in vitro transcribed, and the RNA produced was purified by lithium chloride and resolved on a 1% formaldehyde gel to assess the integrity of the constructs after purification. Lane 1: ssRNA ladder (New England Biolabs, MA, US). Lane 2: In vitro transcribed eGFP RNA after purification. Lane 3 to 7: In vitro transcribed pri-miR-31 mimics after purification (b) The in vitro transcribed RNA was capped, purified by lithium chloride, and assessed on a 2% formaldehyde gel to assess integrity. Lane 1: Low Range ssRNA ladder (New England Biolabs, MA, US). Lane 2 to 3: capped eGFP RNA after purification. Lane 4 to 7: capped pri-miR-31 mimics after purification.

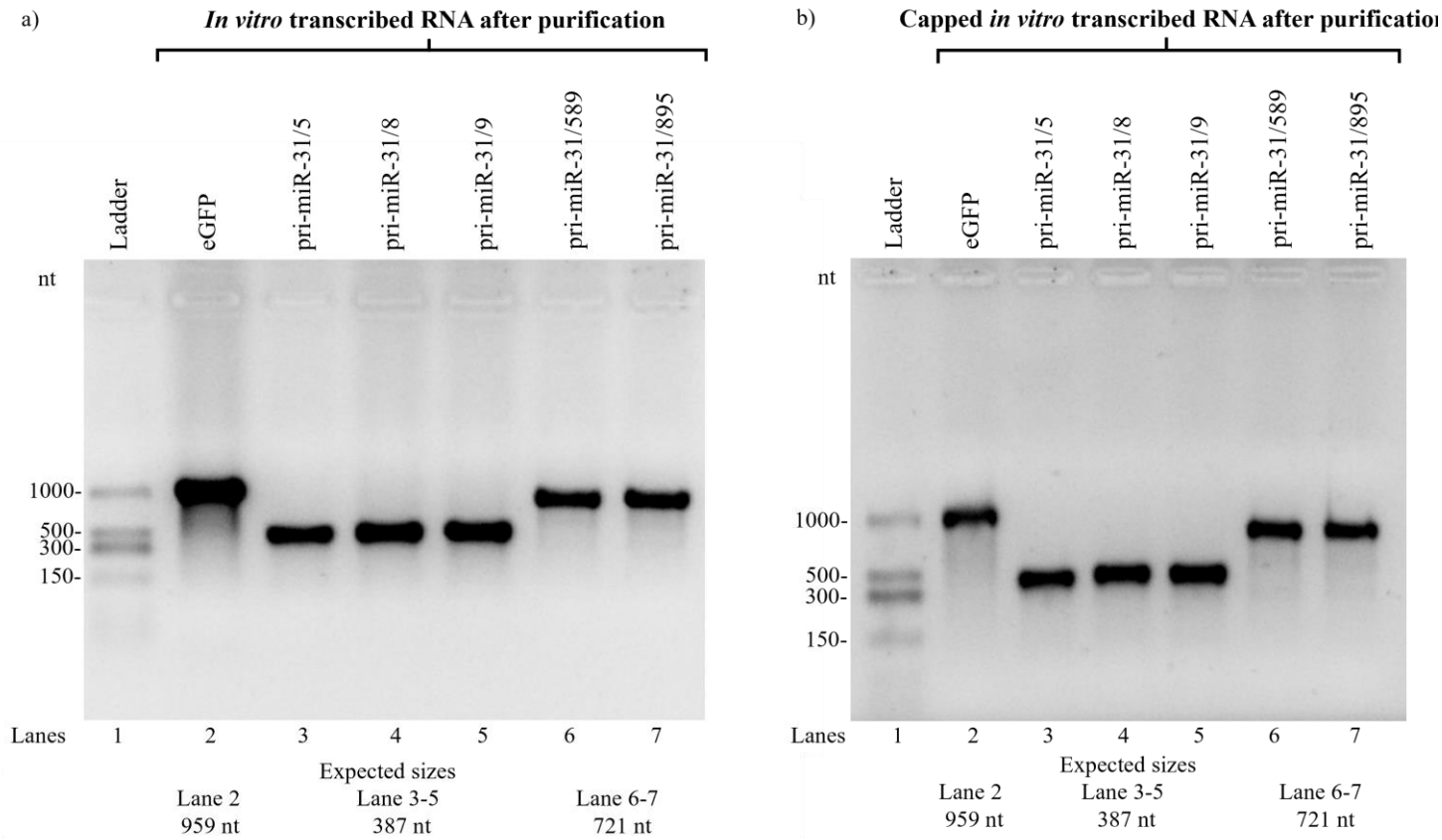


Figure 3.9: Cellulose purified in vitro transcribed RNA before and after capping. (a) The in vitro transcribed RNA produced was purified by cellulose and resolved on a 2% formaldehyde gel to assess the integrity of the constructs after purification. Lane 1: Low Range ssRNA ladder (New England Biolabs, MA, US). Lane 2: eGFP RNA after purification. Lane 3 to 7: pri-miR-31 RNA after purification. (b) The purified in vitro transcribed RNA was capped, purified by lithium chloride, and assessed on a 2% formaldehyde gel to assess the integrity of the constructs after purification. Lane 1: Low Range ssRNA ladder (New England Biolabs, MA, US). Lane 2: capped eGFP RNA after purification. Lane 3 to 7: capped pri-miR-31 RNA after purification.

To determine whether the pri-miR-31 mimics were able to inhibit HBV replication prior to cellulose purification, the amount of HBsAg produced after treatment was measured by performing an ELISA one day after treatment (Figure 3.10). The cells were transfected with the pCH-9/3091 plasmid as the target and the mCherry plasmid as the marker. RFP expression was consistent throughout each transfected well which indicated equivalent DNA transfection efficiencies (Figure S25). GFP expression was consistent throughout each well transfected with eGFP or CleanCap-eGFP which indicated equivalent RNA transfection efficiencies, however the CleanCap-eGFP mRNA demonstrated more intense GFP expression compared to the cells that were transfected with the eGFP mRNA (Figure S25). This was expected as CleanCap-eGFP mRNA is HPLC purified. The cells that were transfected with either of the pri-miR-31 mimics demonstrated a modest reduction in HBsAg when compared to the cells that were transfected with eGFP. The pri-miR-31/5, pri-miR-31/8, pri-miR-31/9, and pri-miR-31/895 mimics demonstrated a 18.9%, 18.9%, 14.1%, 22.7% knockdown with p-values <0.01. The pri-miR-31/589 mimic demonstrated a 19.73% knockdown however the statistical analysis test attested the knockdown to be non-significant. The cells that were transfected with eGFP demonstrated a 15.5% reduction in HBsAg when compared to the cells that were transfected with the CleanCap-eGFP mRNA which indicated that the sequence common to eGFP and the pri-miR-31 mimics may be inducing non-specific silencing. These results together suggested that the pri-miR-31 mimics induced non-specific silencing and modestly inhibited HBV replication in the cells prior to cellulose purification.

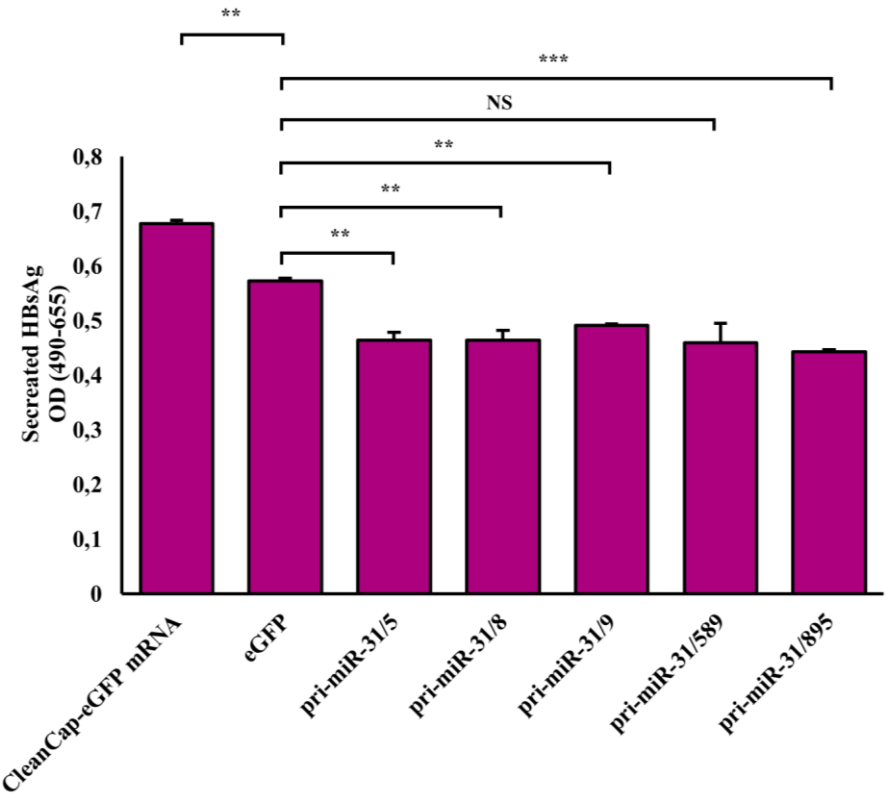


Figure 3.10: Assessment of HBV replication inhibition by the pri-miR-31 mimics prior to cellulose purification. HepG2-hNTCP cells were transfected with pCH-9/3091 (target) and mCherry (marker). One day after DNA transfection, the cells were transfected with CleanCap-eGFP (negative control), eGFP (negative control), pri-miR-31/5, pri-miR-31/8, pri-miR-31/9, pri-miR-31/589 or pri-miR-31/895 RNA. HBsAg expression was assessed one day after RNA transfection by performing an ELISA. The graphs were plotted using the mean and the error bars indicate the standard error of the mean (SEM) (n=3). The statistical significance was calculated using the student's paired two-tailed t-test (*** indicates $p<0.001$; ** indicates $p<0.01$ and NS indicates $p>0.05$).

To determine the ability of the pri-miR-31 mimics to inhibit HBV replication after cellulose purification, the amount of HBsAg produced after treatment was measured by performing an ELISA one and two days after treatment (Figure 3.11). The cells were transfected with the pCH-9/3091 plasmid as the target and the mCherry plasmid as the marker. RFP expression was consistent throughout each well one or two days after RNA transfection which indicated equivalent transfection efficiencies (Figure S26). GFP expression was consistent throughout each well transfected with eGFP or CleanCap-eGFP which indicated equivalent transfection efficiencies, however the CleanCap-eGFP mRNA demonstrated more intense GFP expression compared to the cells that were transfected with the eGFP mRNA (Figure S26). One day after treatment, the eGFP mRNA demonstrated a 31.2% reduction in HBsAg compared to the mock control with p-values <0.05. The pri-miR-31/5, pri-miR-31/8 and pri-miR-31/9, pri-miR-31/589 and pri-miR-31/895 mimics demonstrated a 45.0%, 36.8%, 37.4%, 49.2% and 53.3% reduction in HBsAg compared to the mock control with p-values <0.05. Since the eGFP mRNA was not expected to reduce HBsAg this suggests that the knockdown demonstrated with the pri-miRNA mimics was as a result of non-specific silencing. Thus, the difference between the eGFP mRNA and each of the pri-miR-31 mimics suggested that the mimics produced a 13.8%, 5.6%, 6.2%, 18.0% and 22.1% reduction in HBsAg respectively one day after treatment. Two days after treatment, the eGFP mRNA demonstrated a 58.5% reduction in HBsAg compared to the mock control with p-values <0.01. The pri-miR-31/5, pri-miR-31/8 and pri-miR-31/9, pri-miR-31/589 and pri-miR-31/895 mimics demonstrated an 84.4%, 76.2%, 71.2%, 87.4% and 88.8% reduction in HBsAg compared to the mock control with p-values <0.01. Thus, the difference between the eGFP mRNA and each of the pri-miR-31 mimics suggested that the mimics produced a 25.9%, 17.7%, 12.7%, 28.9% and 30.3% reduction in HBsAg respectively two days after treatment. These results together suggested that the pri-miR-31 mimics induced non-specific silencing and modestly inhibited HBsAg expression in HepG2-hNTCP cells following cellulose purification one and two days after treatment.

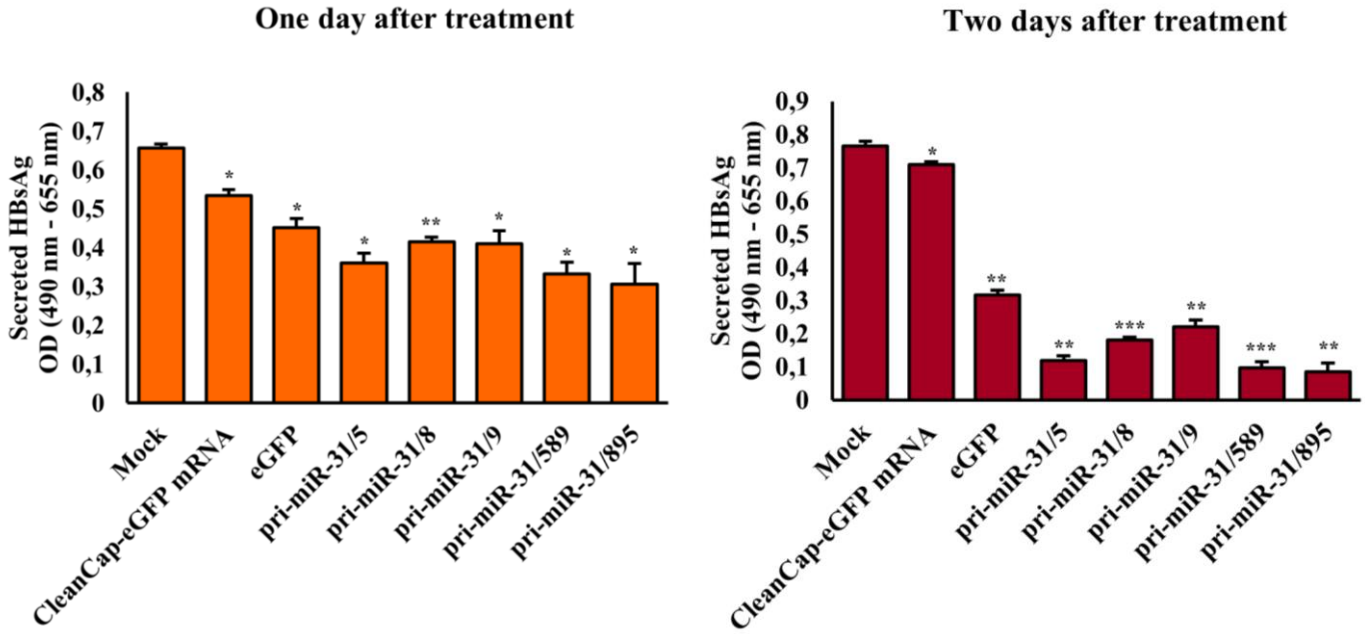


Figure 3.11: Assessment of HBV inhibition by the cellulose purified pri-miR-31 mimics by performing an ELISA. HepG2-hNTCP cells were transfected with pCH-9/3091 (target) and mCherry (marker). One day after transfection, the cells were transfected with CleanCap-eGFP (negative control), eGFP (negative control), pri-miR-31/5, pri-miR-31/8, pri-miR-31/9, pri-miR-31/589 or pri-miR-31/895 RNA. HBsAg expression was assessed one and two days after RNA transfection by performing an ELISA. The graphs were plotted using the mean and the error bars indicate the standard error of the mean (SEM) (n=3). The statistical significance was calculated against the mock control using the student's paired two-tailed t-test (*** indicates $p<0.001$; ** indicates $p<0.01$ and * indicates $p<0.05$).

3.3.2. Cellulose purified pri-miR-31/5 and pri-miR-31/8 mimics moderately induce specific HBV replication inhibition

The specific anti-HBV activity of the cellulose purified pri-miR-31 mimics was assessed after treatment by performing dual-luciferase assays. Dual-luciferase assays are commonly used to assess gene expression as the technique accounts for experimental variability allowing for more accurate results. The assay involves sequentially measuring firefly and *Renilla* luciferase reporter expression within a sample where the independent reporter serves as the baseline to which the experimentally dependent reporter is normalised to. The cells were transfected with the psiCHECK-HBx plasmid as the target and the mCherry plasmid as the marker. The psiCHECK-HBx plasmid contains an independently located firefly luciferase reporter and a *Renilla* luciferase reporter ORF upstream of an *HBx* sequence (Figure S27). The firefly reporter expresses firefly luciferase mRNA and the *Renilla* reporter produces *Renilla* luciferase mRNA with an *HBx* sequence. Thus, firefly luciferase is steadily produced whereas *Renilla* luciferase expression is dependent on the *HBx* sequence. The plasmid was chosen as the ratio of *Renilla* luciferase expression to firefly luciferase expression is useful to assess anti-HBV activity while accounting for experimental variability. The ratio of *Renilla* luciferase expression to firefly luciferase expression was used to assess the specific anti-HBV activity of the cellulose purified pri-miR-31 mimics one and two days after treatment (Figure 3.12).

RFP expression was consistent throughout each well one or two days after RNA transfection which indicated equivalent transfection efficiencies (Figure S28). GFP expression was consistent throughout each well transfected with eGFP or CleanCap-eGFP which indicated equivalent transfection efficiencies for each triplicate (Figure S28). One day after treatment, the CleanCap-eGFP and eGFP mRNA which did not contain a pri-miR-31 sequence, demonstrated a non-significant difference compared to the mock control as expected. This suggested that the eGFP mRNA does not induce non-specific silencing. The difference observed between the pri-miR-31/8 and pri-miR-31/895 mimics compared to the mock control were non-significant, suggesting that these mimics did not inhibit HBV replication. The pri-miR-31/5 mRNA demonstrated a 35.9% decrease in expression ratio over the mock control with p-values <0.01, indicating moderate HBV inhibition. Two days after treatment, the CleanCap-eGFP and eGFP mRNA demonstrated a non-significant difference compared to the mock control as expected. The pri-miR-31/9, pri-miR-31/589 and pri-miR-31/895 mimics exhibited a non-significant difference compared to the mock control suggesting that these mimics did not inhibit HBV replication. The pri-miR-31/5 and pri-miR-31/8 mimics

demonstrated reduced expression ratios by 50% and 53.6% respectively compared to the mock control, with p-values <0.05, suggesting that these mimics moderately inhibited HBV replication. In a study performed by Ely and colleagues, the pri-miR-31/9 mimics demonstrated the lowest reduction in HBsAg whereas the pri-miR-31/589 and pri-miR-31/895 mimics demonstrated the highest reduction in this antigen (Ely et al., 2009). This may explain the absence in specific silencing demonstrated by pri-miR-31/9 however the absence of specific silencing by pri-miR-31/589 and pri-miR-31/895 was unexpected.

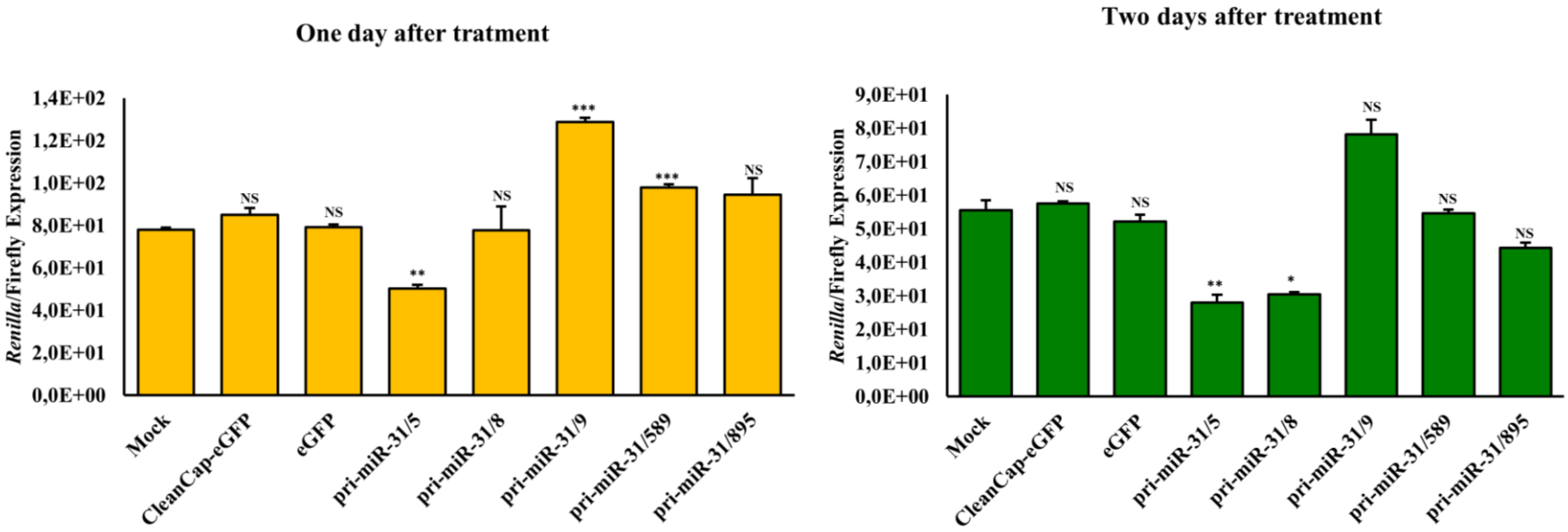


Figure 3.12: Assessment of HBV inhibition by the cellulose purified pri-miR-31 mimics by performing dual-luciferase assays. HepG2-hNTCP cells were transfected with psiCHECK-HBx (target) and mCherry (marker). One day after DNA transfection, the cells were transfected with CleanCap-eGFP (negative control), eGFP (negative control), pri-miR-31/5, pri-miR-31/8, pri-miR-31/9, pri-miR-31/589 or pri-miR-31/895 RNA. The ratio of *Renilla* luciferase expression to firefly luciferase expression was assessed one and two days after RNA transfection by performing dual-luciferase assays. The graphs were plotted using the mean and the error bars indicate the standard error of the mean (SEM) (n=3). The statistical significance was calculated against the mock control using the student's paired two-tailed t-test (*** indicates $p<0.001$; ** indicates $p<0.01$; * indicates $p<0.05$; NS indicates $p>0.05$).

3.3.3. Cellulose purified pri-miR-31 mimics do not affect cellular viability

To assess cytotoxicity of the cellulose purified pri-miR-31 mimics, an MTT assay was performed (Figure 3.13). MTT assays are used to assess cellular viability by measuring the amount of formazan produced after incubation with MTT. MTT is a yellow tetrazolium salt which converts to a purple formazan product through the activity of NAD(P)H-dependent cellular oxidoreductase enzymes. These enzymes are only found in metabolically active cells, thus the quantity of formazan formed reflects the amount of living cells present within the sample. GFP expression was consistent throughout each well transfected with eGFP or CleanCap-eGFP which indicated equivalent transfection efficiencies (Figure S29). The CleanCap-eGFP mRNA and mock control demonstrated a non-significant difference compared to the untransfected control as expected. The cells treated with Triton X-100 exhibited a 71.4% reduction in cellular viability compared to the untransfected control with p-values <0.001. This was expected as Triton X-100 is known to induce cellular cytotoxicity. The eGFP mRNA demonstrated statistically significant reduction in cellular viability however the difference was minor. The pri-miR-31 mimics demonstrated a non-significant difference compared to the untransfected control which indicated that the pri-miR-31 mimics did not affect cellular viability.

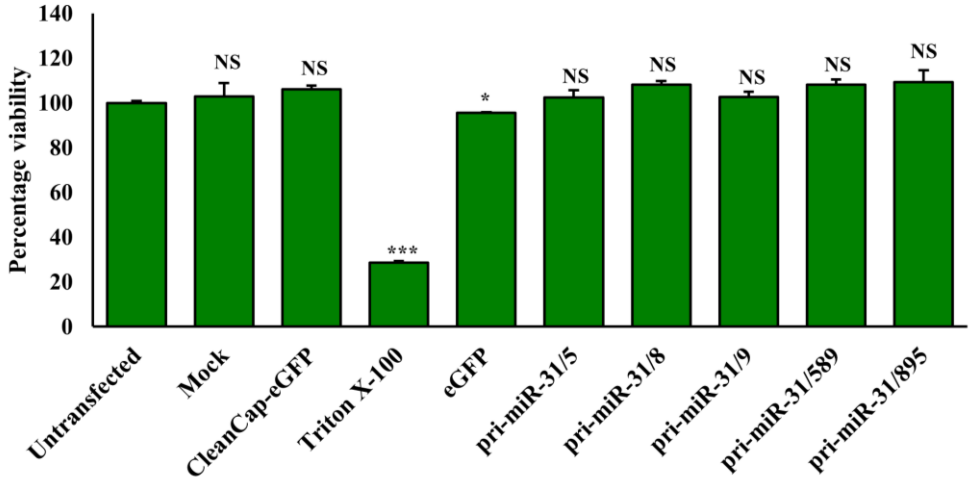


Figure 3.13: Assessment of cellular viability by the cellulose purified pri-miR-31 mimics using an MTT assay. Hek293T cells were transfected with pri-miR-31/5, pri-miR-31/8, pri-miR-31/9, pri-miR-31/589, pri-miR-31/895, eGFP (negative control) or CleanCap-eGFP (negative control) RNA. The cells that were treated with 1% Triton X-100 served as the positive control, those that were left untreated served as the untransfected control and the cells that were treated with the transfection mixture alone served as the mock control. The graph was plotted using the mean normalised to the mean of the untransfected control and the error bars indicate the normalised SEM (n=3). The statistical significance was calculated against the untransfected control using the student's paired two-tailed t-test (*** indicates $p<0.001$; * indicates $p<0.05$; NS indicates $p>0.05$)

3.3.4. Cellulose purified pri-miR-31 mimics induce interferon response

The ability of the pri-miR-31 mimics to activate the innate immune response was assessed by performing a dual-luciferase assay and by real-time RT-qPCR.

The dual-luciferase assay was performed using the phRL-CMV and pUCAsc-ISRE×3 plasmids. The phRL-CMV plasmid has a *Renilla* luciferase reporter sequence that is constitutively expressed under the control of the CMV promoter. The pUCAsc-ISRE×3 plasmid has three copies (×3) of the interferon-stimulated response element (ISRE) (5' TCGGGAAACCGAAACT-3') sequence upstream of the firefly luciferase sequence and these ISREs are responsive to interferon response factors (IRFs). Thus, these plasmids were chosen as the ratio of firefly luciferase expression to *Renilla* luciferase expression is useful to assess interferon response while accounting for experimental variability. GFP expression was consistent throughout each well transfected with the eGFP mRNA or CleanCap-eGFP mRNA which indicated equivalent transfection efficiencies for each triplicate (Figure S30a). The eGFP mRNA and mock control produced similar expression ratios as expected with no significant difference (Figure 3.14). The poly I:C dsRNA demonstrated a 7× increase in expression over the mock control, as expected, with p-values <0.05. The pri-miR-31/5, pri-

miR-31/589 and pri-miR-31/895 mimics produced an increased expression ratio compared to the mock control, however statistical analysis demonstrated the difference to be non-significant, suggesting that these mimics did not induce an interferon response. The pri-miR-31/8 and pri-miR-31/9 mimics compared to the mock control exhibited a 15.0× and 7× increased expression ratio with p-values <0.05 respectively, suggesting that these mimics were recognised by the host immune system and subsequently activated the interferon response. The induction of the interferon response may have been a result of the non-specific silencing observed.

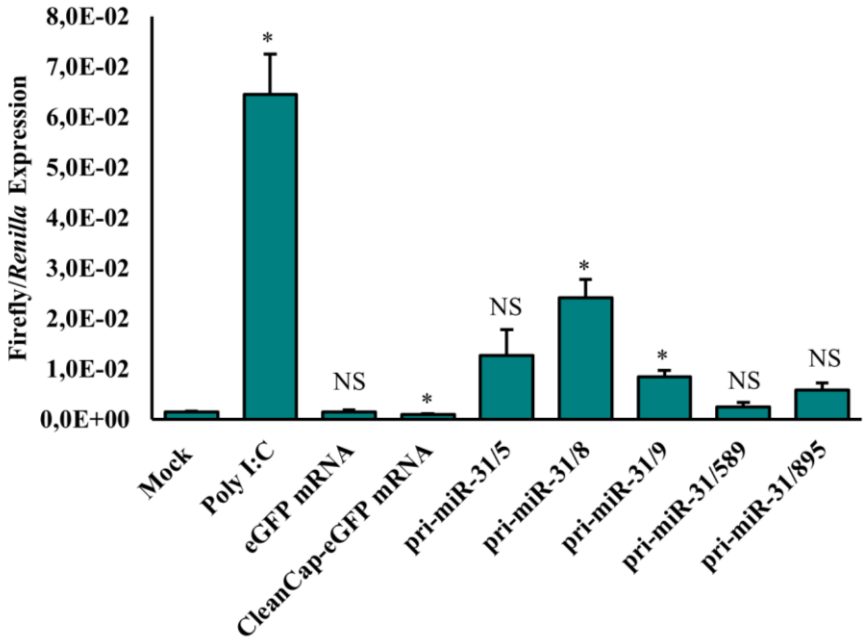


Figure 3.14: Evaluation of interferon response by the cellulose purified pri-miR-31 mimics by performing a dual luciferase assay. Hek293T cells were transfected with phRL-CMV, pUCAsc-ISRE×3 and pri-miR-31/5, pri-miR-31/8, pri-miR-31/9, pri-miR-31/589, pri-miR-31/895, eGFP (negative control), CleanCap-eGFP (negative control) or poly I:C (positive control). Two days after transfection, the ratio of firefly to *Renilla* expression was measured by a dual-luciferase assay. The graph was plotted using the ratio of firefly to *Renilla* luciferase expression and the error bars indicate the SEM (n=3). The statistical significance was calculated against the mock control using the student's paired two-tailed t-test (* indicates $p<0.05$ and NS indicates $p>0.05$).

The RT-qPCR assays were performed in addition to the dual-luciferase assay as it is a more sensitive assay to assess interferon response and provides greater insight into the analysis of this response. RT-qPCR assays are used to measure gene expression by reverse transcribing total RNA into complementary DNA and amplifying the gene of interest to determine the amount of targeted mRNA that was initially present. The detection of foreign nucleic acids by the host innate immune system leads to the production of interferons (IFNs) and the

subsequent expression of IFN stimulated genes (ISGs) such as *IFN-β*, *OAS1* and *MxA*. Thus, the difference in expression between constitutively expressed *GAPDH* and *IFN-β*, *OAS1* or *MxA* was used to determine interferon response. GFP expression was consistent throughout each well transfected with the eGFP mRNA or CleanCap-eGFP mRNA which indicated equivalent transfection efficiencies for each triplicate (Figure S30b). The CleanCap-eGFP mRNA which was used as a negative control did not produce significantly different quantities of *IFN-β*, *OAS1* and *MxA* mRNA compared to the untransfected control as expected, which indicated that the CleanCap-eGFP mRNA did not induce an immune response (Figure 3.15). The poly I:C dsRNA which was used as a positive control produced increased amounts of *IFN-β*, *OAS1* and *MxA* mRNA compared to the untransfected control as expected, which indicated that the poly I:C dsRNA induced an immune response. The pri-miR-31 mimics expressed increased levels of *IFN-β*, *OAS1* and *MxA* mRNA compared to the untransfected control at a confidence level of >95% which demonstrated that the mimics were recognised by the host immune system and subsequently induced an interferon response.

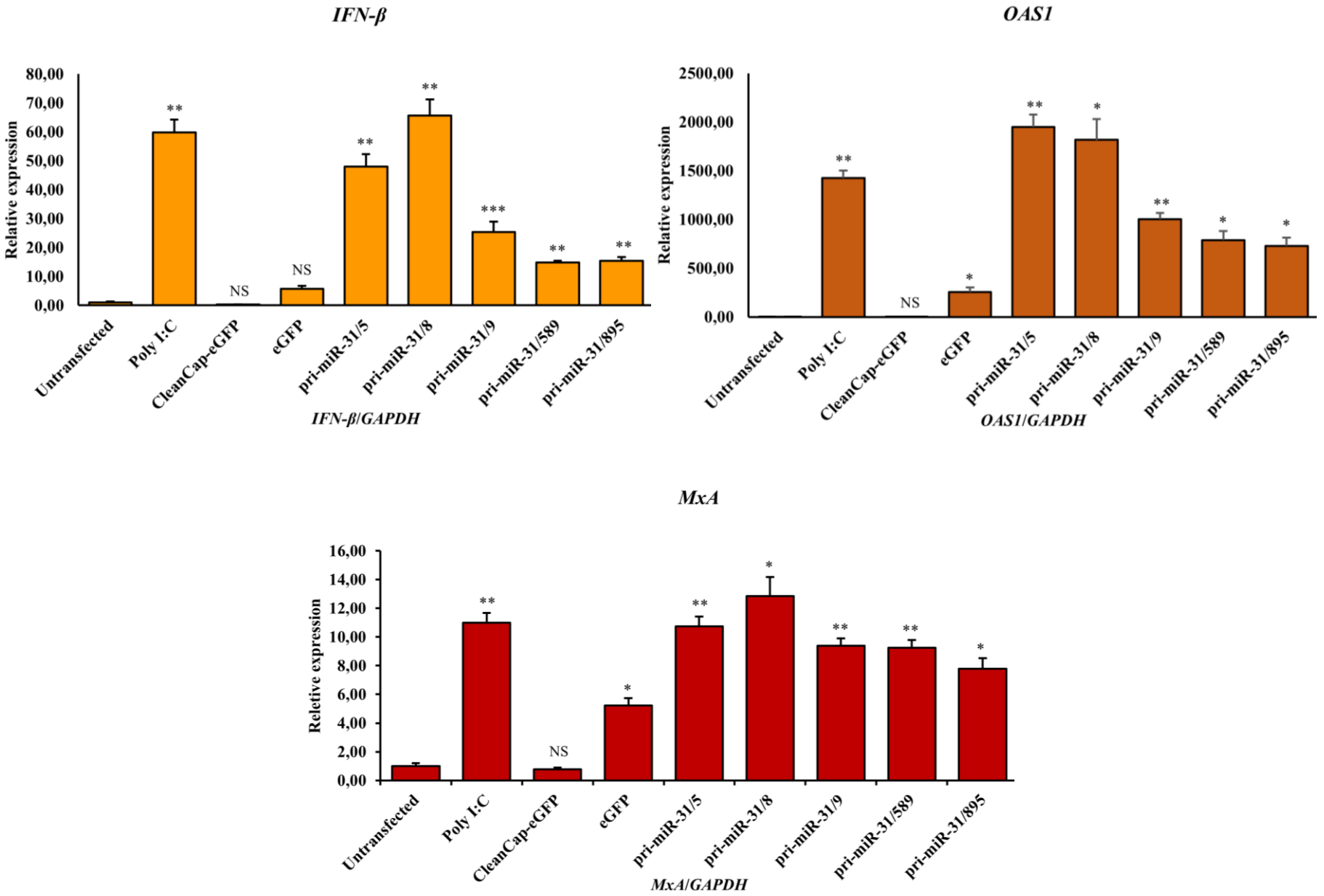

IFN-β
Relative expression
80,00
70,00
60,00
50,00
40,00
30,00
20,00
10,00
0,00
**
NS
NS
**
**
***
**
**
Untransfected
Poly I:C
CleanCap-eGFP
eGFP
pri-miR-31/5
pri-miR-31/8
pri-miR-31/9
pri-miR-31/589
pri-miR-31/895
IFN-β/GAPDH
OAS1
Relative expression
2500,00
2000,00
1500,00
1000,00
500,00
0,00
**
NS
*
**
*
**
*
*
Untransfected
Poly I:C
CleanCap-eGFP
eGFP
pri-miR-31/5
pri-miR-31/8
pri-miR-31/9
pri-miR-31/589
pri-miR-31/895
OAS1/GAPDH
MxA
Reletive expression
16,00
14,00
12,00
10,00
8,00
6,00
4,00
2,00
0,00
**
NS
*
**
*
**
**
*
Untransfected
Poly I:C
CleanCap-eGFP
eGFP
pri-miR-31/5
pri-miR-31/8
pri-miR-31/9
pri-miR-31/589
pri-miR-31/895
MxA/GAPDH

Figure 3.15: Assessment of immune stimulation by the cellulose purified pri-miR-31 mimics by performing RT-qPCR assays. Hek293T cells were transfected with pri-miR-31/5, pri-miR-31/8, pri-miR-31/9, pri-miR-31/589, pri-miR-31/895, eGFP (negative control), CleanCap-eGFP (negative control) or poly I:C (positive control). One day after transfection, the total RNA was extracted, and RT-qPCR assays were performed to determine immune response. The graphs were plotted by calculating the relative expression ratio of the sample genes (*IFN-β*, *OAS1* or *MxA*) to the control gene (*GAPDH*) normalised to their respective untransfected control and the error bars indicate the normalised SEM (n=3). The statistical significance was calculated against the untransfected control using the student's paired two-tailed t-test (*** indicates $p<0.001$; ** indicates $p<0.01$; * indicates $p<0.05$; NS indicates $p>0.05$).

3.3.5. Cellulose purified pri-miR-31 mimics were inefficiently processed

The linearised pmRNA-CMV-eGFP-pA and pT7-pri-miR-31/5 plasmids that were purified and assessed above, were in vitro transcribed, and the RNA produced was purified by lithium chloride precipitation and visualised on a formaldehyde gel to assess the integrity of the constructs after purification (Section 3.3.1 and Figure 3.16a). The eGFP RNA produced an expected band of 959 nt. The pri-miR-31/5 RNA produced a band of 500 nt instead of a band of 387 nt. The difference in size could be accounted to the inconsistent accuracy of the formaldehyde gel electrophoresis technique. The in vitro transcribed RNA was then purified by cellulose and analysed by capillary electrophoresis to ensure integrity of the constructs after purification (Figure 3.16b). The eGFP and pri-miR-31/5 RNA produced expected bands of 959 nt and 387 nt respectively. The cellulose purified RNA was then capped, purified by lithium chloride precipitation, and assessed by capillary electrophoresis to assess the integrity of the constructs after purification (Figure 3.16c). The eGFP and pri-miR-31/5 RNA produced bands slightly higher than expected which could be as a result of the capillary electrophoresis technique. These results all together indicated that the eGFP and pri-miR-31 RNA were suitable for assessment in vitro.

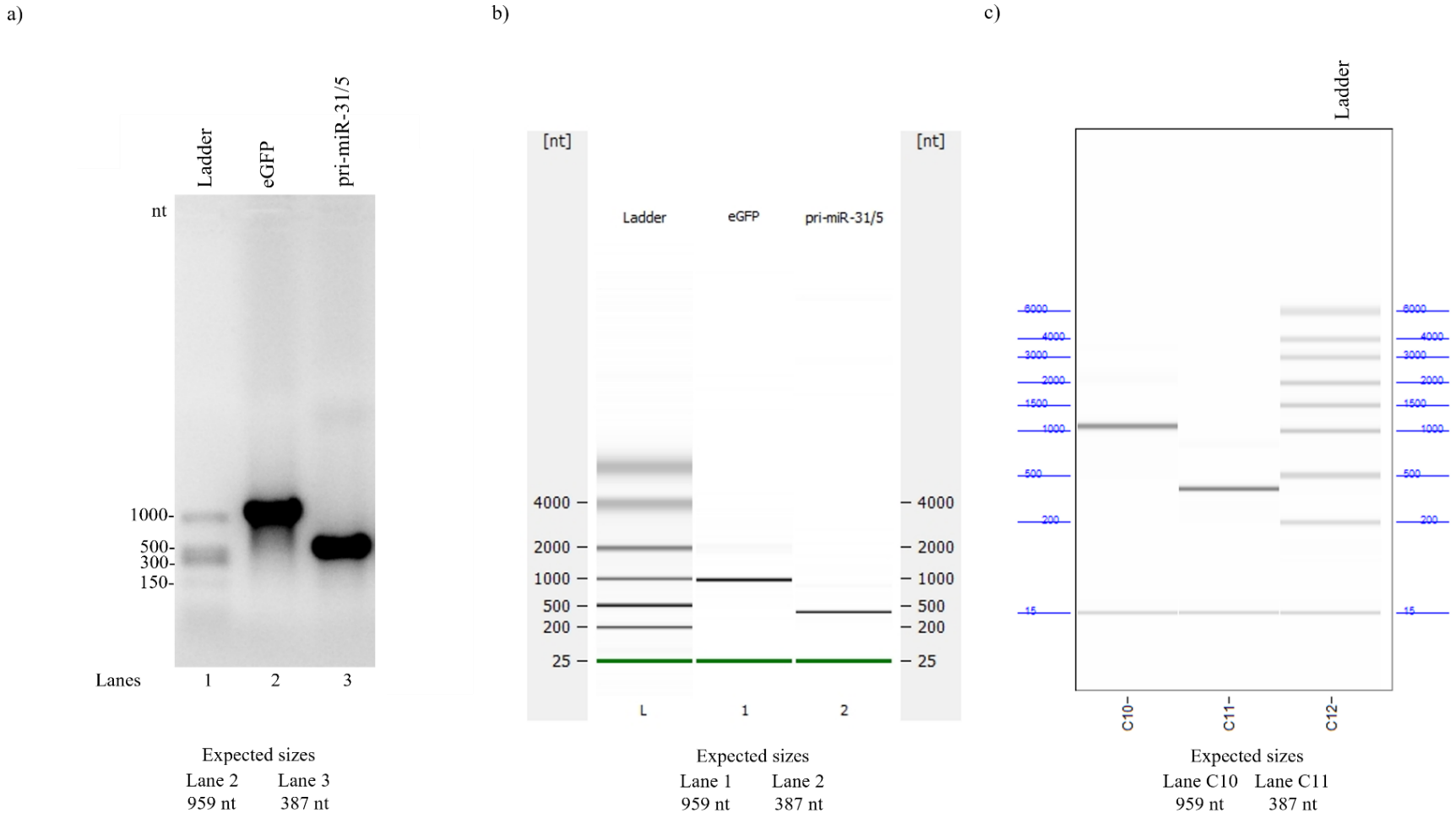


Figure 3.16: In vitro transcribed RNA after LiCl precipitation, cellulose purification and capping. (a) The linearised pmRNA-CMV-eGFP-pA and pT7-pri-miR-31/5 plasmids that were purified and assessed above, were in vitro transcribed, and the RNA produced was purified by lithium chloride precipitation and visualised on a 2 % formaldehyde gel. Lane 1: Low Range ssRNA ladder (New England Biolabs, MA, US). Lane 2: eGFP RNA after purification. Lane 3: pri-miR-31/5 RNA after purification (b) The in vitro transcribed RNA was purified by cellulose and analysed using the Agilent Bioanalyzer System (Agilent, CA, US). Lane 1: eGFP RNA after cellulose purification. Lane 2: pri-miR-31/5

RNA after cellulose purification. (c) The cellulose purified RNA was capped, purified by lithium chloride precipitation, and assessed using the Agilent Fragment Analyzer System (Agilent, CA, US). Lane C10: capped eGFP RNA after purification. Lane C11: capped pri-miR-31/5 RNA after purification.

The processing efficiency of the pri-miR-31/5 mimics were assessed by Northern blot hybridisation analysis. The mimics were expected to enter the cells and initiate the RNAi pathway. The initiation of the pathway was expected to process the pri-miR-31 mimics into pre-miRNA (70-80 nt), then into the miRNA duplex (20-25 bp), and finally form the mature miRNA guide sequence (20-22 nt). The pCMV-pri-miR-31/5 plasmid was used as a positive control as it contains the pri-miR-31/5 sequence and has been previously shown to be processed into the mature miRNA guide sequence (Ely et al., 2009). GFP expression was observed in the plate transfected with the eGFP RNA (Figure S31). The Northern blot hybridisation analysis was performed using a radioactively labelled probe with a complementary sequence against the expected guide to determine if the pri-miR-31/5 mimic was processed as designed (Figure 3.17). The eGFP RNA did not produce a signal corresponding to processing of a guide RNA, which was as expected. The pCMV-pri-miR-31/5 plasmid produced two bands. The first band of an unknown length was presumed to indicate pre-miRNA and the second band of approximately 20 nt was indicative of the expected mature miRNA. The pri-miR-31/5 mimics produced three high molecular weight bands of unknown lengths which were presumed to indicate the mimics that remained unprocessed and two faint bands that corresponded to the bands produced by the pCMV-pri-miR-31/5 plasmid. These results suggest that the majority of the pri-miR-31/5 mimics remained unprocessed and only a fraction was processed into the expected guide sequence. The inefficient processing of the pri-miR-31 mimics could have been as a result of the induction of the interferon response which could have caused the modest inhibition of HBV replication.

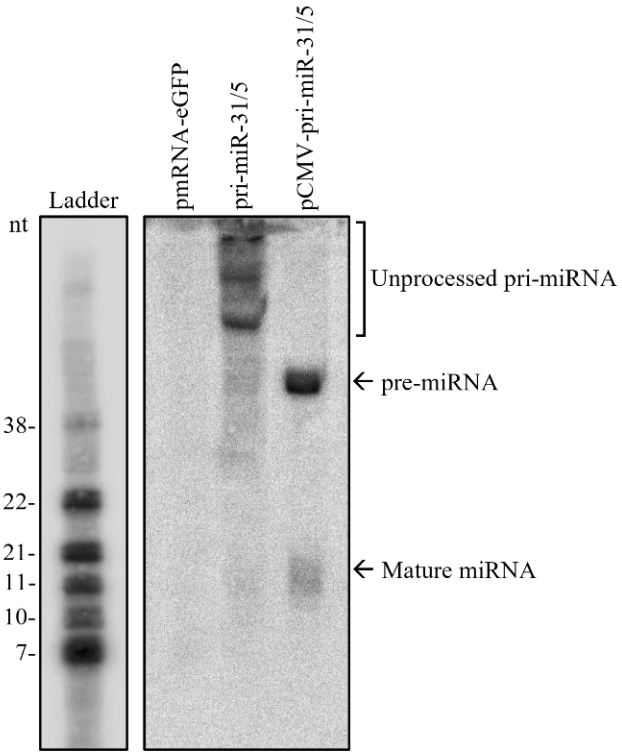


Figure 3.17: Expression and processing of the pri-miR-31/5 mimics by Northern blot hybridisation analysis. Total RNA was extracted from Hek293T cells that were transfected with eGFP (negative control), pri-miR-31/5, or pCMV-pri-miR-31/5 (positive control). The samples were run on a 20% denaturing polyacrylamide gel and Northern blot analysis was performed using a radioactively labelled probe against the expected guide sequence. The ladder was generated by radioactively labelling several oligonucleotides of different lengths and running them together alongside the RNA samples. The sizes indicated are approximations of the RNA sizes.

CHAPTER 4

4. DISCUSSION

Infection with the hepatitis B virus remains a leading global health concern despite the existence of an effective vaccine [reviewed in (Pattyn et al., 2021)]. It is estimated that over 275 million people worldwide are living with the chronic form of the disease and approximately 800 000 people die each year as a consequence of the complications that arise from chronic infection (World Health Organization, 2017). The current mainstream treatments available for patients with chronic HBV are capable of suppressing viral replication however these therapeutic strategies cannot eradicate the virus. Thus, the development of novel therapeutic strategies capable of eradicating the virus are urgently needed. The exploitation of the RNAi pathway by employing expression cassettes that endogenously express anti-HBV pri-miRNA mimics have demonstrated to be efficient in inhibiting viral replication, however achieving safe, efficient, and cost-effective delivery remains a major challenge (Maepa et al., 2017; Ivacik et al., 2015; Mowa et al., 2012; Dyer et al., 2010; Ely et al., 2009, 2008; Carmona et al., 2006). Thus, the purpose of this study was to in vitro transcribe anti-HBV pri-miR-31 mimics as the delivery of RNA sequences using non-viral vectors offers several advantages over DNA therapeutics and their delivery vectors. The rationale was that targeting the HBV transcripts may reduce viral protein production and thereby remove the suppressive effect that some of the proteins have on the immune system which has the potential to reactivate the host's natural defences to clear the virus.

4.1. Construction and assessment of the pT7-pri-miR-31 expression vectors

pT7-pri-miR-31 monomeric and trimeric expression vectors were successfully constructed using conventional molecular cloning techniques for use as templates to in vitro transcribe the anti-HBV pri-miR-31 mimics. These expression vectors contained a T7 promoter for in vitro transcription and pri-miR-31 sequences from gene cassettes which have been shown to efficiently inhibit HBV replication both in vitro and in vivo (Ely et al., 2009, 2008; Milligan et al., 1987). The constructed pT7-pri-miR-31 expression vectors were assessed in HepG2-hNTCP cells prior to in vitro transcription to determine whether these constructs could inhibit HBV replication in vitro. The data obtained demonstrated the ability of the pT7-pri-miR-31 expression vectors to reduce HBsAg which suggested that the design of these expression vectors was suitable and could be used as templates to in vitro transcribe functional pri-miR-31 mimics.

4.2. Efficiency of the in vitro transcribed pri-miR-31 mimics

The ability of the in vitro transcribed pri-miR-31 mimics to mediate effective gene silencing was assessed in cultured mammalian cells. The results obtained from the ELISA assays demonstrated the pri-miR-31 mimics to induce non-specific silencing and modestly inhibit HBsAg. Since previous studies have shown pri-miRNA-31 mimics to work well when expressed from expression cassettes, it suggests that the pri-miRNA-31 mimic sequences are suitable to efficiently inhibit HBsAg (Ely et al., 2009, 2008). However, the design of the in vitro transcribed pri-miRNA-31 mimics demonstrated here are not suitable and can be improved to increase HBsAg inhibition. The difference in silencing observed between the endogenously expressed and in vitro transcribed pri-miR-31 mimics described here and in previous studies were similarly dependent on their target sequences as the pri-miR-31/9 mimics demonstrated the lowest reduction in HBsAg compared to the pri-miR-31/589 and pri-miR-31/895 mimics which demonstrated the highest reduction of this antigen (Ely et al., 2009). The in vitro transcribed pri-miR-31 mimics were also assessed to determine the specific silencing induced by these constructs. The results obtained from the dual-luciferase assays demonstrated the pri-miR-31/5 and pri-miR-31/8 mimics to specifically reduce anti-HBV activity as opposed to the pri-miR-31/9, pri-miR-31/589 and pri-miR-31/895 mimics which did not demonstrate an inhibitory effect. The absence of specific silencing demonstrated by pri-miR-31/9 was expected as these constructs demonstrated the lowest reduction in HBsAg however the absence of specific silencing shown by pri-miR-31/589 and pri-miR-31/895 was unexpected as these mimics demonstrated the highest reduction in HBsAg. These results together suggested that the in vitro transcribed pri-miR-31 mimics were not suitable for mediating efficient gene silencing.

4.3. Processing of the in vitro transcribed pri-miR-31 mimics

The processing efficiency of the in vitro transcribed pri-miR-31/5 mimics were assessed by Northern blot hybridisation analysis after transfection into cultured mammalian cells. The results obtained demonstrated that majority of the pri-miR-31/5 mimics remained unprocessed and only a fraction was processed into the expected guide sequence. These results were different in comparison with observations from previous studies which assessed the silencing efficiency of pri-miR-31 mimics that were endogenously expressed from expression cassettes. The pri-miR-31/5 mimics demonstrated within these studies were efficiently processed into the expected guide sequence (Maepa et al., 2017; Ivacik et al., 2015; Mowa et al., 2012; Ely et al., 2009, 2008). The data obtained also revealed a correlation between guide strand production and silencing efficiency thus the modest inhibition demonstrated by the in vitro

transcribed pri-miR-31/5 mimics described here may have been as a result of insufficient processing (Ely et al., 2009). Since, the in vitro transcribed pri-miR-31/8, pri-miR-31/9, pri-miR-31/589 and pri-miR-31/895 mimics were also shown to modestly reduce HBsAg this suggested that these constructs were also not efficiently processed into the expected guide sequences. The recent study performed by Witteveldt and colleagues, which assessed the miRNA biogenesis pathway in response to the activation of the interferon response, demonstrated this response to prevent the microprocessor complex from binding to the pri-miRNA constructs, which resulted in inefficient processing of these mimics into the expected guide sequences (Witteveldt et al., 2018). Therefore, the inefficient processing observed by the in vitro transcribed pri-miR-31/5 mimics described here could have been as a result of the activation of the interferon response.

4.4. Safety of the in vitro transcribed pri-miR-31 mimics

The safety of the in vitro transcribed pri-miR-31 mimics was determined by assessing the ability of these constructs to induce cellular cytotoxicity and activate the innate immune response.

The ability of the in vitro transcribed pri-miR-31 mimics to induce cellular cytotoxicity was assessed in cultured mammalian cells by performing an MTT assay. Cellular cytotoxicity can be described as the damage caused to living cells due to a toxic agent which can lead to cell death due to the induced oxidative stress from the overproduction of reactive oxygen species (ROS) and nitric oxide (NO) [reviewed in (Zhang, 2018)]. Thus, it was crucial to examine whether the in vitro transcribed pri-miR-31 mimics could induce this effect. The results obtained from the MTT assay demonstrated that the cells remained viable after treatment with the in vitro transcribed pri-miR-31 mimics which indicated that these constructs did not induce cellular cytotoxicity.

The ability of the in vitro transcribed pri-miR-31 mimics to activate the innate immune response was assessed in cultured mammalian cells by performing a dual-luciferase assay and by real-time RT-qPCR. The innate immune system detects foreign ssRNA and dsRNA molecules through the use of pattern recognition receptors (PRRs) such as toll-like receptors (TLRs) and retinoic acid inducible gene I like receptors (RLRs) which leads to the production of interferons (IFNs) and other cytokines (Kato et al., 2006; Heil et al., 2004; Alexopoulou et al., 2001). The interaction of these IFNs with their specific receptors promotes the activation of several signalling pathways that leads to the expression of IFN stimulated genes (ISGs) such as dsRNA-dependant protein kinase (PKR) and 2’-5’-oligoadenylate synthetase (OAS) which are essential in establishing an antiviral state for combating foreign invasion [reviewed

in (Schoggins, 2019)]. The activation of PKR phosphorylates the eukaryotic translation initiation factor 2α (eIF2α) which inhibits viral and host mRNA translation, and the activation of OAS leads to the cleavage activity of ribonuclease L (RNase L) which promotes viral and host mRNA degradation [reviewed in (Hovanessian, 2007)]. Therefore, since PKR and OAS have the potential to induce severe adverse effects within the host, it was crucial to determine whether the in vitro transcribed pri-miR-31 mimics were capable of activating the interferon response. The results obtained demonstrated the in vitro transcribed pri-miR-31 mimics to induce the interferon response however the interferon response was not activated in previous studies which assessed pri-miR-31 mimics that were endogenously expressed from expression cassettes (Ely et al., 2009, 2008). This could have been attributed to the difference in effects induced between the in vitro transcribed RNAs and the expression cassettes as exogenous RNA and DNA induce different responses during transfection. RNA and DNA that are exogenously expressed are internalised into host cells within vesicles that are formed through receptor mediated endocytosis [reviewed in (Ziello et al., 2010)]. These vesicles are then transported to early endosomes where in which the nucleic acids are released through a process of membrane fusion [reviewed in (Maxfield and McGraw, 2004)]. The early endosome then sorts the nucleic acids and accompanying receptors into those that will be directed out of the endosomal compartment or those that will remain [reviewed in (Maxfield and McGraw, 2004)]. The early endosome with the remaining molecules will mature into the late endosome and combine with a lysosome to form the endolysosome (Bright et al., 2016; Stoorvogel et al., 1991). The molecules within the endolysosomal compartment will then be degraded however some can escape and enter the cytoplasm (Bright et al., 2016). TLRs such as TLR3, TLR7 and TLR8 are present within the plasma membrane and endosomal compartment, and RLRs such as retinoic acid inducible gene I (RIG-I) and melanoma differentiation associated protein 5 (MDA5) are present within the cytoplasm [reviewed in (Kawai and Akira, 2009)]. In vitro transcribed RNAs and associated contaminating products can be recognised by these receptors during the transfection process and subsequently activate the interferon response [reviewed in (Mu and Hur, 2021)]. Expression cassettes are generally not recognised by PRRs and are able to be transcribed into complementary RNAs upon entering the nucleus. These complementary RNAs can then undergo the modification process to prevent the constructs from inducing the innate immune response [reviewed in (Karikó and Weissman, 2007)].

4.5. Chemical modifications

The difference between endogenously expressed RNAs and in vitro transcribed RNAs is that both constructs undergo different modification processes [reviewed in (Karikó and Weissman, 2007)]. RNAs that are endogenously expressed are composed of nucleotides of which some are naturally modified following transcription [reviewed in (Karikó and Weissman, 2007)]. These modifications prevent the RNA constructs from being recognised by PRRs and thus inhibits the activation of the innate immune response [reviewed in (Karikó and Weissman, 2007)]. RNAs that are in vitro transcribed which do not contain modified nucleotides have been shown to induce immune stimulation and increase the production of contaminating products that are formed during the in vitro transcription process. However, the incorporation of chemically modified nucleotides within the in vitro transcribed RNAs during transcription has been demonstrated to reduce the generation of contaminating products and prevent the in vitro transcribed RNAs from being recognised by PRRs. Therefore, the incorporation of modified nucleotides during the in vitro transcription process is crucial to prevent these constructs from activating the innate immune response and inducing severe adverse effects.

The most commonly used chemically modified nucleotides include pseudouridine (Ψ), *N1*-methylpseudouridine (m1Ψ), 2-thiouridine (s2U), *N6*-methyladenosine (m6A) and 5-methylcytidine (m5C). In vitro transcribed RNAs and their contaminating products activate PRRs such as RIG-I and TLR3 (which recognises the dsRNA) and TLR7 and TLR8 (which recognises the ssRNA), however the ability of these RNA constructs to bind to these receptors are prevented by the incorporation of s2U together with m5C (Kormann et al., 2011; Heil et al., 2004; Alexopoulou et al., 2001). Several other chemically modified nucleotides that have been incorporated, whether in combinations such as Ψ together with m5C or individually such as Ψ, m1Ψ, s2U, m6A or m5C, were also shown to reduce the activation of TLR3, TLR7 or TLR8, thus decreasing the immunogenicity of these in vitro transcribed RNA constructs (Andries et al., 2015; Karikó et al., 2005). In addition, the Ψ, m1Ψ or m5C chemically modified nucleotides were shown to alter the behaviour of the RNA polymerase such that the production of contaminating dsRNA was reduced [reviewed in (Mu and Hur, 2021)]. Several other methods have been assessed to reduce contaminating dsRNA, that can either be performed during or after in vitro transcription, however, incorporating chemically modified nucleotides during in vitro transcription and purifying the in vitro transcribed constructs thereafter, may prove to be a suitable method of reducing immunogenicity [reviewed in (Mu and Hur, 2021)]. Studies that have assessed in vitro transcribed RNAs after purification, by high performance liquid chromatography (HPLC) or cellulose based methods, have shown

that the constructs with unmodified nucleotides were more immunogenic as opposed to those that were modified with m1Ψ (Nelson et al., 2020; Baiersdörfer et al., 2019).

These studies together demonstrate the importance of chemically modified nucleotides within in vitro transcribed RNA constructs. Thus, the incorporation of chemically modified nucleotides within the pri-miR-31 mimics and purification of these constructs, could possibly prevent the in vitro transcribed RNAs from activating the innate immune response. The activation of the interferon response has been shown by Witteveldt and colleagues to prevent the microprocessor complex from binding to pri-miRNA constructs resulting in inefficient processing of these mimics into the expected guide sequences (Witteveldt et al., 2018). Therefore, the prevention of the interferon response could possibly improve the processing efficiency of the in vitro transcribed pri-miR-31 mimics and subsequently increase the inhibitory effect of these constructs.

4.6. Delivery

The delivery of therapeutic genes into target cells remains a major challenge as there are various factors that impede the safety and efficiency of this process. The therapeutic genes are susceptible to endonucleases degradation, are prone to clearance and can interact with non-specific targets [reviewed in (Weng et al., 2020)]. These constructs also possess an overall negative charge that inhibits cellular uptake and are limited in their ability to escape the endosomal membrane [reviewed in (Weng et al., 2020)]. Therefore, in an attempt to overcome these factors therapeutic genes are commonly delivered using vectors.

The use of non-viral vectors has been extensively explored and these strategies can be categorised into physical and chemical based methods. The physical based methods include electroporation, microinjection, and gene gun approaches. The electroporation approach is the most commonly used physical technique for delivering in vitro transcribed RNA into target cells. This method involves applying electrical forces to the target cells in order to introduce pores within the cellular membrane to facilitate the entry of the therapeutic genes into the permeabilised cells [reviewed in (Herrero et al., 2017)]. This procedure has advanced to human clinical trials and has recently been introduced into various hospitals, however, there are several disadvantages associated with this approach [reviewed in (Heller and Heller, 2015)]. These disadvantages include the possibility of pain, erythema, and discomfort at the sites of electroporation as well as extensive cell death from applying high voltages and increasing the pulse length in an attempt to improve the efficiency and specificity of this procedure [reviewed in (Lambricht et al., 2016)].

The chemical-based methods involve the use of nanocarriers such as lipids, polymers, and peptides. These chemical nanocarriers can protect the nucleic acids from degradation, prevent clearance, promote specific delivery, improve uptake, and enhance endosomal escape. Lipid based nanocarriers include liposomes and lipid nanoparticles. Cationic liposomes are the most commonly used non-viral chemical vectors for delivering in vitro transcribed RNA into target cells. These molecules consist of an outer bilayer membrane and an aqueous core [reviewed in (Balazs and Godbey, 2010)]. The membrane is usually composed of positively and neutrally charged lipids containing hydrophilic heads and hydrophobic tails [reviewed in (Balazs and Godbey, 2010)]. This allows the negatively charged nucleic acids within the aqueous layer to bind to the positively charged heads and form the structure that provides the nucleic acids within the aqueous core protection against external nucleases [reviewed in (Balazs and Godbey, 2010)]. The positively charged lipids that are the most frequently used to construct these cationic liposomes include N-[1-(2,3-dioleyloxy)propyl]-N,N,N-trimethylammonium chloride (DOTMA) and 1,2-dioleoyl-3-trimethylammonium propane (DOTAP) (Holmen et al., 1995; Malone et al., 1989). These cationic lipids in combination with neutrally charged helper lipids such as 1,2-dioleoyl-sn-glycero-3-phosphoethanolamine (DOPE), polyethylene glycol (PEG) and cholesterol have the potential to improve the delivery process. DOPE enables efficient endosomal escape by modifying the membrane of the cationic liposome under acidic conditions to allow fusion with the endosomal membrane (Koltover et al., 1998). PEG improves circulation time and prevents unintentional binding [reviewed in (Suk et al., 2016)]. Cholesterol increases stability by regulating the lipid membrane (Briuglia et al., 2015). The disadvantage of using cationic liposomes is that these molecules possess a constant positive charge which has the potential to induce severe toxicity (Andrade et al., 2022). Therefore, ionisable lipid nanoparticles were recently developed as a safer approach. Ionisable lipids are neutrally charged under physiological conditions and positively charged under acidic conditions to enable efficient escape from the endosomal membrane [reviewed in (Hou et al., 2021)]. Ionisable lipid nanoparticles consist of an outer lipid membrane and an electron-dense core which contains inner lipid structures that enclose the nucleic acids [reviewed in (Hald Albertsen et al., 2022)]. These molecules are usually composed of ionisable lipids, phosphatidylcholine, PEG, and cholesterol [reviewed in (Hou et al., 2021)]. The ionisable lipids that are the most frequently used to construct these lipid nanoparticles include 1,2-dioleyloxy-N,N-dimethyl-3-aminopropane (DODMA) and 1,2-dioleoyl-3-dimethylammoniumpropane (DODAP) [reviewed in (Hald Albertsen et al., 2022)]. These carriers can be engineered to target liver cells (Kim et al., 2021). Therefore, the use of

ionisable lipids to deliver the in vitro transcribed pri-miR-31 mimics has the potential to improve transfection efficiency and replication inhibition.

4.7. Off-target effects

The use of RNAi activators has the potential of causing off-target effects which may lead to the incidence of severe adverse events. The potential of causing off-target effects may be especially influenced by non-specific silencing, activation of the innate immune response and oversaturation of the miRNA pathway (Galka-Marciniak et al., 2016; Grimm et al., 2006; Judge et al., 2005). The off-target effects caused by non-specific silencing are primarily due to the improper processing of the RNAi activators into their intended guide sequence. The pri-miRNA mimic contains a pri-miRNA scaffold and a miRNA insert. The mimic is designed to be processed into a miRNA duplex of which the passenger is released, and the guide strand remains within RISC to target specific mRNA sequences, however improper processing of the pri-miRNA mimic can cause non-specific mRNA sequences to be recognised. The generation of miRNA duplexes with heterogenous seed regions can lead to non-specific mRNA suppression as only a few nucleotides within the seed region of the guide strand are required to bind to the 3' UTR of an mRNA transcript to mediate silencing [reviewed in (Bartel, 2009)]. The release of the guide strand instead of the passenger strand can also lead to non-specific mRNA suppression due to the passenger strand having a lower thermodynamic stability at the 5' end, causing the passenger strand to remain within RISC and target unintentional mRNA sequences (Khvorova et al., 2003; Schwarz et al., 2003). These non-specific effects can be prevented by directing the RNAi activators to the target tissues to inhibit these constructs from interacting with unintentional mRNA sequences and by designing the passenger strand with a higher thermodynamic stability at the 5' end to avoid incorrect strand loading. The off-target effects caused by activation of the innate immune response occurs as a result of PRRs recognising the exogenous RNAi activators and subsequently activating the innate immune response. This can be prevented by incorporating chemically modified nucleotides within the RNAi activators prior to transfection [reviewed in (Karikó and Weissman, 2007)]. The off-target effects induced by oversaturation of the miRNA pathway are primarily due to the limited capacity of Exportin-5 which causes both RNAi activators and naturally occurring miRNAs to compete for processing (Grimm et al., 2006). This is not a concern however with the use of exogenous RNAs as the dosage can be easily controlled. Therefore, the potential of the in vitro transcribed pri-miR-31 mimics to induce off-target effects could be reduced by preventing non-specific silencing, and inhibiting

the activation of the innate immune response, which could possibly improve the silencing efficiency of these constructs.

4.8. Conclusion

This study demonstrated the in vitro transcribed pri-miR-31 mimics to modestly inhibit viral replication, however these constructs were also shown to induce non-specific silencing, activate the interferon response, and were inefficiently processed into the expected guide sequences. Nevertheless, improvements can be made to the system to promote safe and efficient gene silencing. The modest inhibition demonstrated by these constructs could have been attributed to inefficient processing due to the activation of the interferon response and limited trafficking of the pri-miR-31 mimics into the nucleus. The use of chemically modified nucleotides and employing pre-miRNA which do not need to enter the nucleus may improve the safety and efficacy of these constructs. Therefore, this study demonstrated the potential of the in vitro transcribed miRNA mimics in inhibiting HBV, however improvements to the system could increase viral replication inhibition and reduce the immunogenicity of these constructs.

CHAPTER 5

5. APPENDIX

5.1. Preparation, transformation, and propagation of chemically competent *E. coli*

Reagents:

Luria Bertani medium

Five grams of yeast extract, 10 g of tryptone and 5 g of NaCl was dissolved in 1 L of distilled water. The solution was then autoclaved for 20 minutes at 121°C and 1 kg/cm^2 and stored at room temperature.

Transformation buffer

Thirty millilitres of glycerol (15%), 2.9404 g of $CaCl_2.2H_2O$ (100 mM) and 0.6048 g of PIPES (10 mM) was added to 150 ml of distilled water. The pH was adjusted to 7.0 with NaOH and distilled water was added to a final volume of 200 ml. The solution was autoclaved for 20 minutes at 121°C and 1 kg/cm^2 and stored at -20°C.

1000× ampicillin stock

One gram of ampicillin was dissolved in 5 ml of distilled water with 5 ml of absolute ethanol and stored at -20°C.

Ampicillin positive Luria Bertani agar plates

Five grams of yeast extract, 10 g of tryptone, 5 g of NaCl and 10 g of agar was dissolved in 1 L of distilled water. The solution was autoclaved for 20 minutes at 121°C and 1 kg/cm^2 and left to cool to approximately 50°C. Thereafter, 1 ml of ampicillin (1000×) was added, and the agar solution was poured into petri dishes. The plates were left to solidify at room temperature before the plates were stored at 4°C.

IPTG (isopropyl-β-D-thiogalactopyranosid) stock (100 mg/ml)

Ten millilitres of distilled water was used to dissolve 200 mg of IPTG. The solution was then filter sterilised with a 0.22 µm syringe filter and stored at -20ºC.

X-gal (5-bromo-4-chloro-3-indolyl-βD-galactopyranoside) stock (20 mg/ml)

Two hundred milligrams of X-gal was added to 10 ml of dimethylformamide and stored at -20 ºC covered in aluminium foil.

Protocols:

Bacterial pre-culture was prepared by inoculating 4 µl of *E. coli* stock into 4 ml of Luria Bertani medium and incubating the cell suspension overnight at 37°C with shaking at 150 rpm. Sub-cultures were then produced by transferring each half of the pre-culture into 100 ml

of Luria Bertani medium and incubating the cell suspension at 37°C with shaking at 150 rpm for 4 hours.

Two hundred millilitres of *E. coli* sub-culture were then split equally into four 50 ml centrifuge tubes and centrifuged at 4 000 rpm for 30 minutes at 4°C. Thereafter, the supernatants were discarded, and each pellet was resuspended in 15 ml of transformation buffer. The mixtures were then placed on ice for 30 minutes and centrifuged at 2 500 rpm for 15 minutes at 4°C. Following centrifugation, each pellet was resuspended in 1 ml of transformation buffer. The resuspensions containing the chemically competent *E. coli* were then combined and aliquoted into 200 µl volumes. These aliquots were then stored at -80°C and thawed on ice before use.

Plasmid DNA was added to chemically competent *E. coli* and incubated on ice for 25 minutes. Following incubation, the cells were heat shocked at 42°C for 90 seconds and placed on ice for a further 5 minutes. The transformed *E. coli* were then spread evenly on pre-warmed ampicillin positive Luria Bertani agar plates (100 µg/ml) and placed upside down in a bacteriological incubator overnight at 37°C.

Selected colonies were each inoculated into Luria Bertani medium supplemented with ampicillin (100 µg/ml) and incubated overnight at 37°C with shaking at 150 rpm.

5.2. DNA purification and analysis

Reagents:

Buffer P1 (Resuspension buffer)

To prepare buffer P1, 3.72 g of $Na_2EDTA.2H_2O$ and 6.06 g of Tris base was added to 800 ml of distilled water. The pH was adjusted to 8.0 with HCl and distilled water was added to a final volume of 1 L. The solution was then autoclaved for 20 minutes at 121°C and 1 kg/cm^2. Thereafter, 100 mg of RNase was added, and the buffer was stored at 4°C.

Buffer P2 (Lysis solution)

Five hundred millilitres of distilled water was used to dissolve 8 grams of NaOH pellets. Thereafter, 10 g of SDS was added and the solution was made to a final volume of 1 L with distilled water. The buffer was then stored at room temperature.

Buffer P3 (Neutralising solution)

To prepare buffer P3, 294.5 g of potassium acetate was added to 500 ml of distilled water. The pH was adjusted to 5.5 with acetic acid and distilled water was added to a final volume of 1 L. The solution was then stored at 4°C.

Buffer QBT (Equilibration buffer)

Eight hundred millilitres of distilled water was added to 43.83 g of NaCl and 10.46 g of MOPS. The pH was adjusted to 7.0 with NaOH and 150 ml of isopropanol was added. Thereafter, 15 ml of Triton-X solution (10%) was added, and the solution was made to a final volume of 1 L with distilled water. The buffer was then stored at room temperature.

Buffer QC (Wash buffer)

To prepare buffer QC, 58.44 g of NaCl and 10.46 g of MOPS was dissolved in 800 ml of distilled water. The pH was adjusted to 7.0 with NaOH and 150 ml of isopropanol was added. Thereafter, distilled water was added to a final volume of 1 L and the solution was stored at room temperature.

Buffer QF (Wash buffer)

To prepare buffer QF, 73.05 g of NaCl and 6.06 g of Tris base was dissolved in 800 ml of distilled water. The pH was adjusted to 8.5 with HCl and 150 ml of isopropanol was added. Thereafter, distilled water was added to a final volume of 1 L and the solution was stored at room temperature.

50× TAE running buffer

Two hundred and forty-two grams of Tris base, 100 ml of EDTA (0.5 M) and 57.1 ml of glacial acetic acid was added to distilled water. The pH was adjusted to 8.0 and distilled water was added to a final volume of 1 L. The solution was then stored at room temperature.

Protocols:

5.2.1. Large scale plasmid DNA purification

Large scale plasmid purifications were performed using the QIAGEN® Plasmid Maxi Kit (Qiagen, Germany) according to the manufacturer's instructions with minor adjustments. Briefly, the bacterial culture was centrifuged at 5 000 ×g for 15 minutes at 4°C, the supernatant was discarded, and the bacterial pellet was resuspended in 10 ml of buffer P1. Thereafter, 10 ml of buffer P2 was added, and the solution was mixed by inverting six times. The solution was then incubated at room temperature for 5 minutes and 10 ml of prechilled buffer P3 was added. After mixing by inverting, the solution was left to incubate on ice for 20 minutes before it was centrifuged at 4 000 rpm for 20 minutes at 4°C. To equilibrate the Qiagen-tip 500 column (Qiagen, NW, DE), 10 ml of buffer QBT was added and allowed to empty with gravity. The supernatant was applied to the equilibrated tip and allowed to move through the resin of the column by gravity flow. Thereafter, the column was washed by adding 30 ml of buffer QC twice and allowing it to empty to the action of gravity. The

column was transferred to a clean vessel and 15 ml of buffer QF was added to elute the DNA. The eluted DNA was then mixed with 10.5 ml of isopropanol and centrifuged at 4 000 rpm for 60 minutes at 4°C. Next, the pellet was washed with 5 ml of 70% ethanol and centrifuged at 15 000 ×g for 10 minutes. The supernatant was discarded, and the pellet was centrifuged for a further 5 minutes. The remaining ethanol was removed, and the pellet was left to air dry for 5 minutes before it was resuspended in 200 µl of sterile water and stored at -20°C. The concentration of the plasmid DNA was determined by spectrophotometry.

5.2.2. Small scale plasmid DNA purification

Small scale plasmid purifications were performed using the EconoSpin™ All-in-One Mini Spin Columns (Epoch Life Science, TX, US) according to the manufacturer's instructions. Ten millilitres of bacterial culture was centrifuged at 2 000 rpm for 15 minutes and the pellet was resuspended in 250 µl of buffer P1. Thereafter, 250 µl of buffer P2 was added and the solution was mixed by inverting six times. The solution was then incubated at room temperature for 5 minutes before 350 µl of buffer P3 was added. After mixing, the solution was centrifuged at 12 000 rpm for 10 minutes. The supernatant was then added to the EconoSpin™ All-in-One Mini Spin Column (Epoch Life Science, TX, US) and centrifuged at 4 000 rpm for 1 minute. Thereafter, the flow-through was discarded and 500 µl of WS buffer was added to the column and centrifuged at 12 000 rpm for 1 minute. This was repeated and the flow-through was discarded. The column was then centrifuged for a further 2 minutes to remove the residual ethanol. Following centrifugation, the flow-through was discarded and the column was transferred to a sterile 1.5 ml microcentrifuge tube. To elute the DNA, 50 µl of distilled water was added onto the membrane of the column and allowed to stand for 5 minutes. The tube was centrifuged at 12 000 ×g for 1 minute and the eluted DNA was stored at -20°C. The concentration of the plasmid DNA was then determined by spectrophotometry.

5.2.3. Small scale high yield plasmid DNA purification

Small scale high yield plasmid purifications were performed without the use of purification columns. Briefly, the bacterial culture was centrifuged at 4 000 rpm for 15 minutes and the resulting pellet was resuspended in 300 µl of buffer P1. The cell resuspension was then transferred to a sterile microcentrifuge tube where 300 µl of buffer P2 was added and mixed by inverting. The microcentrifuge tube was then left to incubate at room temperature for 5 minutes before 300 µl of buffer P3 was added. Thereafter, the solution was mixed by inverting and centrifuged at 12 000 rpm for 10 minutes. The supernatant was then transferred to a sterile microcentrifuge tube and an equal volume (~900 µl) of isopropanol was added. Thereafter, the solution was mixed by inverting and left to incubate at -20ºC for 30 minutes

before it was centrifuged at 12 000 rpm for 30 minutes. Following centrifugation, the supernatant was discarded, and the residual liquid was removed. The pellet was left to air dry for 2 minutes before it was resuspended in 100 µl of sterile water. The concentration was then determined by spectrophotometry and the plasmid DNA was stored at -20°C.

5.2.4. Restriction enzyme digestion

Restriction enzyme digestions were performed using endonucleases acquired from Thermo Fisher Scientific and New England Biolabs according to the manufacturers' instructions.

5.2.5. Agarose gel electrophoresis

The desired gel percentage in weight of agarose powder (Lonza, Rockland, US) (1% agarose gel = 1 g of agarose powder) was heated in a microwave for 5 minutes with 100 ml of 1× TAE running buffer until the agarose completely dissolved. The agarose gel solution was left to cool to approximately 50°C before 2 µl of ethidium bromide was added. Thereafter, the mixture was slowly swirled and poured into a casting tray with an appropriate gel comb. The gel was then left to solidify for approximately 20 minutes before it was placed into an electrophoresis tank and submerged with 1× TAE running buffer. The samples were prepared by adding the appropriate concentration of plasmid DNA and 6× loading dye (Thermo Fisher Scientific, MA, USA) to a final concentration of 1× with sterile water. The prepared samples were then loaded into the wells of the agarose gel alongside an appropriate DNA ladder. The gel was left to run at 100 V for 45-90 minutes before it was visualised using the Omega Fluor ™ gel imaging system (Aplegen, CA, US).

5.2.6. DNA fragment purification

Agarose gel purification to isolate and purify DNA fragments of interest was performed using the MinElute Gel Extraction solutions and protocol (Qiagen, Germany) according to the manufacturer's instructions, however, with minor adjustments, and Econospin columns (Epoch Life Science, TX, US). The DNA fragment of interest was excised from the agarose gel and weighed in a sterile microcentrifuge tube (100 mg of gel = 1 volume or 100 µl). Thereafter, 3 volumes of buffer QG was added to 1 volume of gel and incubated at 50°C for 10 minutes. Following incubation, 1 volume of isopropanol was added to the dissolved gel, and the solution was briefly mixed by inverting. The solution was then transferred to a MinElute column that was placed in a collection tube. The tube was centrifuged at 12 400 rpm for 1 minute at room temperature and the flow-through was discarded. Thereafter, 500 µl of buffer QG was added to the column and the tube was centrifuged at 12 400 rpm for 1 minute. The flow-through was then discarded and 750 µl of buffer PE was added to the column before the tube was centrifuged at 12 400 rpm for 1 minute. Following centrifugation, the flow-

through was discarded and the column was centrifuged for an additional 1 minute to remove the excess buffer. The column was then transferred to a sterile 1.5 ml microcentrifuge tube and 20 µl of buffer EB was added. The column was left to stand for 5 minutes before it was centrifuged at 12 400 rpm for 1 minute to elute the DNA.

PCR products were purified by adding a 3:1 volume of buffer QG and a 1:1 volume of isopropanol and transferring the mixture to a MinElute column that was placed in a collection tube. The rest of the method was continued as above from the first centrifugation step.

5.2.7. Ethanol precipitation

Sodium acetate (3 M NaOAc, pH 5.2) was added to the DNA suspension to a final concentration of 0.3 M with water. Thereafter, 2.5× volume of 100% ethanol was added, and the solution was incubated at -20 ºC for 30 minutes. The solution was then centrifuged at 12 000 rpm for 30 minutes at 4 ºC before the supernatant was removed. The remaining pellet was resuspended in 500 µl of 70% ethanol and centrifuged at 12 000 rpm for 5 minutes at 4 ºC before the supernatant was removed. The pellet was then left to air-dry for 5 minutes before it was resuspended in an appropriate volume of sterile water.

5.3. RNA synthesis, purification, and analysis

Reagents:

10× MOPS buffer

One hundred and forty-six grams of EDTA, 41.85 g of MOPS and 4.10 g of NaAc was dissolved in 400 ml of distilled water. The pH was adjusted to 7 with 10 M of NaOH and distilled water was added to a final volume of 500 ml. The solution was then autoclaved for 20 minutes at 121°C and 1 kg/cm^2 and stored at room temperature covered in aluminium foil.

Protocols:

5.3.1. Lithium chloride precipitation

Lithium chloride precipitation solution (7.5 M LiCl, 50 mM EDTA) was added to the RNA suspension to a final concentration of 2.5 M with nuclease-free water. The mixture was then chilled at -20ºC for either 30 minutes or overnight before it was centrifuged at 14 000 ×g for 15 minutes. Thereafter, the pellet was washed with 70% ethanol and centrifuged for an additional 5 minutes. The residual ethanol was removed, and the pellet was air-dried before being resuspended in an appropriate volume of nuclease-free water.

5.4. Tissue culture

Reagents:

1000× pen/strep (100 000 U/ml; 100 000 µg/ml)

To prepare the solution, 0.9 g of penicillin and 1.5 g of streptomycin was dissolved in 15 ml of PBS. The solution was filter sterilised and stored in 0.5 ml aliquots at -20 ºC.

200× HEPES (1 M)

The solution was prepared by dissolving 11.92 g of HEPES in 25 ml of distilled water. Thereafter, the solution was filter sterilised and stored in 500 µl aliquots at -20ºC.

1000× Insulin (5 mg/ml)

Twenty-five milligrams of insulin (Life Technologies, CA, US) was added to 5 ml of HCl (5 mM) and filter sterilised. The solution was stored in 500 µl aliquots at -20ºC.

1000× Hydrocortisone (50 mM)

The solution was prepared by dissolving 0.18 g of hydrocortisone in 10 ml of methanol. Thereafter, the solution was filter sterilised and stored in 500 µl aliquots at 4ºC.

1000× G418 (Geneticin) (400 mg/ml)

Five grams of G418 (Life Technologies, CA, US) was dissolved in 8.99 ml of PBS and filter sterilised. The solution was stored in 500 µl aliquots at 4ºC.

Saline-EDTA solution (0.01% EDTA)

The solution was prepared by adding 1 ml of filter sterilised 10% EDTA to 1 litre of saline.

DMEM stock

Five sachets of DMEM high glucose powder (Life Technologies, CA, US) was dissolved with 18.5 g of $NaHCO_3$ in 4705 ml of sterile water, and then adjusted to a pH of 6.7-6.8. The solution was filter sterilised into 500 ml bottles using the Pall VacuCap 90 PF (PALL Life Sciences, NY, USA) vacuum filtration device and incubated overnight at 37ºC to observe contamination. The DMEM stock solution was stored at 4ºC.

Complete DMEM

To make 500 ml, 0.5 ml of 1000× pen/strep was added to 50 ml of FBS (Sigma, SL, USA) and filter sterilised (0.22 µm filter) into 449.5 ml of DMEM stock. The complete DMEM solution was stored at 4ºC.

Complete DMEM/F12

To make 500 ml, 2.5 ml of 200× HEPES, 1 ml of 1000× pen/strep, 500 µl 1000× hydrocortisone, 500 µl 1000× insulin and 500 µl 1000× G418 was added to 50 ml of FBS (Sigma, SL, USA) and filter sterilised (0.22 µm filter) into 442.5 ml of DMEM/F12 (Life Technologies, CA, US). The complete DMEM/F12 solution was stored at 4ºC.

5.5. Northern blot hybridisation

Reagents:

10× TBE buffer

Fifty-five grams of Boric acid and 108 g of Tris Base was dissolved in 900 ml of DEPC water. Thereafter, 40 ml of 0.5 M EDTA was added, and the solution was adjusted to a pH of 8.0. The solution was then autoclaved for 20 minutes at 121°C and 1 kg/cm^2 and stored at room temperature.

10% APS (Ammonium persulphate solution)

The solution was prepared by dissolving 0.1g of ammonium persulfate in 1 ml of sterile water.

20× SSC buffer (Saline-sodium citrate buffer)

To prepare 500 ml, 87.66 g of sodium chloride and 44.11 g of sodium citrate was dissolved in 400 ml of distilled water. The solution was adjusted to a pH of 7.0 with HCl and made to a final volume of 500 ml with distilled water. Thereafter, the solution was autoclaved for 20 minutes at 121°C and 1 kg/cm^2 and stored at room temperature.

10% SLS buffer (Sodium lauryl sulphate buffer)

Fifty grams of sodium lauryl sulphate was dissolved in distilled water to a final volume of 500 ml and stored at room temperature.

Low stringency wash buffer

To prepare 70 ml, 37.5 ml of distilled water, 7.5 ml of 20× SSC buffer and 0.75 ml of 10% SLS buffer was added in order and made to a final volume of 75 ml with distilled water.

High stringency wash buffer

To prepare 50 ml, 25 ml of distilled water, 1.25 ml of 20× SSC buffer and 0.5 ml of 10% SLS buffer was added in order and made to a final volume of 75 ml with distilled water.

5.6. Supplementary figures

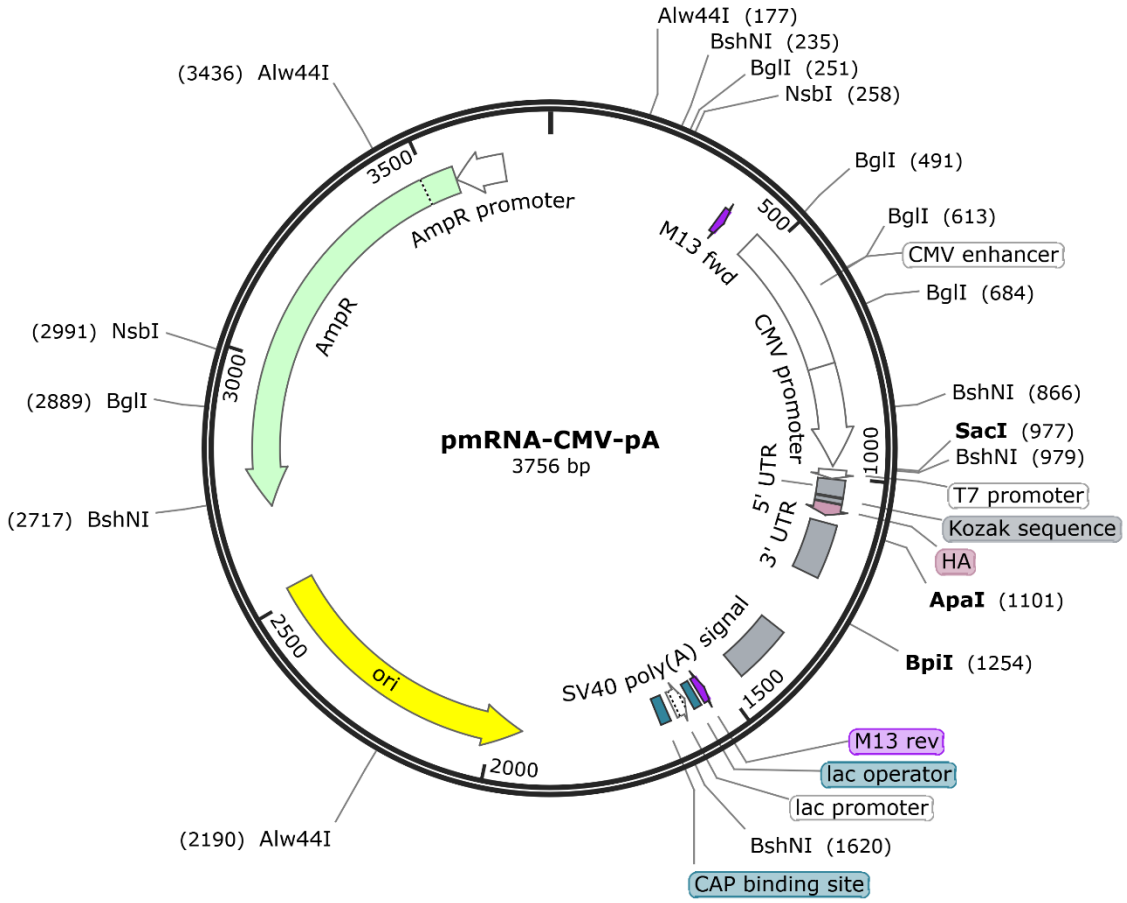


Figure S1: pmRNA-CMV-pA plasmid map. The pmRNA-CMV-pA plasmid has a T7 promoter, a 5' UTR, a Kozak sequence, an HA tag and a 3' UTR with a poly(A) site for the expression of in vitro transcribed RNA. It also has a CMV promoter and a pA signal flanking these sequences to allow expression of the transgene directly from the plasmid. *Bsh*NI, *Alw*44I, *Sac*I, *Apa*I and *Bpi*I enzyme cleavage sites are indicated on the plasmid map. *Bsh*NI has five cleavage sites, *Alw*44I has three cleavage sites, *Sac*I cleaves before the T7 promoter, *Apa*I cleaves at the start of the 3' UTR and *Bpi*I cuts within the poly(A) sequence and is used for linearisation. The plasmid map was created using SnapGene®.

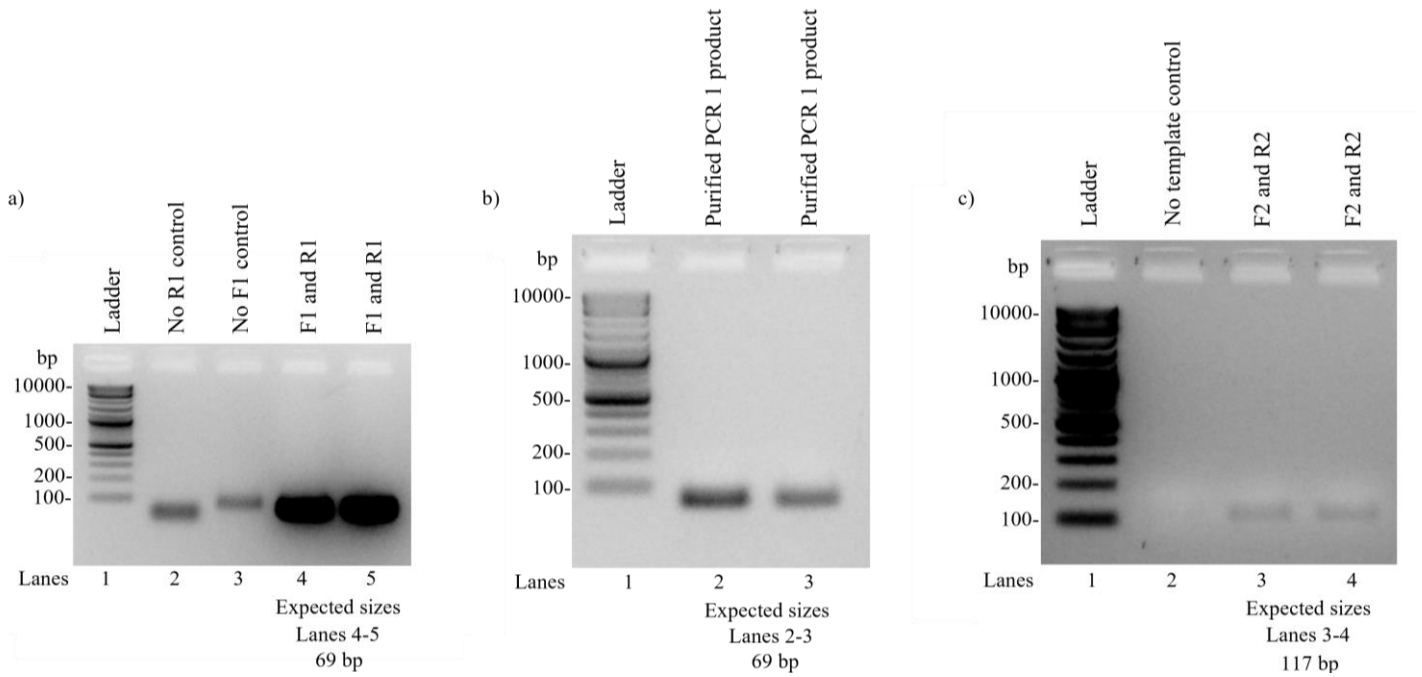


Figure S2: Generation of the double-stranded insert. The double-stranded insert was generated in two separate PCR extension reactions with F1, R1, F2 and R2 oligonucleotides as primers. (a) The amplicons from the first PCR were resolved on a 2% agarose gel. Lane 1: 1 kb plus DNA ladder (New England Biolabs, MA, US). Lane 2: control which excluded the R1 primer. Lane 3: control which excluded the F1 primer. Lanes 4 and 5: PCR products which contained the F1 and R1 primers. (b) The amplicons from the first PCR were purified and visualised on a 2% agarose gel to assess the integrity of the purified constructs. Lane 1: 1 kb plus DNA ladder (New England Biolabs, MA, US). Lanes 2 and 3: purified products from the first PCR. (c) The amplicons from the first PCR were used as templates in the second reaction and the resulting products were resolved on a 2% agarose gel. Lane 1: 1 kb plus DNA ladder (New England Biolabs, MA, US). Lane 2: no template control which excluded the PCR products from the first PCR. Lanes 3 and 4: PCR products from the second PCR which contained the F2 and R2 primers.

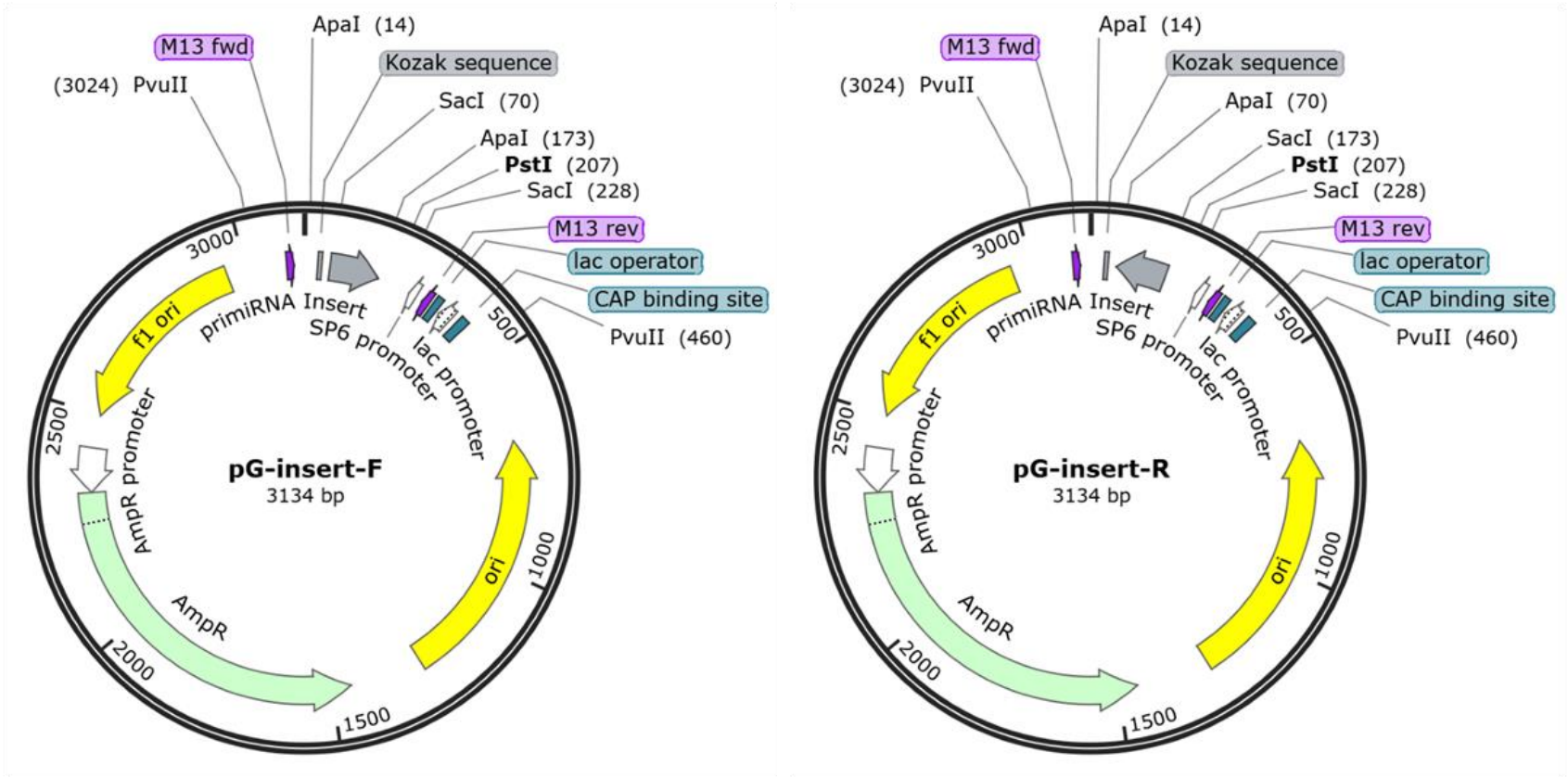


Figure S3: pG-insert plasmid maps. The pG-insert plasmid maps were generated by joining the pGEM®-T Easy vector with the generated insert in the forward orientation to create the pG-insert-F map and in the reverse orientation to create the pG-insert-R map. *Pvu*II, *Apa*I, *Sac*I, and *Pst*I enzyme cleavage sites are indicated on the plasmid maps. The plasmid maps were created using SnapGene®.

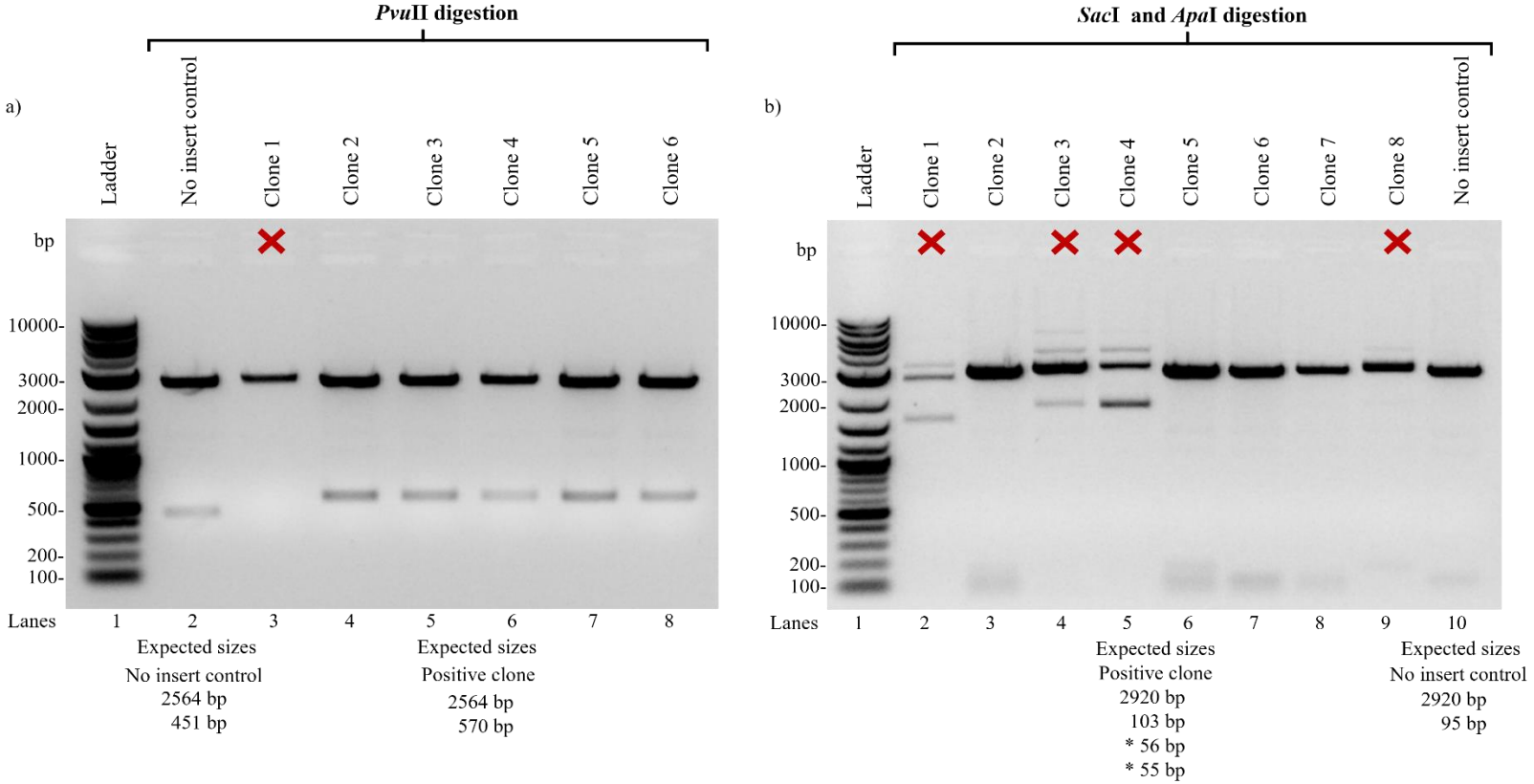


Figure S4: Screening for pG-insert positive clones after the purified insert was ligated into pGEM®-T Easy vector. The purified insert was ligated into the pGEM®-T Easy vector, and the subsequent pG-insert clones were screened with (a) *Pvu*II on a 1% agarose gel and (b) *Sac*I and *Apa*I on a 1% agarose gel. (a) and (b) The red cross indicates the clones with the incorrect banding pattern. Lane 1: 1 kb plus DNA ladder (New England Biolabs, MA, US). (a) Lane 2: no insert control plasmid digested with *Pvu*II. Lanes 3 to 8: clones digested with *Pvu*II. (b) Lanes 2 to 9: clones digested with *Sac*I and *Apa*I. Lane 10: no insert control plasmid digested with *Sac*I and *Apa*I. The asterisk indicates the fragments that were not visible on the gel which was likely due to the extended electrophoresis run time that may have caused these bands to fade and disappear completely.

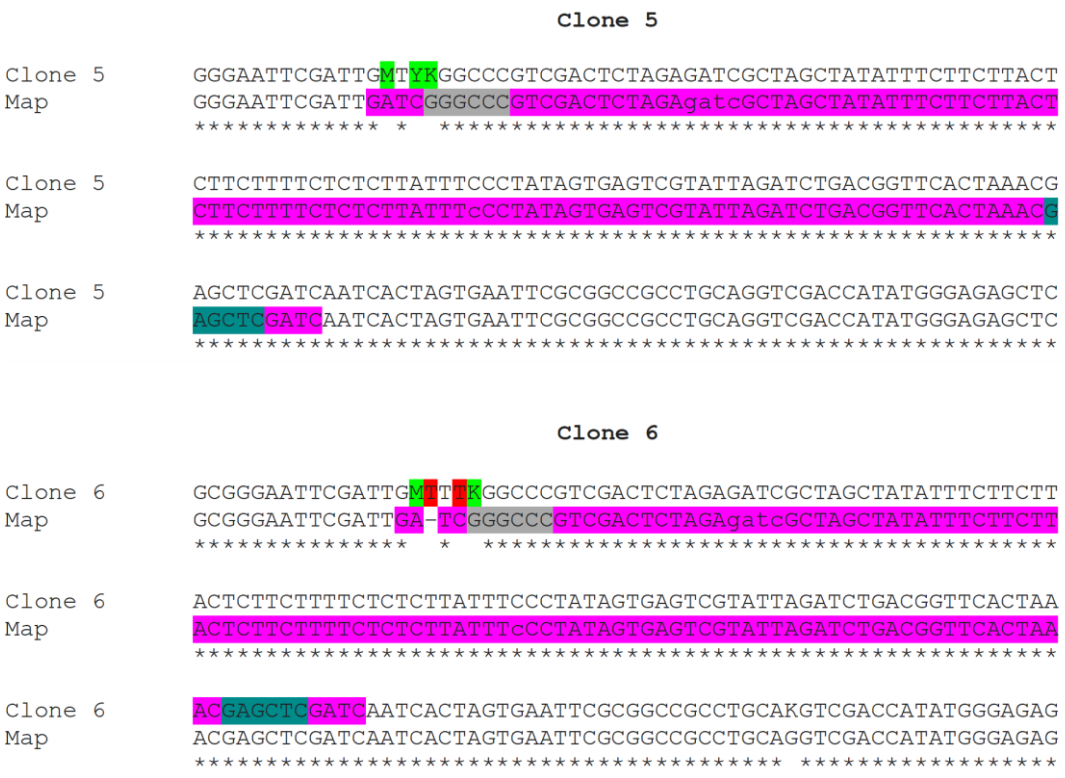


Figure S5: Sequencing analysis of the insert region of clone 5 and 6. Sequence alignment comparing the chromatography data obtained from clones 5 and 6 to the pG-insert-R plasmid map. Sequencing was performed from the M13 forward primer. The sequences highlighted in pink indicate the insert. The sequences highlighted in grey and teal within the insert sequences indicate the *Apa*I and *Sac*I restriction sites respectively. The letters highlighted in green indicate the ambiguous bases with a signal of the correct base whereas the letters highlighted in red indicate the ambiguous bases without a signal of the correct base.

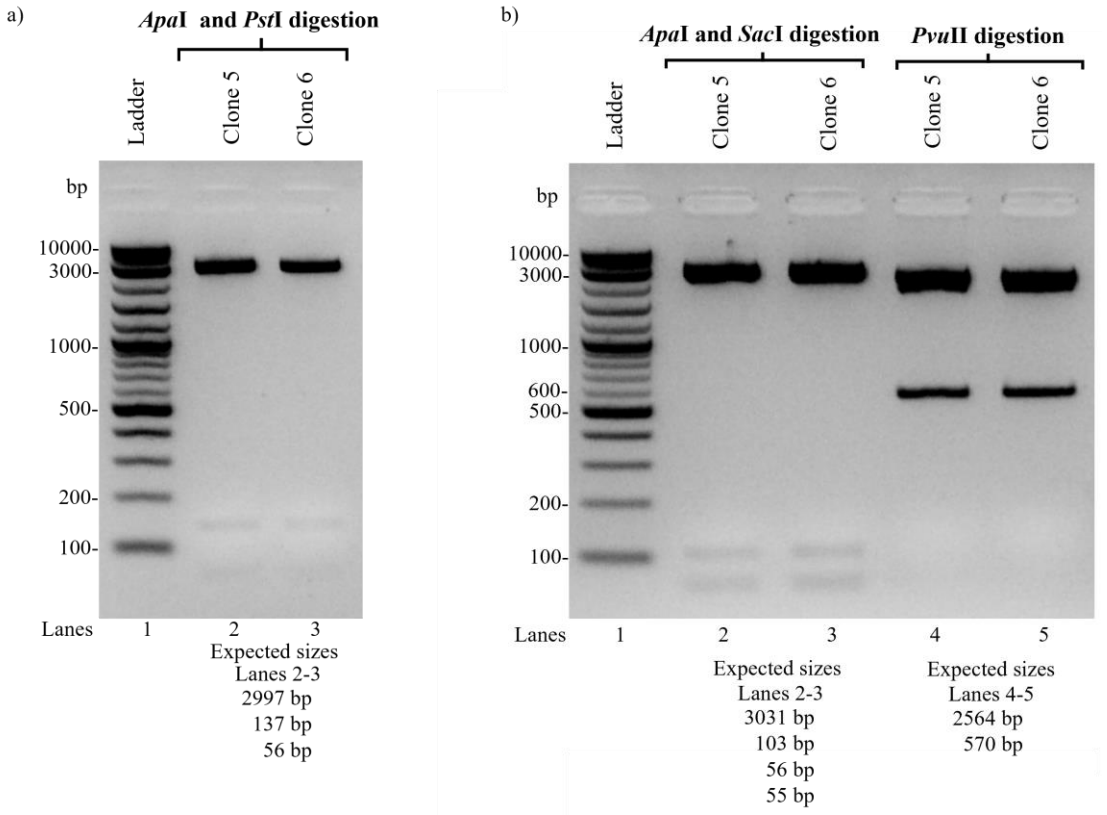


Figure S6: Screening of clone 5 and clone 6 using *Apa*I and *Pst*I to ensure recognition of the *Apa*I cleavage site after propagation and purification. Confirmed positive pG-insert-R clones were screened with *Apa*I and *Pst*I simultaneously on a 2% agarose gel to ensure recognition of the *Apa*I cleavage site (a) Lane 1: 1 kb plus DNA ladder (New England Biolabs, MA, US). Lane 2: clone 5 digested with *Apa*I and *Pst*I. Lane 3: clone 6 digested with *Apa*I and *Pst*I. (b) Clones 5 and 6 were propagated, purified, and screened by restriction enzyme digestion on a 2% agarose gel. Lane 1: 1 kb plus DNA ladder (New England Biolabs, MA, US). Lane 2: clone 5 digested with *Apa*I and *Sac*I. Lane 3: clone 6 digested with *Apa*I and *Sac*I. Lane 4: clone 5 digested with *Puv*II. Lane 5: clone 6 digested with *Puv*II.

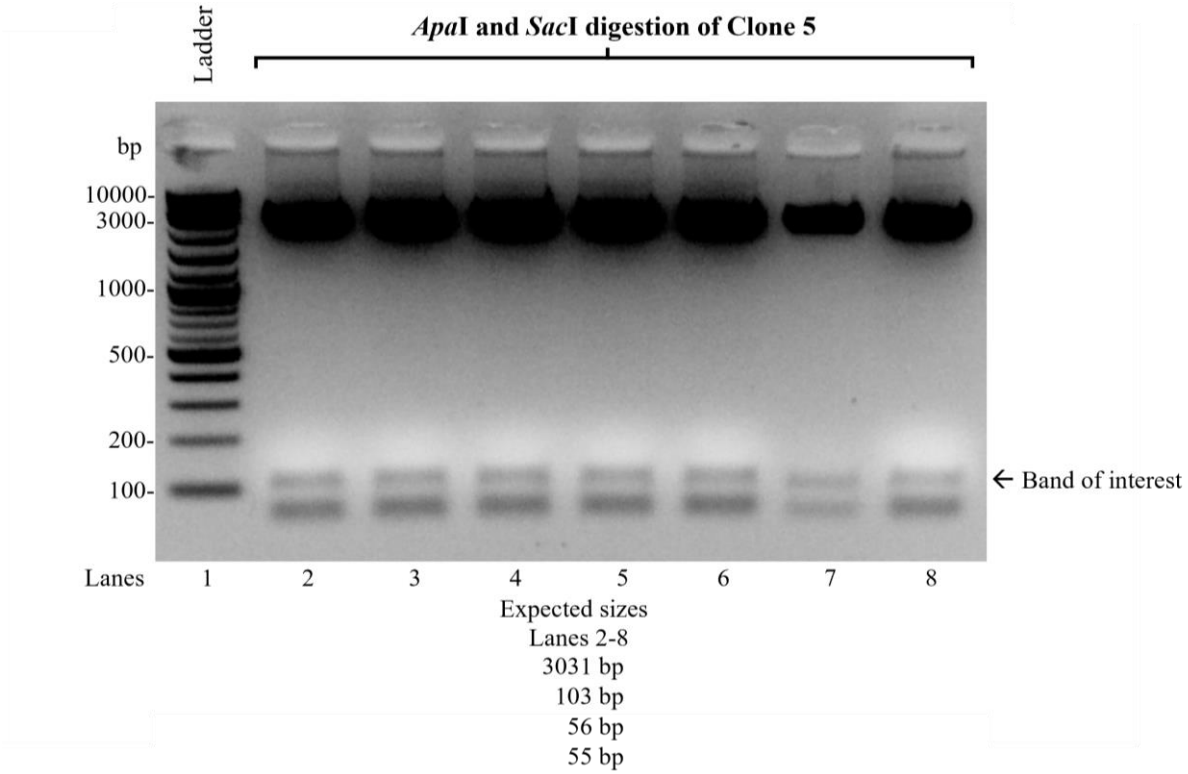


Figure S7: Restriction enzyme digestion of clone 5 using *Apa*I and *Sac*I to separate the insert from the pG-insert-R vector. Clone 5 was digested with *Apa*I and *Sac*I simultaneously to separate the insert from the vector and to create overhangs that were compatible with the overhangs of the pmRNA-CMV-pA plasmid backbone. The fragments were run on a 2% agarose gel. Lane 1: 1 kb plus DNA ladder (New England Biolabs, MA, US). Lanes 2 to 8: clone 5 digested with *Apa*I and *Sac*I. The band of interest which denoted the 103 bp insert was indicated with the arrow.

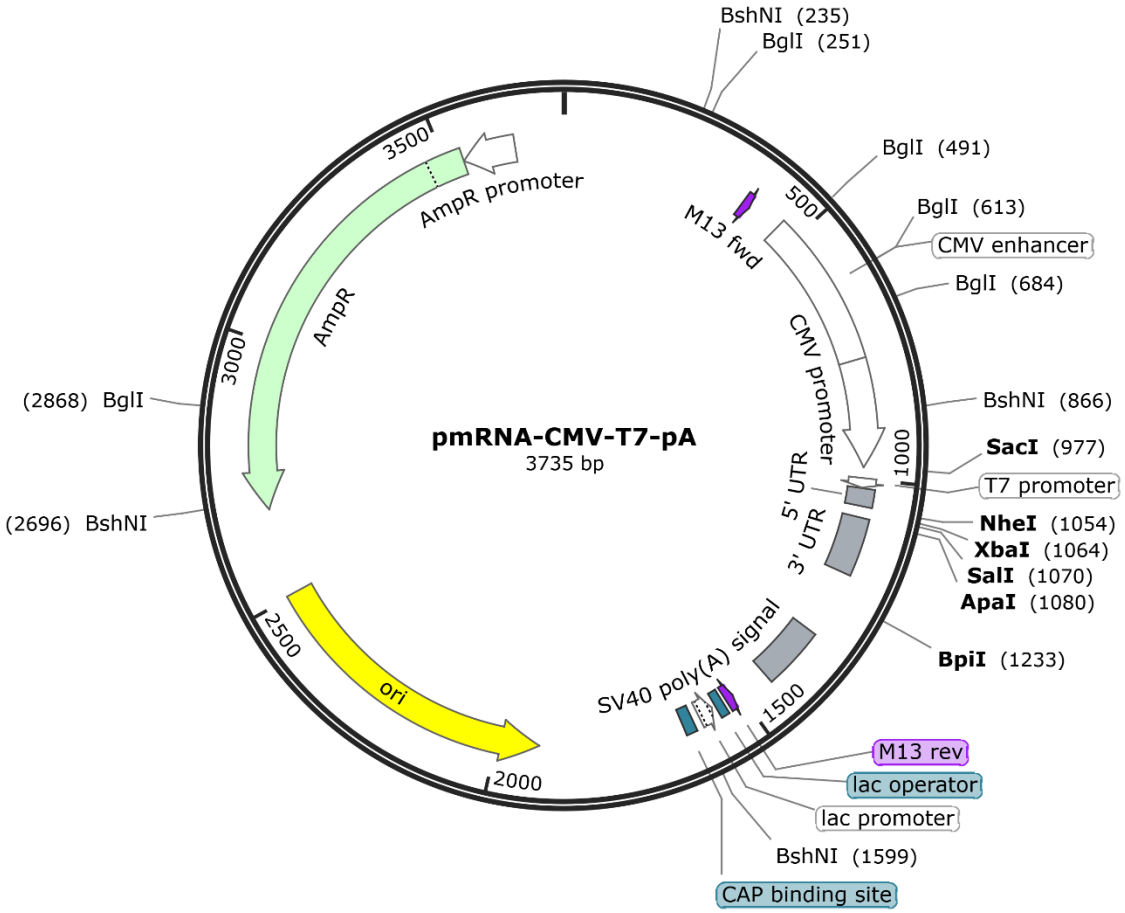


Figure S8: pmRNA-CMV-T7-pA plasmid map. The pmRNA-CMV-T7-pA plasmid map was generated by joining the pmRNA-CMV-pA backbone sequence with the generated insert sequence. *Bsh*NI, *Bgl*I, *Sac*I, *Nhe*I, *Xba*I, *Sal*I, *Apa*I and *Bpi*I enzyme cleavage sites are indicated on the plasmid map. The plasmid map was created using SnapGene®.

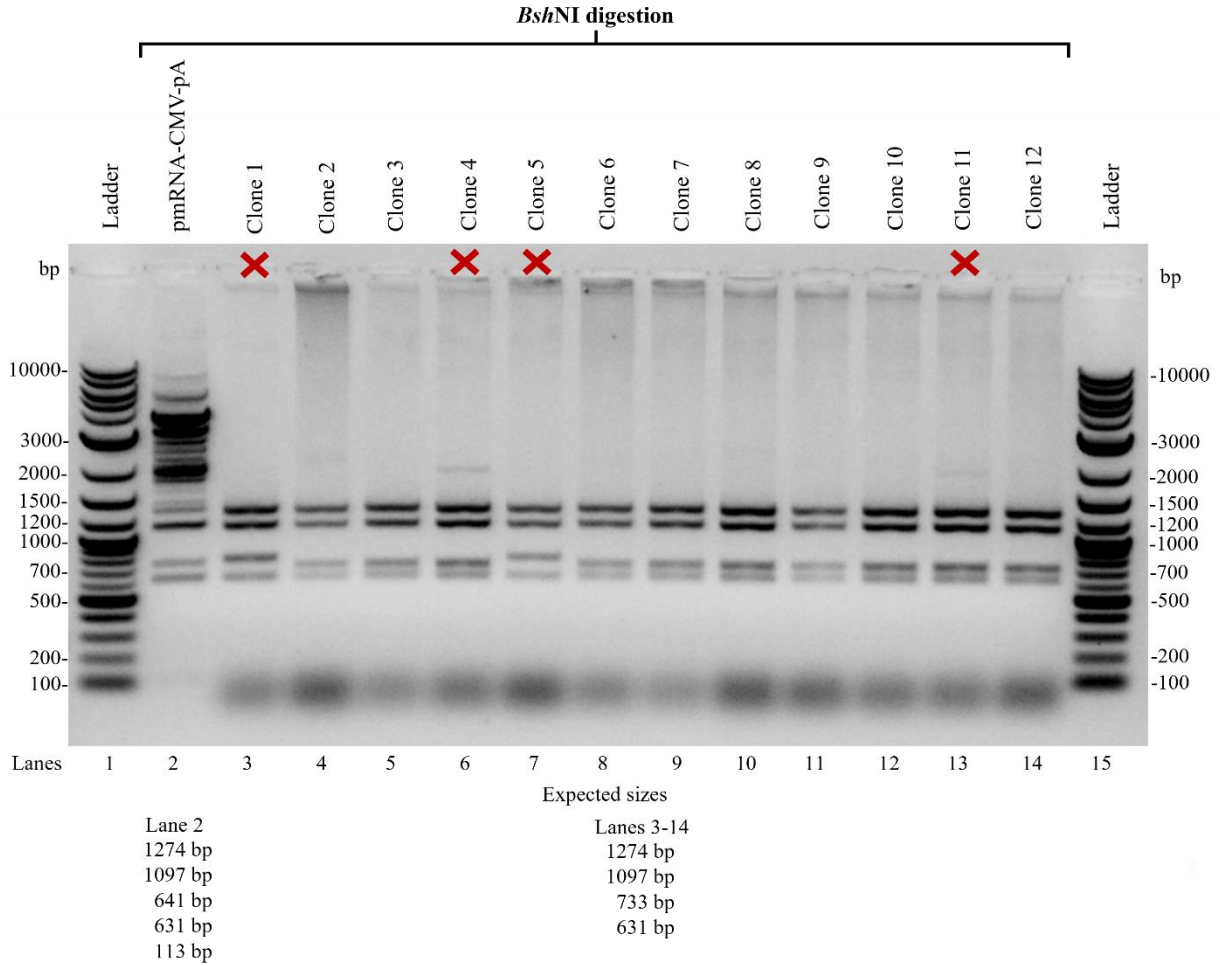


Figure S9: pmRNA-CMV-T7-pA clones screened with *Bsh*NI. The isolated insert was ligated into the pmRNA-CMV-pA backbone to create the pmRNA-CMV-T7-pA plasmid and the subsequent clones were screened with *Bsh*NI on a 1% agarose gel. Lane 1 and 15: 1 kb plus DNA ladder (New England Biolabs, MA, US). Lane 2: pmRNA-CMV-pA plasmid digested with *Bsh*NI. Lanes 3 to 14: clones digested with *Bsh*NI.

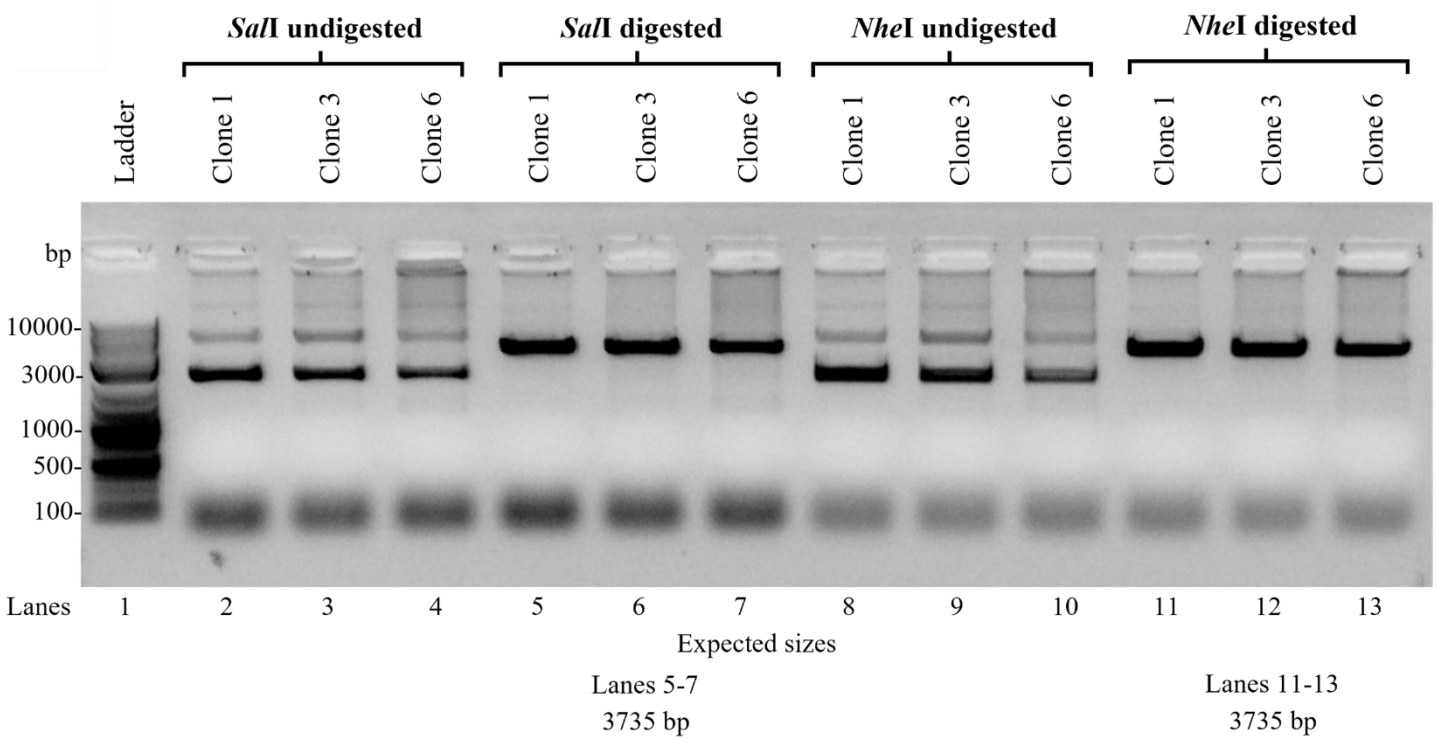


Figure S10: pmRNA-CMV-T7-pA clones digested with *Sal*I and *Nhe*I. The isolated insert was ligated into the pmRNA-CMV-pA backbone to create the pmRNA-CMV-T7-pA plasmid and the subsequent clones were digested with *Sal*I and *Nhe*I separately to ensure that the enzymes were able to recognise these restriction sites. Lane 1: 1 kb plus DNA ladder (New England Biolabs, MA, US). Lane 5 to 7: clones digested with *Sal*I. Lanes 11 to 13: clones digested with *Nhe*I. Lanes 2 to 4 and 8 to 10: undigested controls.

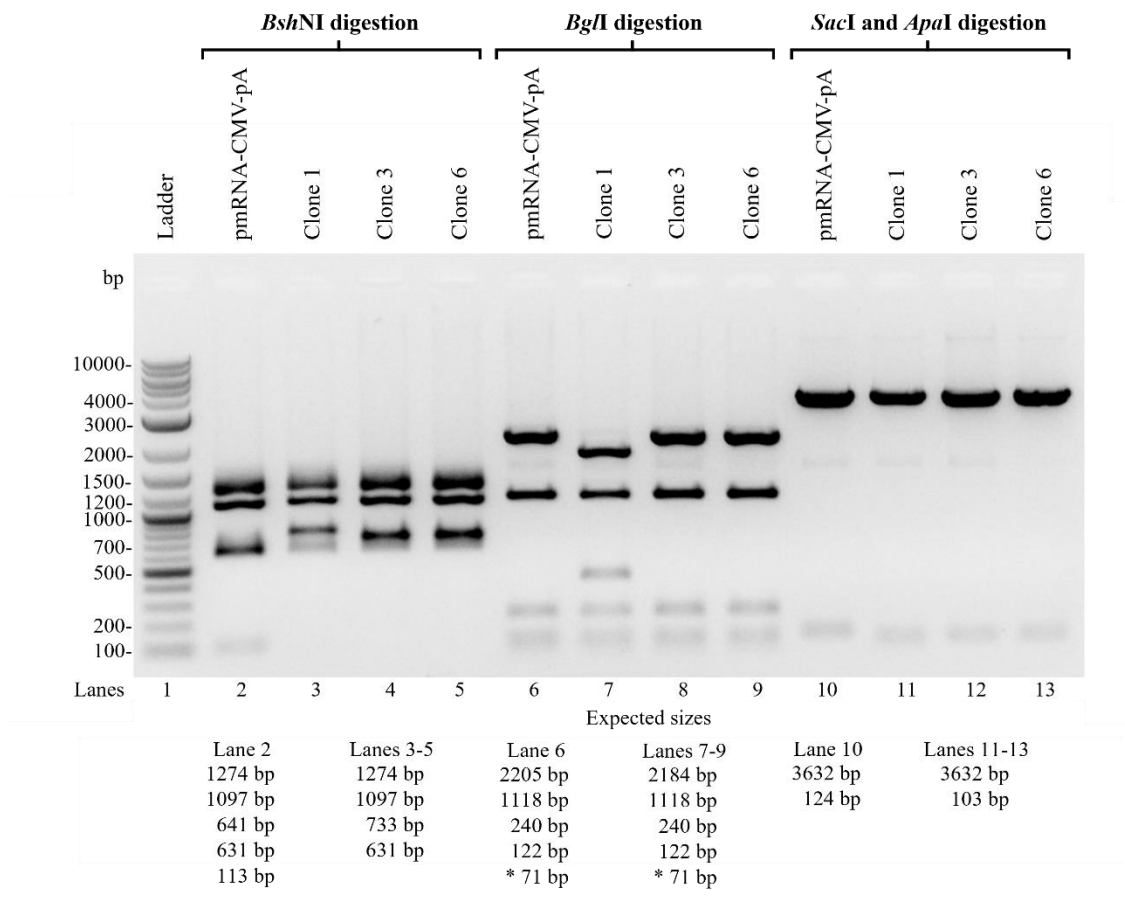


Figure S11: pmRNA-CMV-T7-pA clones screened with *Bsh*NI and *Bgl*I separately and *Sac*I and *Apa*I simultaneously. The pmRNA-CMV-T7-pA clones were screened with *Bsh*NI and *Bgl*I separately and *Apa*I and *Sac*I simultaneously. Lane 1: 1 kb plus DNA ladder (New England Biolabs, MA, US). Lane 2: pmRNA-CMV-pA plasmid digested with *Bsh*NI. Lanes 3 to 5: clones digested with *Bsh*NI. Lane 6: pmRNA-CMV-pA plasmid digested with *Bgl*I. Lanes 7 to 9: clones digested with *Bgl*I. Lane 10: pmRNA-CMV-pA plasmid digested with *Apa*I and *Sac*I. Lanes 11 to 13: clones digested with *Apa*I and *Sac*I. The asterisk indicates the fragments that were not visible on the gel which was likely due to the extended electrophoresis run time that may have caused these bands to fade and disappear completely.

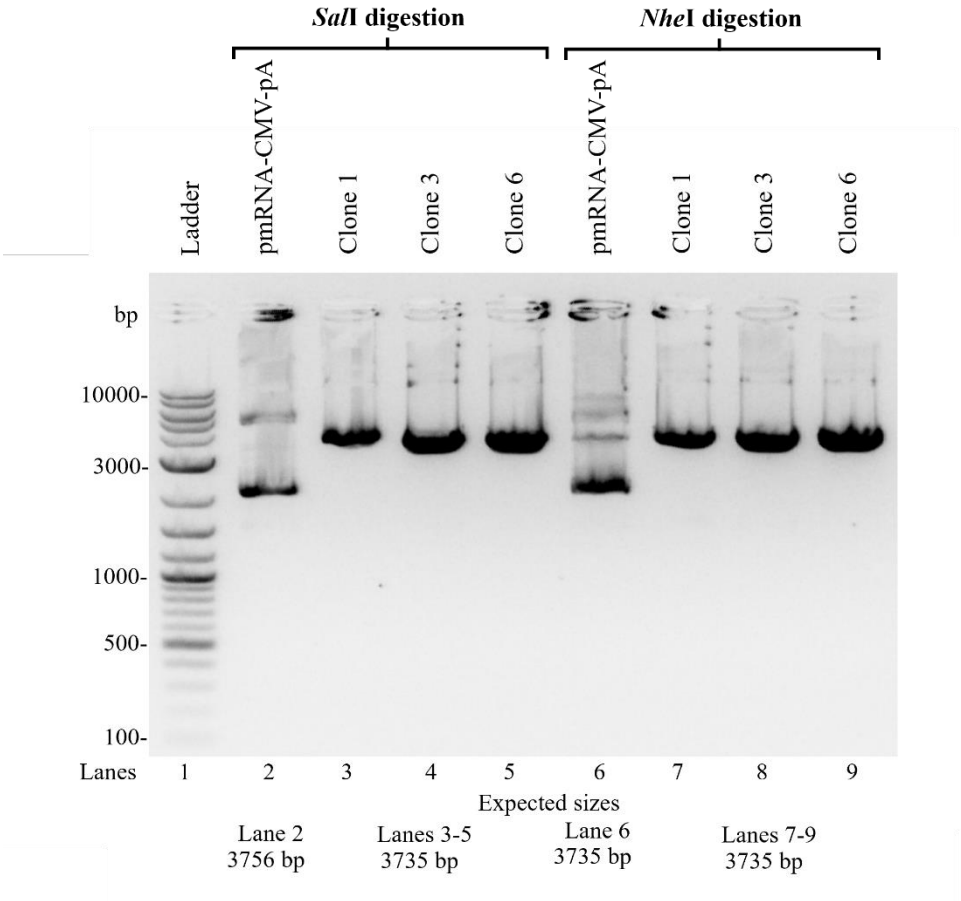


Figure S12: pmRNA-CMV-T7-pA clones screened with *Sal*I and *Nhe*I separately. The pmRNA-CMV-T7-pA clones were screened with *Nhe*I and *Sal*I. Lane 1: 1 kb plus DNA ladder (New England Biolabs, MA, US). Lane 2: pmRNA-CMV-pA plasmid digested with *Sal*I. Lanes 3 to 5: clones digested with *Sal*I. Lanes 6: pmRNA-CMV-pA plasmid digested with *Nhe*I. Lanes 7 to 9: clones digested with *Nhe*I.

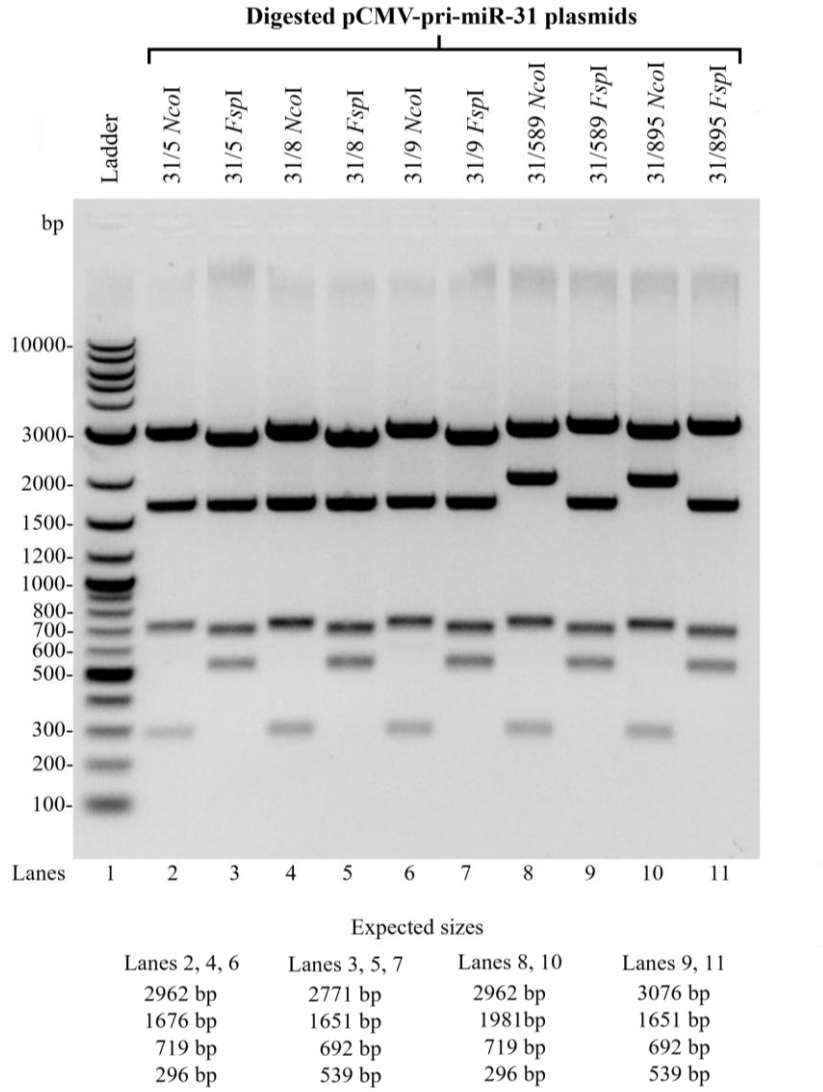


Figure S13: Identification of the pCMV-pri-miR-31 plasmids. The pCMV-pri-miR-31/5, pCMV-pri-miR-31/8, pCMV-pri-miR-31/9, pCMV-pri-miR-31/589 and pCMV-pri-miR-31/895 plasmids were screened with *Nco*I and *Fsp*I separately to confirm the identity of the plasmids. Lane 1: 1 kb plus DNA ladder (New England Biolabs, MA, US). Lanes 2 to11: pCMV-pri-miR-31 plasmids digested with *Nco*I and *Fsp*I separately.

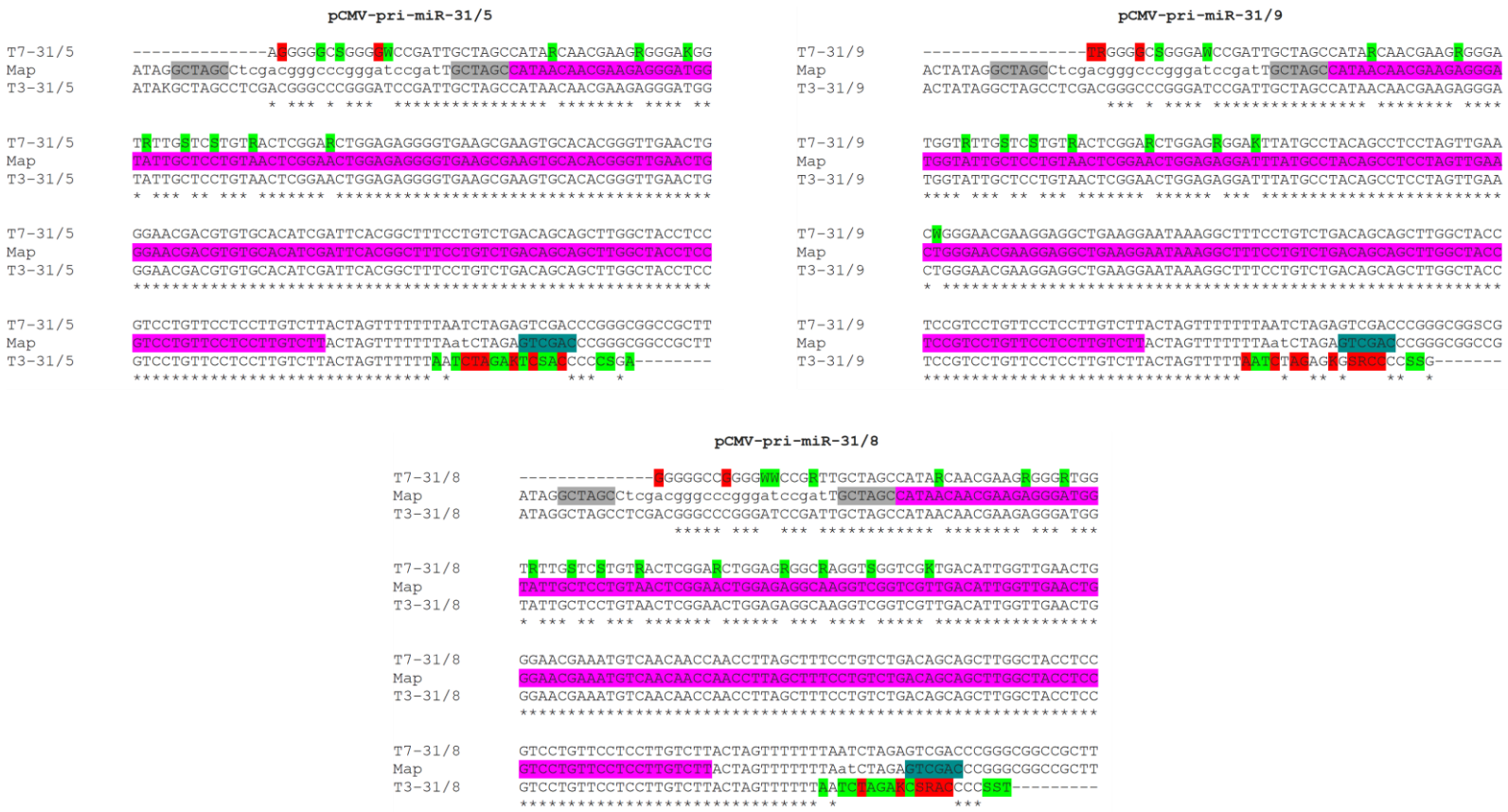


Figure S14: Sequencing analysis of the pri-miR-31 encoding region of the monomeric pCMV-pri-miR-31 expression vectors. Sequence alignment comparing the chromatography data obtained to the respective pCMV-pri-miR-31 plasmid maps. Sequencing was performed in the forward direction from the T7 promoter and in the reverse direction from the T3 promoter. The chromatography data obtained from the T3 promoters were reverse complemented. The sequences highlighted in pink indicate the pri-miR-31 encoding regions. The sequences highlighted in grey and teal indicate the *Nhe*I and *Sal*I restriction sites respectively. The letters highlighted in green indicate the ambiguous bases with a signal of the correct base whereas the letters highlighted in red indicate the ambiguous bases without a signal of the correct base.

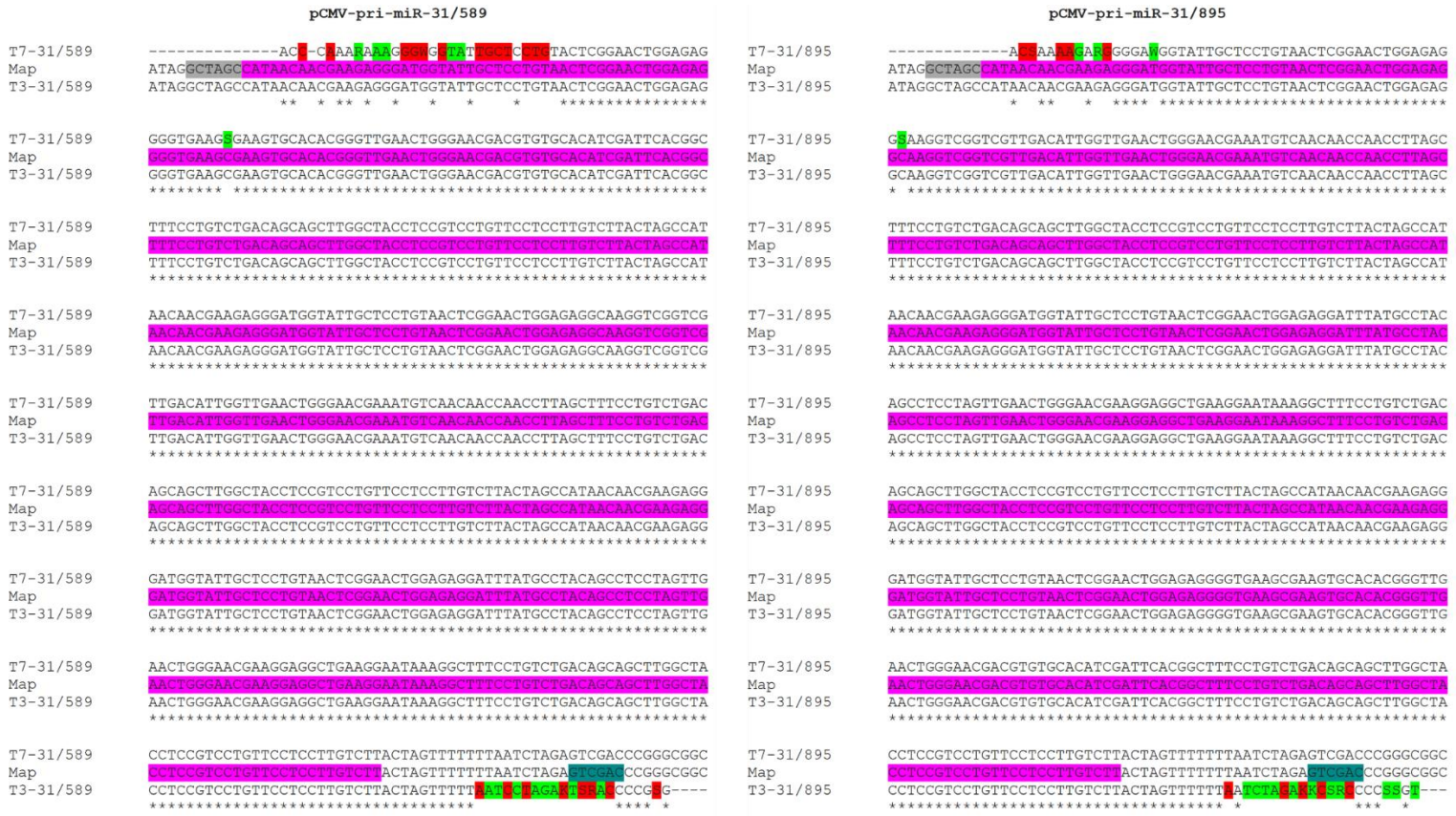


Figure S15: Sequencing analysis of the pri-miR-31 encoding region of the trimeric pCMV-pri-miR-31 expression vectors. Sequence alignment comparing the chromatography data obtained to the respective pCMV-pri-miR-31 plasmid maps. Sequencing was performed in the forward direction from the T7 promoter and in the reverse direction from the T3 promoter. The chromatography data obtained from the T3 promoters were reverse complemented. The sequences highlighted in pink indicate the pri-miR-31 encoding regions. The sequences highlighted in grey and teal indicate the *Nhe*I and *Sal*I restriction sites respectively. The letters highlighted in green indicate the ambiguous bases with a signal of the correct base whereas the letters highlighted in red indicate the ambiguous bases without a signal of the correct base.

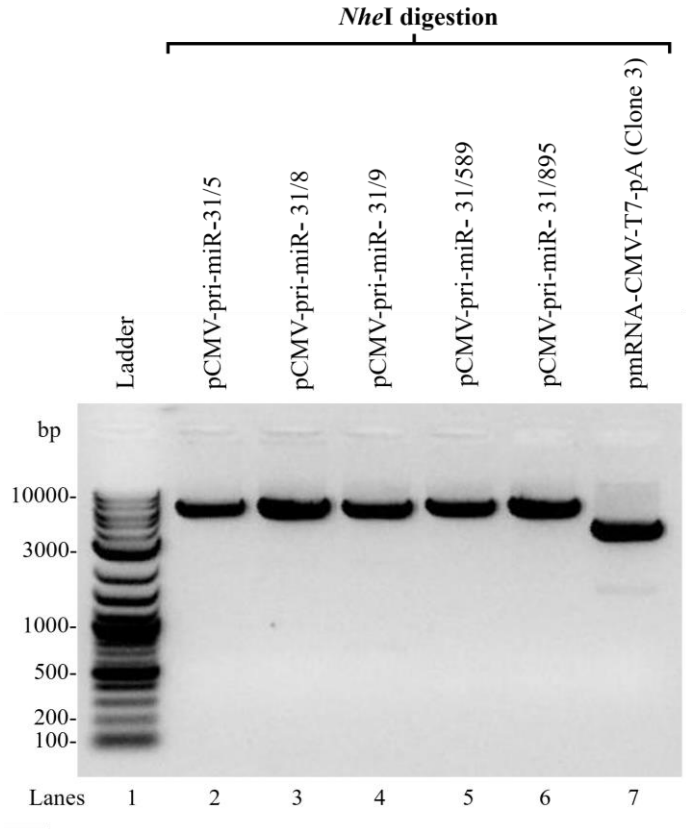


Figure S16: pmRNA-CMV-T7-pA and pCMV-pri-miR-31 plasmids digested with *Nhe*I. The pmRNA-CMV-T7-pA and pCMV-pri-miR-31 plasmids were digested with *NheI* and purified by ethanol precipitation before the fragments were visualised on a 1% agarose gel to assess the integrity of the constructs. Lane 1: 1 kb plus DNA ladder (New England Biolabs, MA, US). Lanes 2 to 6: *NheI* digested pCMV-pri-miR-31 plasmids after purification. Lane 7: *NheI* digested pmRNA-CMV-T7-pA plasmid after purification.

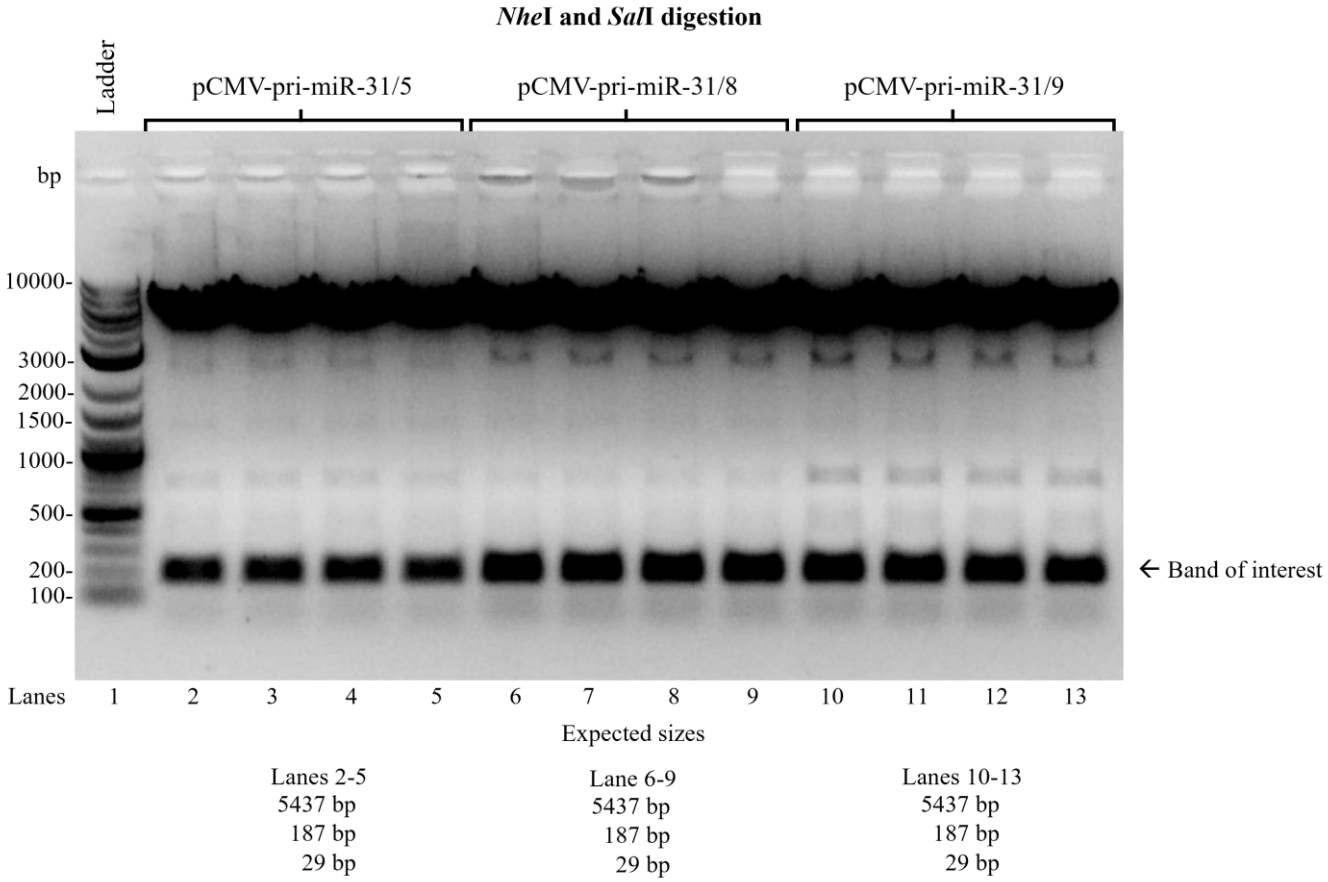


Figure S17: pCMV-pri-miR-31 monomeric expression vectors after digestion with *Nhe*I and *Sal*I. The pCMV-pri-miR-31 monomeric expression vectors were visualised on a 1% agarose gel after digestion with *Nhe*I and *Sal*I. Lane 1: 1 kb plus DNA ladder (New England Biolabs, MA, US). Lanes 2 to 13: pCMV-pri-miR-31 plasmids after digestion with *Nhe*I and *Sal*I. The arrow indicates the bands of interest that contain the respective pri-miR-31 sequences. The unexpected bands may have been a result of star activity.

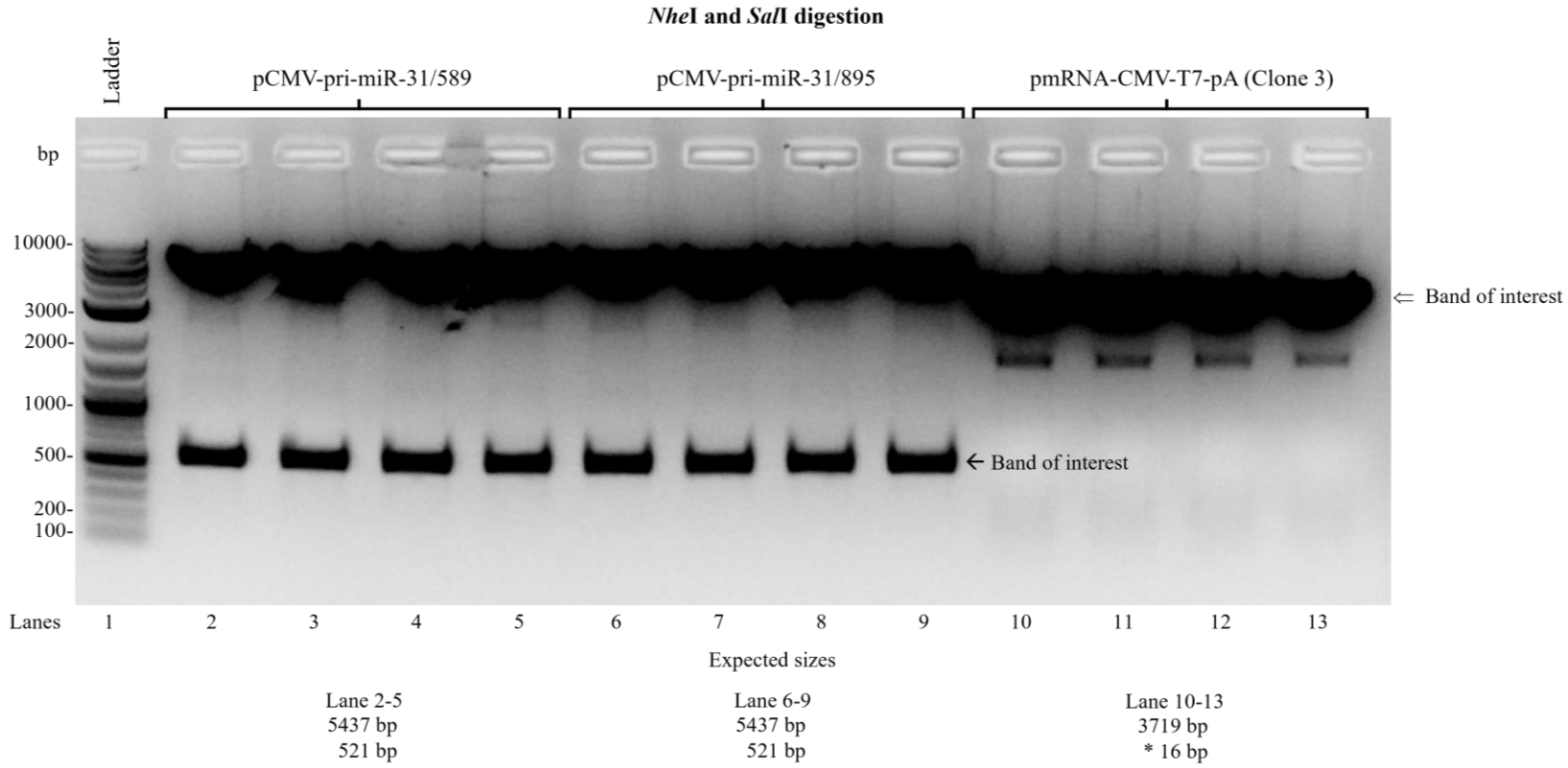


Figure S18: pCMV-pri-miR-31 trimeric expression vectors and pmRNA-CMV-T7-pA plasmid after digestion with *Nhe*I and *Sal*I. The pCMV-pri-miR-31 trimeric expression vectors and pmRNA-CMV-T7-pA plasmid were visualised on a 1% agarose gel after digestion with *Nhe*I and *Sal*I. Lane 1: 1 kb plus DNA ladder (New England Biolabs, MA, US). Lanes 2 to 9: pCMV-pri-miR-31 plasmids after digestion with *Nhe*I and *Sal*I. Lane 10 to 13: pmRNA-CMV-T7-pA plasmid after digestion with *Nhe*I and *Sal*I. The single lined arrow indicates the bands of interest that contain the respective pri-miR-31 sequences. The double lined arrow indicates the bands of interest that contain the pmRNA-CMV-T7-pA plasmid with *Nhe*I and *Sal*I overhangs. The unexpected bands may have been a result of star activity. The asterisk indicates the fragments that were not visible on the gel which was likely due to the extended electrophoresis run time that may have caused these bands to fade and disappear completely.

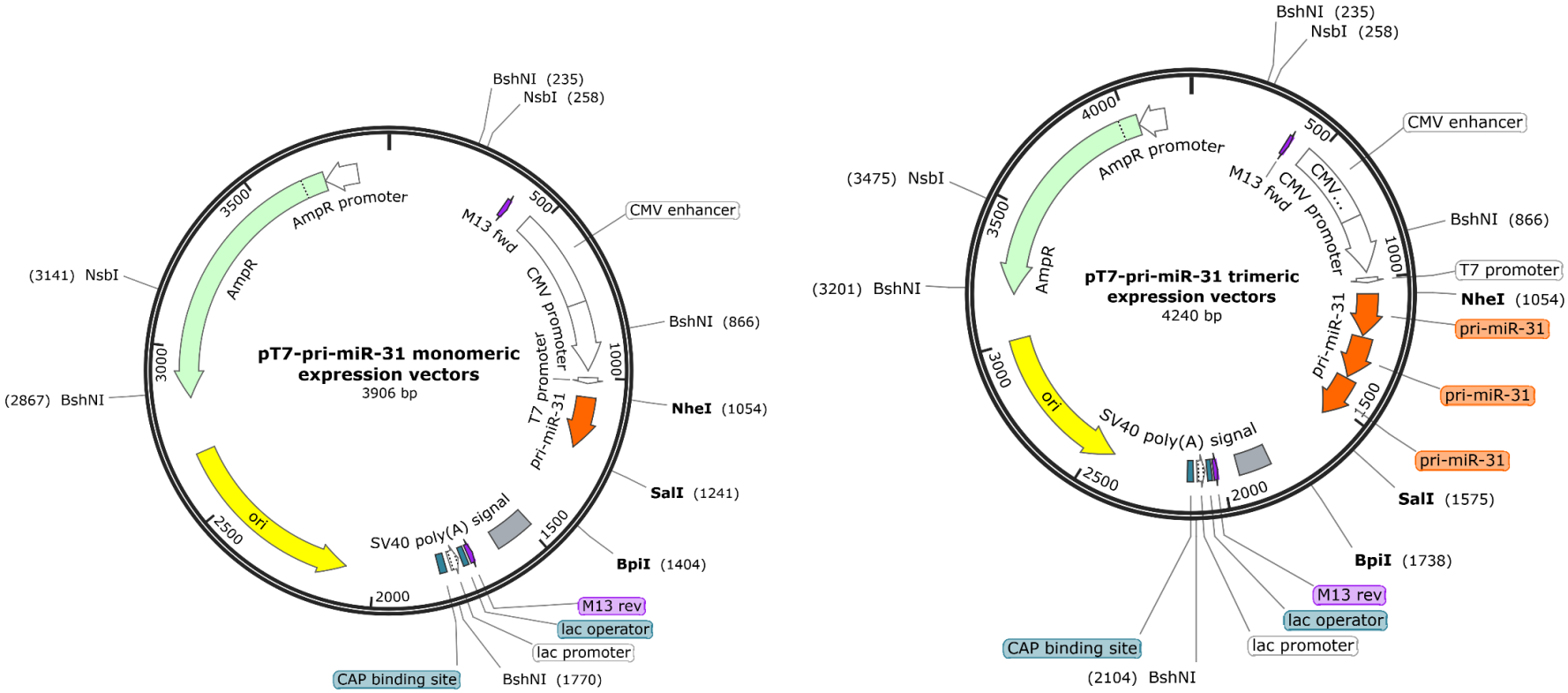


Figure S19: Schematic representation of the pT7-pri-miR-31 expression vectors. The plasmid map on the left represents the pT7-pri-miR-31/5, pT7-pri-miR-31/8 and pT7-pri-miR-31/9 monomeric expression vectors as these plasmids are of the same length and consist of the same sequence except for their respective pri-miR-31 encoding sequence indicated in orange. The plasmid map on the right represents the pT7-pri-31/589 and pT7-pri-31/895 trimeric expression vectors as these plasmids are of the same length and consist of the same sequence except for their respective pri-miR-31 encoding sequence indicated in orange. The plasmid maps were created using SnapGene®.

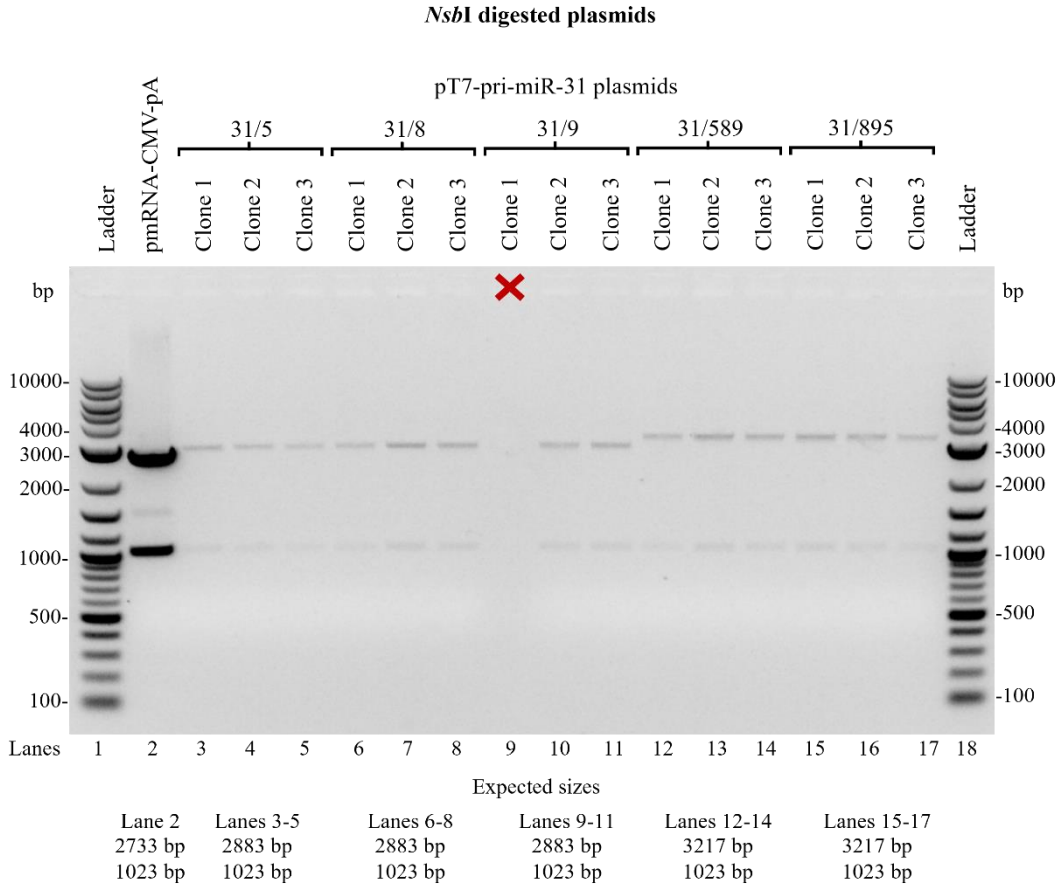


Figure S20: pT7-pri-miR-31 clones screened with *Nsb*I. The pT7-pri-miR-31 clones were digested with *Nsb*I and assessed on a 1% agarose gel to identify the positive clones. Lane 1 and 18: 1 kb plus DNA ladder (New England Biolabs, MA, US). Lane 2: pmRNA-CMV-pA plasmid digested with *Nsb*I. Lanes 3 to 17: pT7-pri-miR-31 clones digested with *Nsb*I.

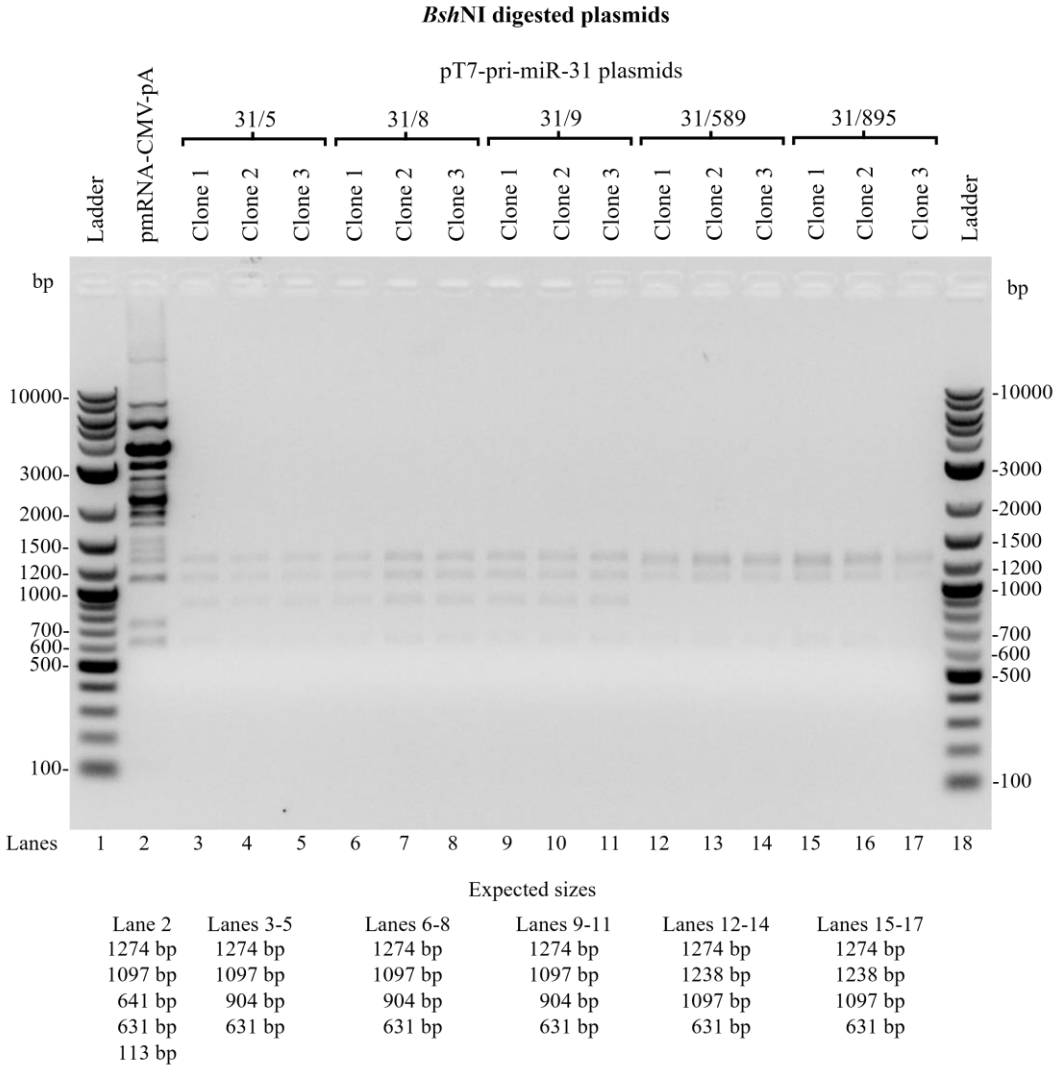


Figure S21: pT7-pri-miR-31 clones screened with *Bsh*NI. The pT7-pri-miR-31 clones were digested with *Bsh*NI and assessed on a 1% agarose gel to identify the positive clones. Lane 1 and 18: 1 kb plus DNA ladder (New England Biolabs, MA, US). Lane 2: pmRNA-CMV-pA plasmid digested with *Bsh*NI. Lanes 3 to 17: pT7-pri-miR-31 clones digested with *Bsh*NI.

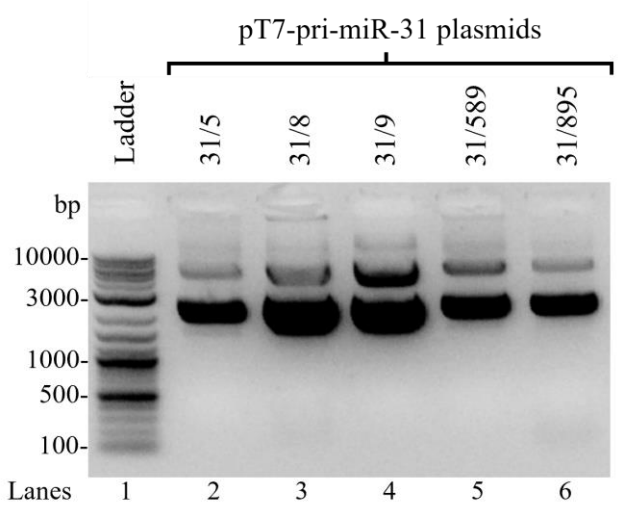


Figure S22: pT7-pri-miR-31 plasmids after propagation and purification. The pT7-pri-miR-31 plasmids were visualised on a 1% agarose gel to assess the integrity of the constructs after propagation and purification. Lane 1: 1 kb plus DNA ladder (New England Biolabs, MA, US). Lanes 2 to 6: purified pT7-pri-miR-31 plasmids.

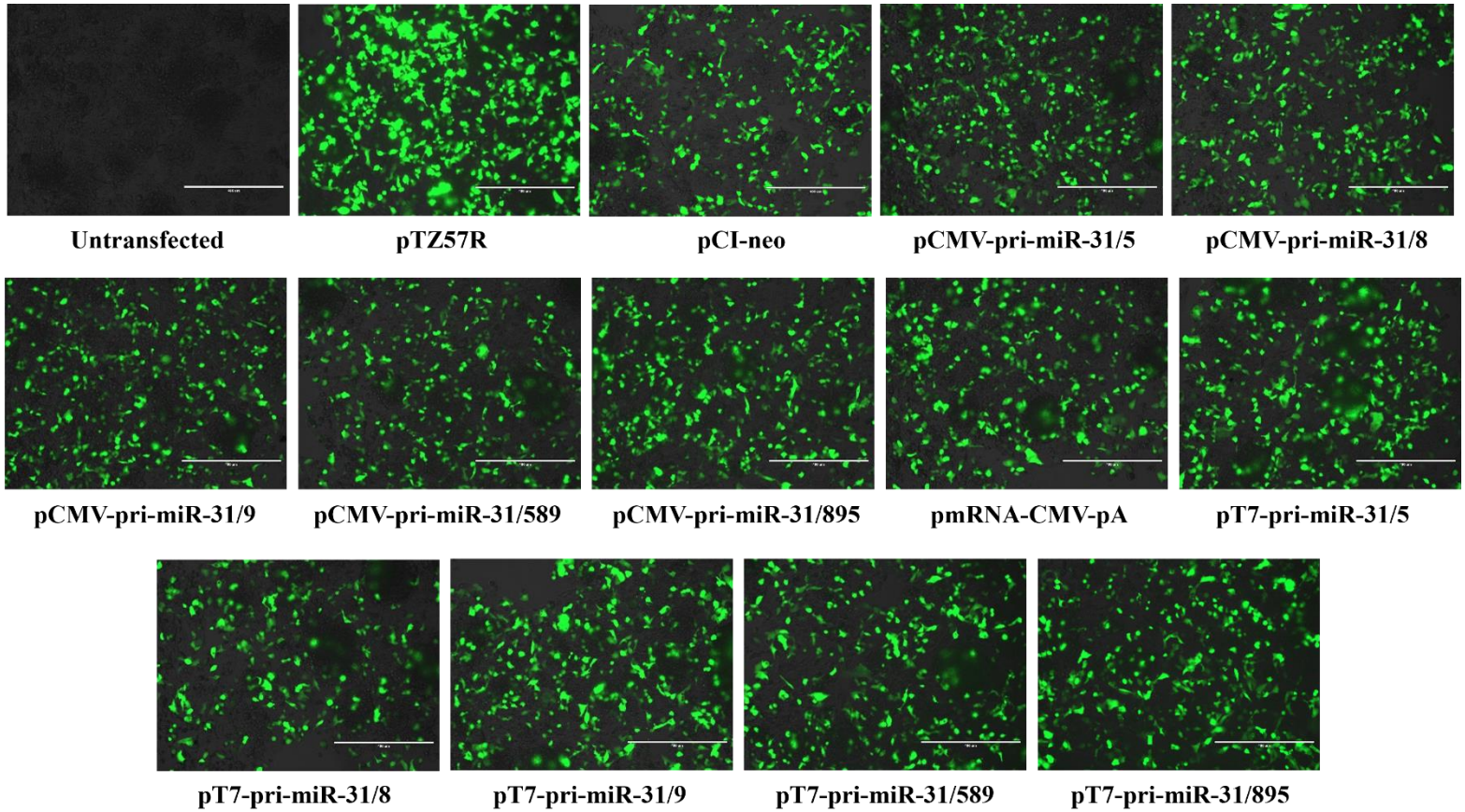


Figure S23: Fluorescence observed in the assay to assess HBV inhibition of the pT7-pri-miR-31 expression vectors. On the day of transfection, HepG2-hNTCP cells were transfected with pCH-9/3091 (target), pCI-neo-eGFP (marker) and an experimental plasmid as indicated. Two days after transfection, the cells were analysed by fluorescence microscopy. The transfections were performed in triplicate and each fluorescent image demonstrated here represents the GFP expression obtained from each of the three wells.

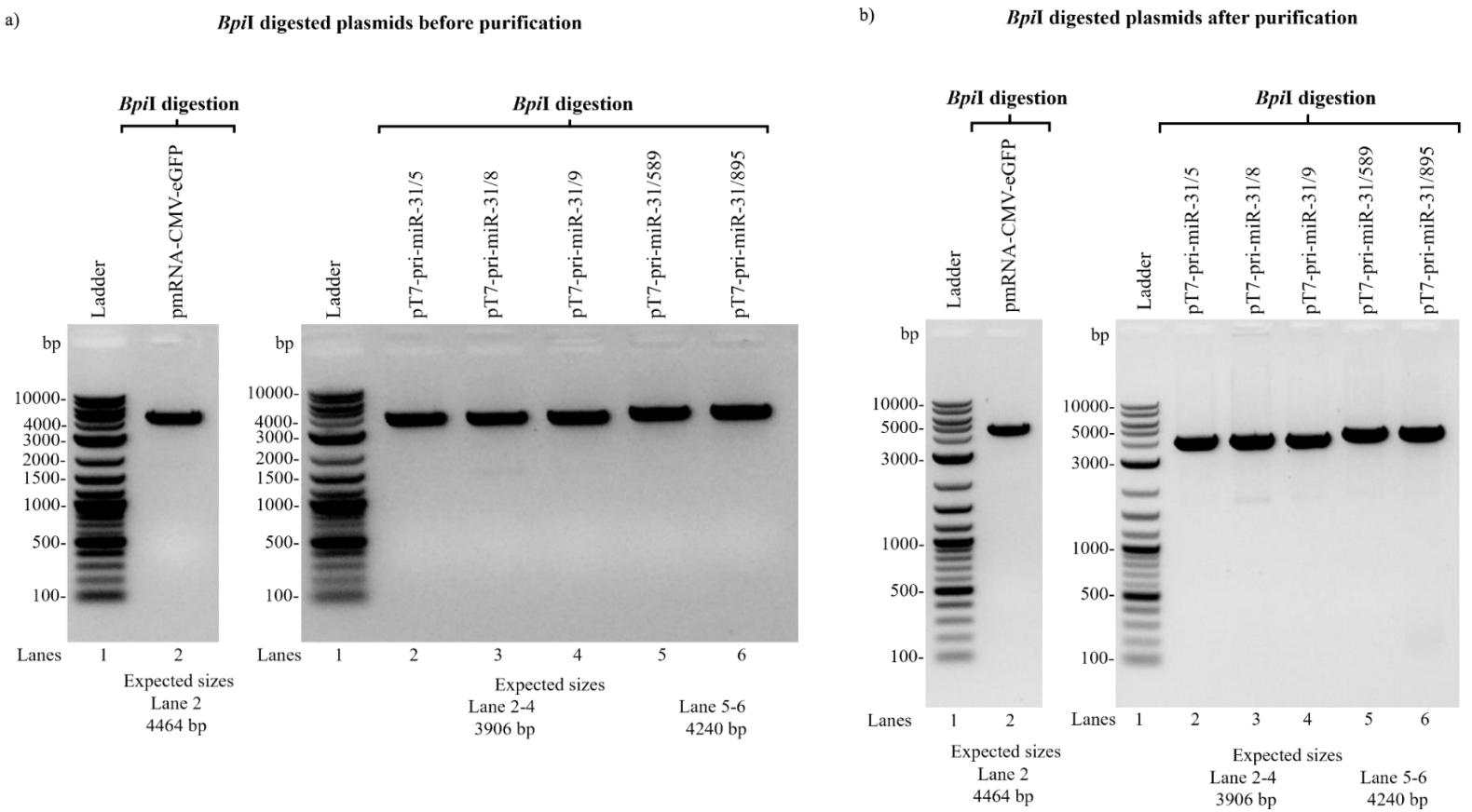


Figure S24: Linearised pT7-pri-miR-31 plasmids before and after purification. (a) The pmRNA-CMV-eGFP-pA and pT7-pri-miR-31 plasmids were digested with *Bpi*I and assessed on a 1% agarose gel to ensure linearisation. Lane 1 (gel 1 and gel 2): 1 kb plus DNA ladder (New England Biolabs, MA, US). Lane 2 (gel 1): pmRNA-CMV-eGFP-pA plasmid digested with *Bpi*I. Lanes 2 to 6 (gel 2): pT7-pri-miR-31 plasmids digested with *Bpi*I. (b) The linearised pT7-pri-miR-31 plasmids were purified and resolved on a 1% agarose gel to assess integrity after purification. Lane 1 (gel 1 and gel 2): 1 kb plus DNA ladder (New England Biolabs, MA, US). Lane 2 (gel 1): pmRNA-CMV-eGFP-pA plasmid digested with *Bpi*I. Lanes 2 to 6 (gel 2): pT7-pri-miR-31 plasmids digested with *Bpi*I.

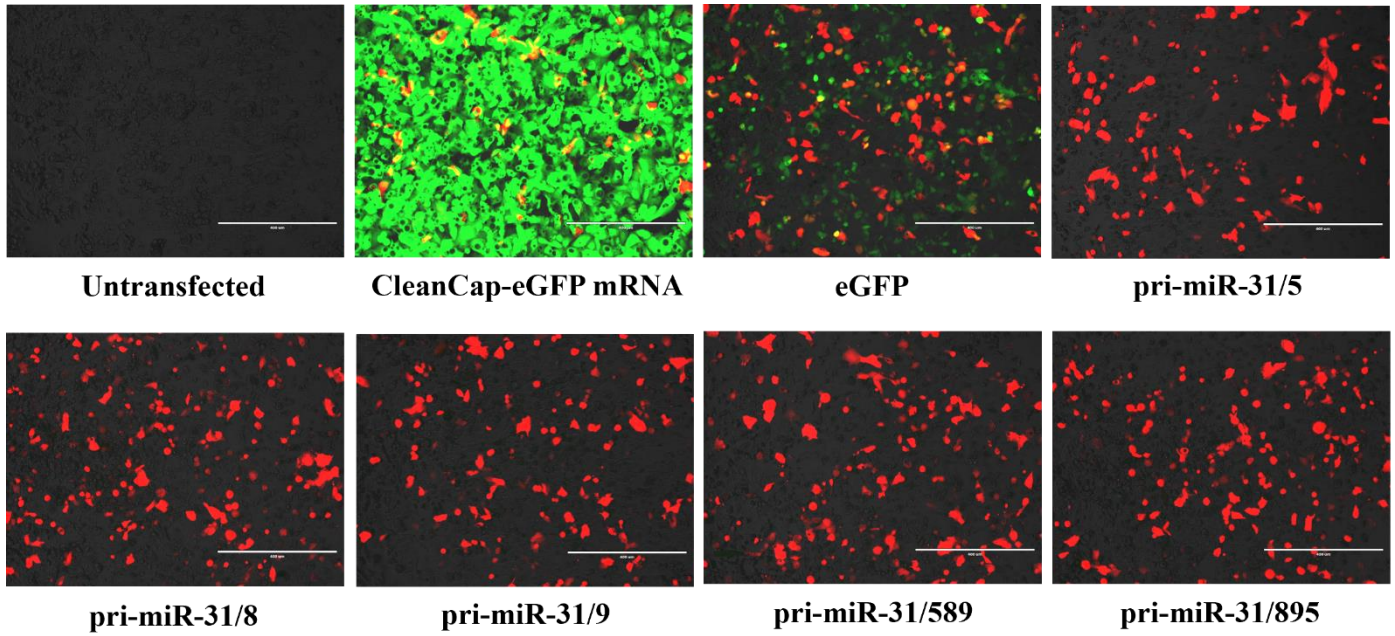
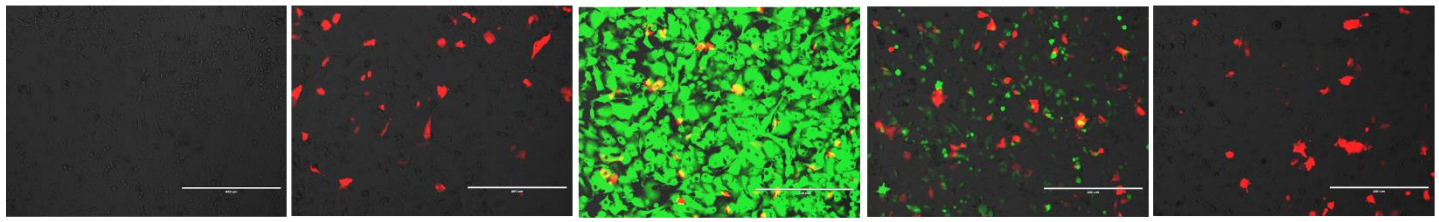
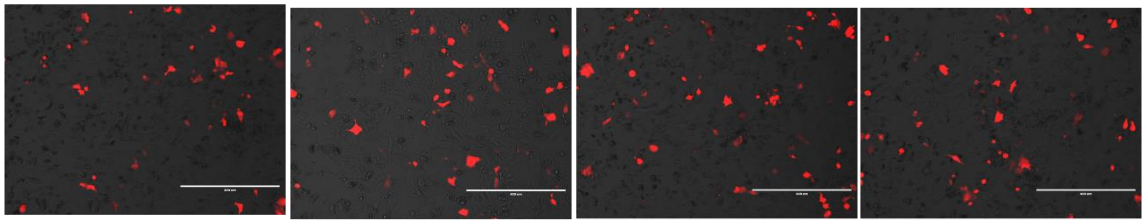


Figure S25: Fluorescence observed in the assay to assess HBV inhibition of the pri-miR-31 mimics prior to cellulose purification. On the day of transfection, HepG2-hNTCP cells were transfected with pCH-9/3091 (target) and mCherry (marker). One day after DNA transfection the cells were transfected with an experimental plasmid as indicated. One day after RNA transfection, the cells were analysed by fluorescence microscopy. The transfections were performed in triplicate and each fluorescent image demonstrated here represents the GFP and RFP expression obtained from each of the three wells.

One day after treatment

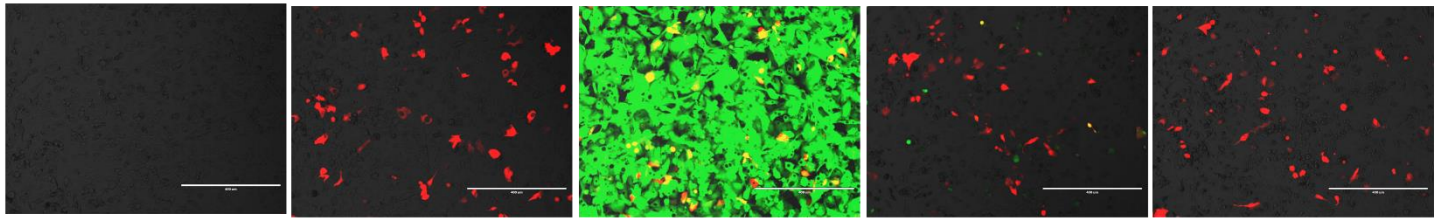


Untransfected | Mock | CleanCap-eGFP mRNA | eGFP | pri-miR-31/5

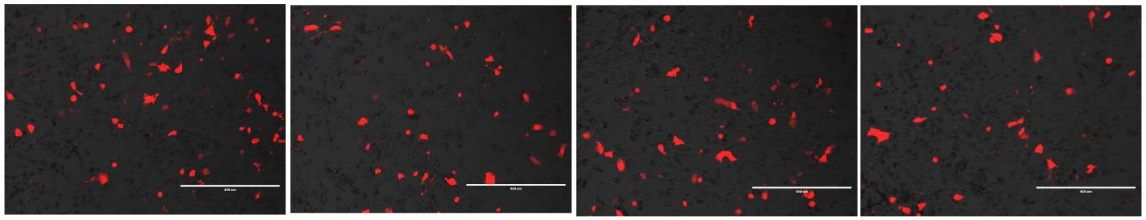


pri-miR-31/8 | pri-miR-31/9 | pri-miR-31/589 | pri-miR-31/895

Two days after treatment



Untransfected | Mock | CleanCap-eGFP mRNA | eGFP | pri-miR-31/5



pri-miR-31/8 | pri-miR-31/9 | pri-miR-31/589 | pri-miR-31/895

Figure S26: Fluorescence observed in the assay to assess HBV inhibition of the pri-miR-31 mimics after cellulose purification. On the day of transfection, HepG2-hNTCP cells were transfected with pCH-9/3091 (target) and mCherry (marker), and the cells that were transfected with only pCH-9/3091 and mCherry served as the mock control. One day after DNA transfection, the cells were transfected with an experimental plasmid as indicated. One and two days after RNA transfection, the cells were analysed by fluorescence microscopy. The transfections were performed in triplicate and each fluorescent image demonstrated here represents the GFP and RFP expression obtained from each of the three wells.

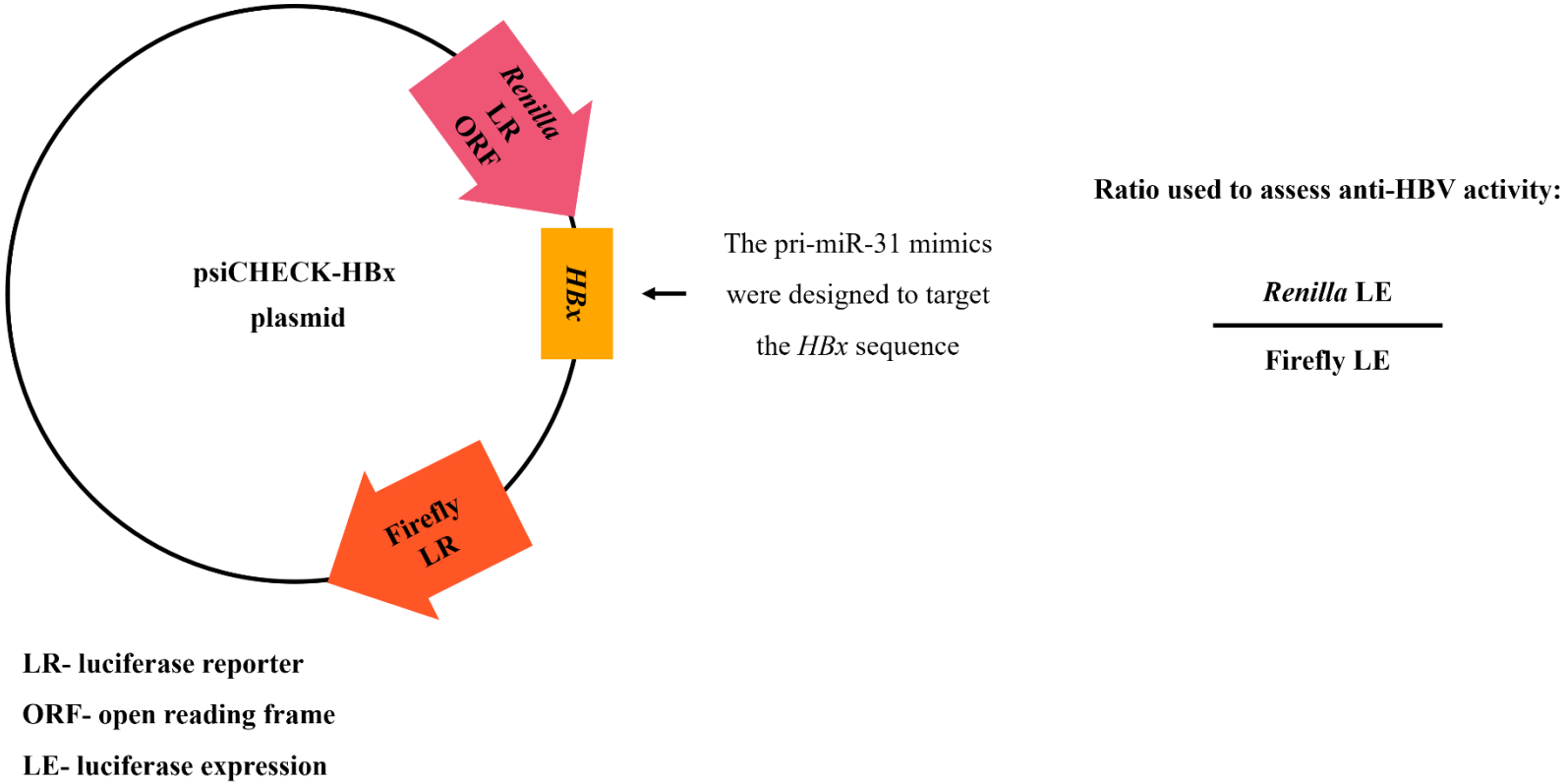
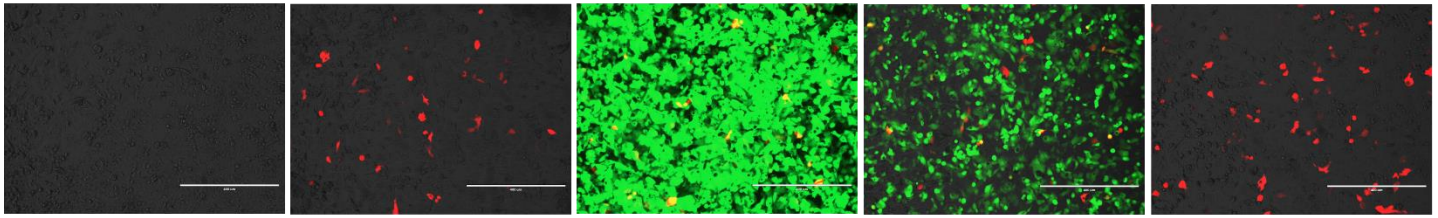
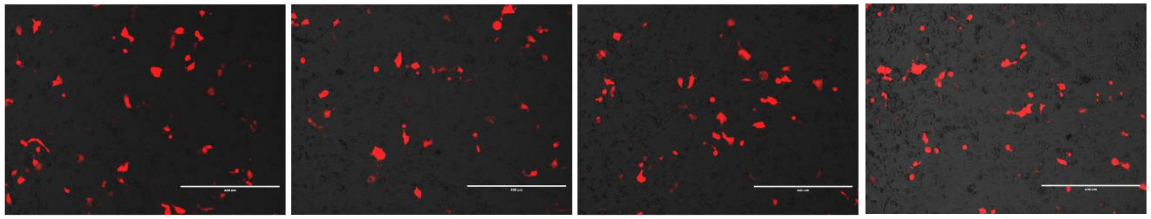


Figure S27: Schematic representation of the psiCHECK-HBx plasmid. The psiCHECK-HBx plasmid contains an independently located firefly luciferase reporter and a *Renilla* luciferase reporter ORF upstream of an *HBx* sequence. The firefly reporter expresses firefly luciferase mRNA and the *Renilla* reporter produces *Renilla* luciferase mRNA with an *HBx* sequence. Thus, firefly luciferase is steadily produced whereas *Renilla* luciferase expression is dependent on the *HBx* sequence. The pri-miR-31 mimics were designed to target the *HBx* sequence, therefore the ratio of *Renilla* luciferase expression to firefly luciferase expression was used to assess anti-HBV activity while accounting for experimental variability.

One day after treatment

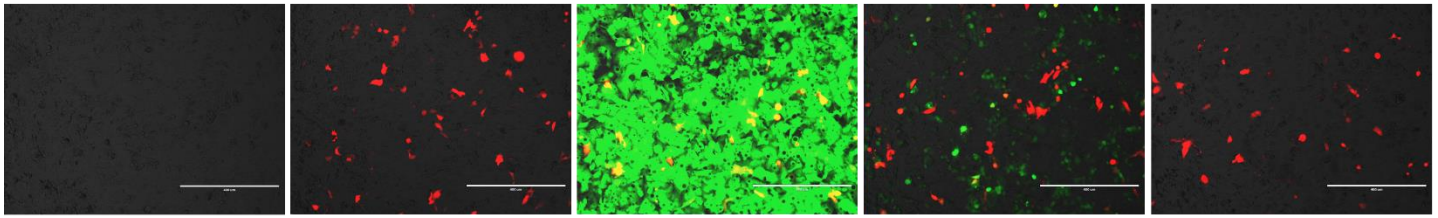


Untransfected | Mock | CleanCap-eGFP mRNA | eGFP | pri-miR-31/5

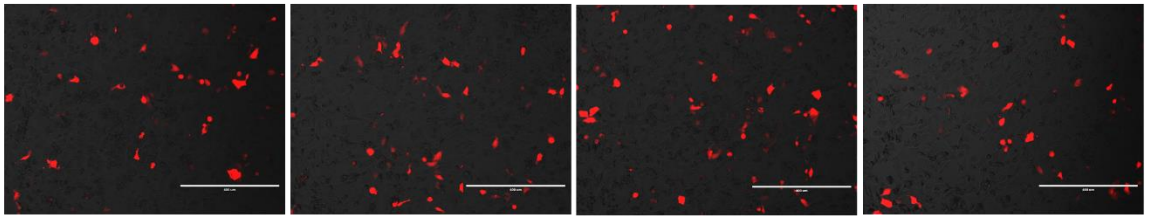


pri-miR-31/8 | pri-miR-31/9 | pri-miR-31/589 | pri-miR-31/895

Two days after treatment



Untransfected | Mock | CleanCap-eGFP mRNA | eGFP | pri-miR-31/5



pri-miR-31/8 | pri-miR-31/9 | pri-miR-31/589 | pri-miR-31/895

Figure S28: Fluorescence observed in the assay to assess specific HBV inhibition of the pri-miR-31 mimics after cellulose purification. On the day of transfection, HepG2-hNTCP cells were transfected with psiCHECK-HBx (target) and mCherry (marker), and the cells that were transfected with only psiCHECK-HBx and mCherry served as the mock control. One day after DNA transfection, the cells were transfected with an experimental plasmid as indicated. One and two days after RNA transfection, the cells were analysed by fluorescence microscopy. The transfections were performed in triplicate and each fluorescent image demonstrated here represents the GFP and RFP expression obtained from each of the three wells.

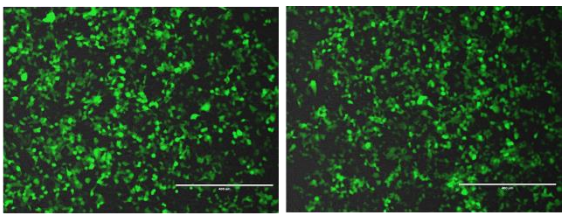


Figure S29: Fluorescence observed in the assay to assess cytotoxicity of the pri-miRNA-31 mimics. On the day of transfection, Hek293T cells were transfected with an experimental plasmid (only CleanCap-eGFP and eGFP are demonstrated here). One day after transfection, the cells were analysed by fluorescence microscopy and an MTT assay was performed. The transfections were performed in triplicate and each fluorescent image demonstrated here represents the GFP expression obtained from each of the three wells.

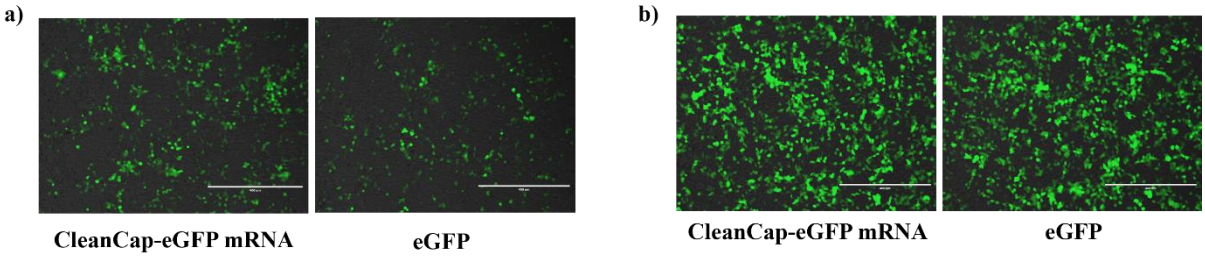
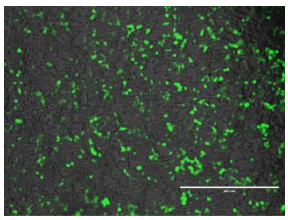


Figure S30: Fluorescence observed in the assays to assess immunogenicity of the pri-miRNA-31 mimics. (a) On the day of transfection, Hek293T cells were transfected with phRL-CMV, pUCAsc-ISRE×3 and an experimental plasmid (only CleanCap-eGFP and eGFP are demonstrated here). Two days after transfection, the cells were analysed by fluorescence microscopy and a dual-luciferase assay was performed. (b) On the day of transfection, Hek293T cells were transfected with an experimental plasmid (only CleanCap-eGFP and eGFP are demonstrated here). One day after transfection, the cells were analysed by fluorescence microscopy and RT-qPCR assays were performed. (a and b) The transfections were performed in triplicate and each fluorescent image demonstrated here represents the GFP expression obtained from each of the three wells.



eGFP

Figure S31: Fluorescence observed in the analysis to assess processing efficiency of the pri-miRNA-31 mimics. On the day of transfection, Hek293T cells were transfected with an experimental plasmid (only eGFP is demonstrated here). One day after transfection, the cells were analysed by fluorescence microscopy and Northern blot hybridisation analysis was performed to determine the mature miRNA guide sequences formed. The transfections were performed in triplicate and each fluorescent image demonstrated here represents the GFP expression obtained from each of the three wells.

6. REFERENCES

Alexopoulou, L., Holt, A.C., Medzhitov, R., Flavell, R.A., 2001. Recognition of double-stranded RNA and activation of NF-κB by Toll-like receptor 3. Nature 413, 732–738. https://doi.org/10.1038/35099560

Ambesajir, A., Kaushik, A., Kaushik, J.J., Petros, S.T., 2012. RNA interference: A futuristic tool and its therapeutic applications. Saudi J. Biol. Sci. 19, 395–403. https://doi.org/10.1016/j.sjbs.2012.08.001

Andrade, S., Loureiro, J.A., Ramirez, S., Catumbela, C.S.G., Soto, C., Morales, R., Pereira, M.C., 2022. Multi-Dose Intravenous Administration of Neutral and Cationic Liposomes in Mice: An Extensive Toxicity Study. Pharmaceuticals 15, 761. https://doi.org/10.3390/ph15060761

Andries, O., Mc Cafferty, S., De Smedt, S.C., Weiss, R., Sanders, N.N., Kitada, T., 2015. N(1)-methylpseudouridine-incorporated mRNA outperforms pseudouridine-incorporated mRNA by providing enhanced protein expression and reduced immunogenicity in mammalian cell lines and mice. J. Control. Release Off. J. Control. Release Soc. 217, 337–344. https://doi.org/10.1016/j.jconrel.2015.08.051

Baiersdörfer, M., Boros, G., Muramatsu, H., Mahiny, A., Vlatkovic, I., Sahin, U., Karikó, K., 2019. A Facile Method for the Removal of dsRNA Contaminant from In Vitro-Transcribed mRNA. Mol. Ther. Nucleic Acids 15, 26–35. https://doi.org/10.1016/j.omtn.2019.02.018

Balazs, D.A., Godbey, W.T., 2010. Liposomes for Use in Gene Delivery. J. Drug Deliv. 2011, e326497. https://doi.org/10.1155/2011/326497

Bartel, D.P., 2009. MicroRNAs: target recognition and regulatory functions. Cell 136, 215–233. https://doi.org/10.1016/j.cell.2009.01.002

Bartenschlager, R., Junker-Niepmann, M., Schaller, H., 1990. The P gene product of hepatitis B virus is required as a structural component for genomic RNA encapsidation. J. Virol. 64, 5324–5332. https://doi.org/10.1128/JVI.64.11.5324-5332.1990

Belloni, L., Allweiss, L., Guerrieri, F., Pediconi, N., Volz, T., Pollicino, T., Petersen, J., Raimondo, G., Dandri, M., Levrero, M., 2012. IFN-α inhibits HBV transcription and replication in cell culture and in humanized mice by targeting the epigenetic regulation of the nuclear cccDNA minichromosome. J. Clin. Invest. 122, 529–537. https://doi.org/10.1172/JCI58847

Bernstein, E., Caudy, A.A., Hammond, S.M., Hannon, G.J., 2001. Role for a bidentate ribonuclease in the initiation step of RNA interference. Nature 409, 363–366. https://doi.org/10.1038/35053110

Böttcher, B., Wynne, S.A., Crowther, R.A., 1997. Determination of the fold of the core protein of hepatitis B virus by electron cryomicroscopy. Nature 386, 88–91. https://doi.org/10.1038/386088a0

Bright, N.A., Davis, L.J., Luzio, J.P., 2016. Endolysosomes Are the Principal Intracellular Sites of Acid Hydrolase Activity. Curr. Biol. CB 26, 2233–2245. https://doi.org/10.1016/j.cub.2016.06.046

Briuglia, M.-L., Rotella, C., McFarlane, A., Lamprou, D.A., 2015. Influence of cholesterol on liposome stability and on in vitro drug release. Drug Deliv. Transl. Res. 5, 231–242. https://doi.org/10.1007/s13346-015-0220-8

Bruss, V., Ganem, D., 1991. The role of envelope proteins in hepatitis B virus assembly. Proc. Natl. Acad. Sci. U. S. A. 88, 1059–1063.

Carmona, S., Ely, A., Crowther, C., Moolla, N., Salazar, F.H., Marion, P.L., Ferry, N., Weinberg, M.S., Arbuthnot, P., 2006. Effective inhibition of HBV replication in vivo by anti-HBx short hairpin RNAs. Mol. Ther. J. Am. Soc. Gene Ther. 13, 411–421. https://doi.org/10.1016/j.ymthe.2005.10.013

Chen, J., Wu, M., Liu, K., Zhang, W., Li, Y., Zhou, X., Bai, L., Yuan, Z., 2015. New insights into hepatitis B virus biology and implications for novel antiviral strategies. Natl. Sci. Rev. 2, 296–313. https://doi.org/10.1093/nsr/nwv044

Chen, M., Sällberg, M., Hughes, J., Jones, J., Guidotti, L.G., Chisari, F.V., Billaud, J.-N., Milich, D.R., 2005. Immune Tolerance Split between Hepatitis B Virus Precore and Core Proteins. J. Virol. 79, 3016–3027. https://doi.org/10.1128/JVI.79.5.3016-3027.2005

Chuang, W.-L., Jia, J., Chan, H.L.Y., Han, K.-H., Tanwandee, T., Tan, D., Chen, X., Gane, E., Piratvisuth, T., Chen, L., Xie, Q., Sung, J.J.-Y., Messinger, D., Wat, C., Bakalos, G., Liaw, Y.F., 2018. Responses are durable for up to 5 years after completion of peginterferon alfa-2a treatment in hepatitis B e antigen-positive patients. Aliment. Pharmacol. Ther. 47, 1306–1316. https://doi.org/10.1111/apt.14595

Cooksley, W.G.E., Piratvisuth, T., Lee, S.-D., Mahachai, V., Chao, Y.-C., Tanwandee, T., Chutaputti, A., Chang, W.Y., Zahm, F.E., Pluck, N., 2003. Peginterferon alpha-2a (40 kDa): an advance in the treatment of hepatitis B e antigen-positive chronic hepatitis B. J. Viral Hepat. 10, 298–305. https://doi.org/10.1046/j.1365-2893.2003.00450.x

Dane, D.S., Cameron, C.H., Briggs, M., 1970. Virus-like particles in serum of patients with Australia-antigen-associated hepatitis. Lancet Lond. Engl. 1, 695–698. https://doi.org/10.1016/s0140-6736(70)90926-8

de Fraga, R.S., Van Vaisberg, V., Mendes, L.C.A., Carrilho, F.J., Ono, S.K., 2020. Adverse events of nucleos(t)ide analogues for chronic hepatitis B: a systematic review. J. Gastroenterol. 55, 496–514. https://doi.org/10.1007/s00535-020-01680-0

De Paula, D., Bentley, M.V.L.B., Mahato, R.I., 2007. Hydrophobization and bioconjugation for enhanced siRNA delivery and targeting. RNA N. Y. N 13, 431–456. https://doi.org/10.1261/rna.459807

Decorsière, A., Mueller, H., van Breugel, P.C., Abdul, F., Gerossier, L., Beran, R.K., Livingston, C.M., Niu, C., Fletcher, S.P., Hantz, O., Strubin, M., 2016. Hepatitis B virus X protein identifies the Smc5/6 complex as a host restriction factor. Nature 531, 386–389. https://doi.org/10.1038/nature17170

Diab, A., Foca, A., Zoulim, F., Durantel, D., Andrisani, O., 2018. The diverse functions of the hepatitis B core/capsid protein (HBc) in the viral life cycle: Implications for the development of HBc-targeting antivirals. Antiviral Res. 149, 211–220. https://doi.org/10.1016/j.antiviral.2017.11.015

Dyer, V., Ely, A., Bloom, K., Weinberg, M., Arbuthnot, P., 2010. tRNA Lys3 promoter cassettes that efficiently express RNAi-activating antihepatitis B virus short hairpin RNAs. Biochem. Biophys. Res. Commun. 398, 640–646. https://doi.org/10.1016/j.bbrc.2010.06.122

Edmunds, W.J., Medley, G.F., Nokes, D.J., Hall, A.J., Whittle, H.C., 1993. The influence of age on the development of the hepatitis B carrier state. Proc. Biol. Sci. 253, 197–201. https://doi.org/10.1098/rspb.1993.0102

Ely, A., Naidoo, T., Arbuthnot, P., 2009. Efficient silencing of gene expression with modular trimeric Pol II expression cassettes comprising microRNA shuttles. Nucleic Acids Res. 37, e91–e91. https://doi.org/10.1093/nar/gkp446

Ely, A., Naidoo, T., Mufamadi, S., Crowther, C., Arbuthnot, P., 2008. Expressed anti-HBV primary microRNA shuttles inhibit viral replication efficiently in vitro and in vivo. Mol. Ther. J. Am. Soc. Gene Ther. 16, 1105–1112. https://doi.org/10.1038/mt.2008.82

Funk, A.L., Lu, Y., Yoshida, K., Zhao, T., Boucheron, P., van Holten, J., Chou, R., Bulterys, M., Shimakawa, Y., 2021. Efficacy and safety of antiviral prophylaxis during pregnancy to prevent mother-to-child transmission of hepatitis B virus: a systematic review and meta-analysis. Lancet Infect. Dis. 21, 70–84. https://doi.org/10.1016/S1473-3099(20)30586-7

Galka-Marciniak, P., Olejniczak, M., Starega-Roslan, J., Szczesniak, M.W., Makalowska, I., Krzyzosiak, W.J., 2016. siRNA release from pri-miRNA scaffolds is controlled by the

sequence and structure of RNA. Biochim. Biophys. Acta 1859, 639–649. https://doi.org/10.1016/j.bbagrm.2016.02.014

Giladi, H., Ketzinel-Gilad, M., Rivkin, L., Felig, Y., Nussbaum, O., Galun, E., 2003. Small interfering RNA inhibits hepatitis B virus replication in mice. Mol. Ther. J. Am. Soc. Gene Ther. 8, 769–776. https://doi.org/10.1016/s1525-0016(03)00244-2

Grimm, D., Streetz, K.L., Jopling, C.L., Storm, T.A., Pandey, K., Davis, C.R., Marion, P., Salazar, F., Kay, M.A., 2006. Fatality in mice due to oversaturation of cellular microRNA/short hairpin RNA pathways. Nature 441, 537–541. https://doi.org/10.1038/nature04791

Gust, I.D., Burrell, C.J., Coulepis, A.G., Robinson, W.S., Zuckerman, A.J., 1986. Taxonomic classification of human hepatitis B virus. Intervirology 25, 14–29. https://doi.org/10.1159/000149651

Ha, M., Kim, V.N., 2014. Regulation of microRNA biogenesis. Nat. Rev. Mol. Cell Biol. 15, 509–524. https://doi.org/10.1038/nrm3838

Hald Albertsen, C., Kulkarni, J.A., Witzigmann, D., Lind, M., Petersson, K., Simonsen, J.B., 2022. The role of lipid components in lipid nanoparticles for vaccines and gene therapy. Adv. Drug Deliv. Rev. 188, 114416. https://doi.org/10.1016/j.addr.2022.114416

Han, J., Lee, Y., Yeom, K.-H., Kim, Y.-K., Jin, H., Kim, V.N., 2004. The Drosha-DGCR8 complex in primary microRNA processing. Genes Dev. 18, 3016–3027. https://doi.org/10.1101/gad.1262504

Heil, F., Hemmi, H., Hochrein, H., Ampenberger, F., Kirschning, C., Akira, S., Lipford, G., Wagner, H., Bauer, S., 2004. Species-specific recognition of single-stranded RNA via toll-like receptor 7 and 8. Science 303, 1526–1529. https://doi.org/10.1126/science.1093620

Heller, R., Heller, L.C., 2015. Gene electrotransfer clinical trials. Adv. Genet. 89, 235–262. https://doi.org/10.1016/bs.adgen.2014.10.006

Herrero, M.J., Sendra, L., Miguel, A., Aliño, S.F., 2017. Physical Methods of Gene Delivery, in: Brunetti-Pierri, N. (Ed.), Safety and Efficacy of Gene-Based Therapeutics for Inherited Disorders. Springer International Publishing, Cham, pp. 113–135. https://doi.org/10.1007/978-3-319-53457-2_6

Ho, P.Y., Yu, A.-M., 2016. Bioengineering of noncoding RNAs for research agents and therapeutics. Wiley Interdiscip. Rev. RNA 7, 186–197. https://doi.org/10.1002/wrna.1324

Holmen, S.L., Vanbrocklin, M.W., Eversole, R.R., Stapleton, S.R., Ginsberg, L.C., 1995. Efficient lipid-mediated transfection of DNA into primary rat hepatocytes. In Vitro Cell. Dev. Biol. Anim. 31, 347–351. https://doi.org/10.1007/BF02634283

Hou, X., Zaks, T., Langer, R., Dong, Y., 2021. Lipid nanoparticles for mRNA delivery. Nat. Rev. Mater. 6, 1078–1094. https://doi.org/10.1038/s41578-021-00358-0

Hovanessian, A.G., 2007. On the discovery of interferon-inducible, double-stranded RNA activated enzymes: the 2'-5'oligoadenylate synthetases and the protein kinase PKR. Cytokine Growth Factor Rev. 18, 351–361. https://doi.org/10.1016/j.cytogfr.2007.06.003

Hwang, E.W., Cheung, R., 2011. Global epidemiology of hepatitis B virus (HBV) infection. North Am. J. Med. Sci. 4.

Hyams, K.C., 1995. Risks of chronicity following acute hepatitis B virus infection: a review. Clin. Infect. Dis. Off. Publ. Infect. Dis. Soc. Am. 20, 992–1000. https://doi.org/10.1093/clinids/20.4.992

Idilman, R., Gunsar, F., Koruk, M., Keskin, O., Meral, C.E., Gulsen, M., Elhan, A.H., Akarca, U.S., Yurdaydin, C., 2015. Long-term entecavir or tenofovir disoproxil fumarate therapy in treatment-naïve chronic hepatitis B patients in the real-world setting. J. Viral Hepat. 22, 504–510. https://doi.org/10.1111/jvh.12358

Ivacik, D., Ely, A., Ferry, N., Arbuthnot, P., 2015. Sustained inhibition of hepatitis B virus replication in vivo using RNAi-activating lentiviruses. Gene Ther. 22, 163–171. https://doi.org/10.1038/gt.2014.94

Iwamoto, M., Saso, W., Nishioka, K., Ohashi, H., Sugiyama, R., Ryo, A., Ohki, M., Yun, J.-H., Park, S.-Y., Ohshima, T., Suzuki, R., Aizaki, H., Muramatsu, M., Matano, T., Iwami, S., Sureau, C., Wakita, T., Watashi, K., 2020. The machinery for endocytosis of epidermal growth factor receptor coordinates the transport of incoming hepatitis B virus to the endosomal network. J. Biol. Chem. 295, 800–807. https://doi.org/10.1074/jbc.AC119.010366

Iwamoto, M., Saso, W., Sugiyama, R., Ishii, K., Ohki, M., Nagamori, S., Suzuki, R., Aizaki, H., Ryo, A., Yun, J.-H., Park, S.-Y., Ohtani, N., Muramatsu, M., Iwami, S., Tanaka, Y., Sureau, C., Wakita, T., Watashi, K., 2019. Epidermal growth factor receptor is a host-entry cofactor triggering hepatitis B virus internalization. Proc. Natl. Acad. Sci. U. S. A. 116, 8487–8492. https://doi.org/10.1073/pnas.1811064116

Jia, F., Deng, F., Tong, S., Li, S., Ren, H., Yin, W., 2020. Efficacy of oral antiviral drugs to prevent mother-to-child transmission of hepatitis B virus: a network meta-analysis. Hepatol. Int. 14, 338–346. https://doi.org/10.1007/s12072-020-10024-2

Jonas, S., Izaurralde, E., 2015. Towards a molecular understanding of microRNA-mediated gene silencing. Nat. Rev. Genet. 16, 421–433. https://doi.org/10.1038/nrg3965

Judge, A.D., Sood, V., Shaw, J.R., Fang, D., McClintock, K., MacLachlan, I., 2005. Sequence-dependent stimulation of the mammalian innate immune response by synthetic siRNA. Nat. Biotechnol. 23, 457–462. https://doi.org/10.1038/nbt1081

Junker-Niepmann, M., Bartenschlager, R., Schaller, H., 1990. A short cis-acting sequence is required for hepatitis B virus pregenome encapsidation and sufficient for packaging of foreign RNA. EMBO J. 9, 3389–3396.

Karayiannis, P., 2017. Hepatitis B virus: virology, molecular biology, life cycle and intrahepatic spread. Hepatol. Int. 11, 500–508. https://doi.org/10.1007/s12072-017-9829-7

Karikó, K., Buckstein, M., Ni, H., Weissman, D., 2005. Suppression of RNA recognition by Toll-like receptors: the impact of nucleoside modification and the evolutionary origin of RNA. Immunity 23, 165–175. https://doi.org/10.1016/j.immuni.2005.06.008

Karikó, K., Muramatsu, H., Ludwig, J., Weissman, D., 2011. Generating the optimal mRNA for therapy: HPLC purification eliminates immune activation and improves translation of nucleoside-modified, protein-encoding mRNA. Nucleic Acids Res. 39, e142. https://doi.org/10.1093/nar/gkr695

Karikó, K., Weissman, D., 2007. Naturally occurring nucleoside modifications suppress the immunostimulatory activity of RNA: implication for therapeutic RNA development. Curr. Opin. Drug Discov. Devel. 10, 523–532.

Kato, H., Takeuchi, O., Sato, S., Yoneyama, M., Yamamoto, M., Matsui, K., Uematsu, S., Jung, A., Kawai, T., Ishii, K.J., Yamaguchi, O., Otsu, K., Tsujimura, T., Koh, C.-S., Reis e Sousa, C., Matsuura, Y., Fujita, T., Akira, S., 2006. Differential roles of MDA5 and RIG-I helicases in the recognition of RNA viruses. Nature 441, 101–105. https://doi.org/10.1038/nature04734

Kawai, T., Akira, S., 2009. The roles of TLRs, RLRs and NLRs in pathogen recognition. Int. Immunol. 21, 317–337. https://doi.org/10.1093/intimm/dxp017

Khanam, A., Chua, J.V., Kottilil, S., 2021. Immunopathology of Chronic Hepatitis B Infection: Role of Innate and Adaptive Immune Response in Disease Progression. Int. J. Mol. Sci. 22, 5497. https://doi.org/10.3390/ijms22115497

Khvorova, A., Reynolds, A., Jayasena, S.D., 2003. Functional siRNAs and miRNAs exhibit strand bias. Cell 115, 209–216. https://doi.org/10.1016/s0092-8674(03)00801-8

Kim, M., Jeong, M., Hur, S., Cho, Y., Park, J., Jung, H., Seo, Y., Woo, H.A., Nam, K.T., Lee, K., Lee, H., 2021. Engineered ionizable lipid nanoparticles for targeted delivery of

RNA therapeutics into different types of cells in the liver. Sci. Adv. 7, eabf4398. https://doi.org/10.1126/sciadv.abf4398

Knaus, T., Nassal, M., 1993. The encapsidation signal on the hepatitis B virus RNA pregenome forms a stem-loop structure that is critical for its function. Nucleic Acids Res. 21, 3967–3975.

Kobayashi, H., Tomari, Y., 2016. RISC assembly: Coordination between small RNAs and Argonaute proteins. Biochim. Biophys. Acta 1859, 71–81. https://doi.org/10.1016/j.bbagrm.2015.08.007

Koltover, I., Salditt, T., Rädler, J.O., Safinya, C.R., 1998. An inverted hexagonal phase of cationic liposome-DNA complexes related to DNA release and delivery. Science 281, 78–81. https://doi.org/10.1126/science.281.5373.78

Kormann, M.S.D., Hasenpusch, G., Aneja, M.K., Nica, G., Flemmer, A.W., Herber-Jonat, S., Huppmann, M., Mays, L.E., Illenyi, M., Schams, A., Griese, M., Bittmann, I., Handgretinger, R., Hartl, D., Rosenecker, J., Rudolph, C., 2011. Expression of therapeutic proteins after delivery of chemically modified mRNA in mice. Nat. Biotechnol. 29, 154–157. https://doi.org/10.1038/nbt.1733

Krawczyk, A., Ludwig, C., Jochum, C., Fiedler, M., Heinemann, F.M., Shouval, D., Roggendorf, M., Roggendorf, H., Lindemann, M., 2014. Induction of a robust T- and B-cell immune response in non- and low-responders to conventional vaccination against hepatitis B by using a third generation PreS/S vaccine. Vaccine 32, 5077–5082. https://doi.org/10.1016/j.vaccine.2014.06.076

Kuhn, A.N., Beiβert, T., Simon, P., Vallazza, B., Buck, J., Davies, B.P., Tureci, O., Sahin, U., 2012. mRNA as a versatile tool for exogenous protein expression. Curr. Gene Ther. 12, 347–361. https://doi.org/10.2174/156652312802762536

Kwon, S., Kwon, M., Im, S., Lee, K., Lee, H., 2022. mRNA vaccines: the most recent clinical applications of synthetic mRNA. Arch. Pharm. Res. 45, 245–262. https://doi.org/10.1007/s12272-022-01381-7

Lai, C.-L., Wong, D., Ip, P., Kopaniszen, M., Seto, W.-K., Fung, J., Huang, F.-Y., Lee, B., Cullaro, G., Chong, C.K., Wu, R., Cheng, C., Yuen, J., Ngai, V., Yuen, M.-F., 2017. Reduction of covalently closed circular DNA with long-term nucleos(t)ide analogue treatment in chronic hepatitis B. J. Hepatol. 66, 275–281. https://doi.org/10.1016/j.jhep.2016.08.022

Lambricht, L., Lopes, A., Kos, S., Sersa, G., Préat, V., Vandermeulen, G., 2016. Clinical potential of electroporation for gene therapy and DNA vaccine delivery. Expert Opin. Drug Deliv. 13, 295–310. https://doi.org/10.1517/17425247.2016.1121990

Lamontagne, R.J., Bagga, S., Bouchard, M.J., 2016. Hepatitis B virus molecular biology and pathogenesis. Hepatoma Res. 2, 163–186. https://doi.org/10.20517/2394-5079.2016.05

Lau, G.K.K., Piratvisuth, T., Luo, K.X., Marcellin, P., Thongsawat, S., Cooksley, G., Gane, E., Fried, M.W., Chow, W.C., Paik, S.W., Chang, W.Y., Berg, T., Flisiak, R., McCloud, P., Pluck, N., Peginterferon Alfa-2a HBeAg-Positive Chronic Hepatitis B Study Group, 2005. Peginterferon Alfa-2a, lamivudine, and the combination for HBeAg-positive chronic hepatitis B. N. Engl. J. Med. 352, 2682–2695. https://doi.org/10.1056/NEJMoa043470

Lee, Y., Kim, M., Han, J., Yeom, K.-H., Lee, S., Baek, S.H., Kim, V.N., 2004. MicroRNA genes are transcribed by RNA polymerase II. EMBO J. 23, 4051–4060. https://doi.org/10.1038/sj.emboj.7600385

Leistner, C.M., Gruen-Bernhard, S., Glebe, D., 2008. Role of glycosaminoglycans for binding and infection of hepatitis B virus. Cell. Microbiol. 10, 122–133. https://doi.org/10.1111/j.1462-5822.2007.01023.x

Levanova, A., Poranen, M.M., 2018. RNA Interference as a Prospective Tool for the Control of Human Viral Infections. Front. Microbiol. 9.

Lewellyn, E.B., Loeb, D.D., 2011. The Arginine Clusters of the Carboxy-Terminal Domain of the Core Protein of Hepatitis B Virus Make Pleiotropic Contributions to Genome Replication. J. Virol. 85, 1298–1309. https://doi.org/10.1128/JVI.01957-10

Liang, T.J., 2009. Hepatitis B: the virus and disease. Hepatol. Baltim. Md 49, S13-21. https://doi.org/10.1002/hep.22881

Loeb, D.D., Hirsch, R.C., Ganem, D., 1991. Sequence-independent RNA cleavages generate the primers for plus strand DNA synthesis in hepatitis B viruses: implications for other reverse transcribing elements. EMBO J. 10, 3533–3540.

Lucifora, J., Arzberger, S., Durantel, D., Belloni, L., Strubin, M., Levrero, M., Zoulim, F., Hantz, O., Protzer, U., 2011. Hepatitis B virus X protein is essential to initiate and maintain virus replication after infection. J. Hepatol. 55, 996–1003. https://doi.org/10.1016/j.jhep.2011.02.015

Lucifora, J., Xia, Y., Reisinger, F., Zhang, K., Stadler, D., Cheng, X., Sprinzl, M.F., Koppensteiner, H., Makowska, Z., Volz, T., Remouchamps, C., Chou, W.-M., Thasler, W.E., Hüser, N., Durantel, D., Liang, T.J., Münk, C., Heim, M.H., Browning, J.L., Dejardin, E., Dandri, M., Schindler, M., Heikenwalder, M., Protzer, U., 2014. Specific and Nonhepatotoxic Degradation of Nuclear Hepatitis B Virus cccDNA. Science 343, 1221–1228. https://doi.org/10.1126/science.1243462

Lund, E., Güttinger, S., Calado, A., Dahlberg, J.E., Kutay, U., 2004. Nuclear export of microRNA precursors. Science 303, 95–98. https://doi.org/10.1126/science.1090599

Maepa, M.B., Ely, A., Grayson, W., Arbuthnot, P., 2017. Sustained Inhibition of HBV Replication In Vivo after Systemic Injection of AAVs Encoding Artificial Antiviral Primary MicroRNAs. Mol. Ther. Nucleic Acids 7, 190–199. https://doi.org/10.1016/j.omtn.2017.04.007

Maepa, M.B., Roelofse, I., Ely, A., Arbuthnot, P., 2015. Progress and Prospects of Anti-HBV Gene Therapy Development. Int. J. Mol. Sci. 16, 17589–17610. https://doi.org/10.3390/ijms160817589

Malone, R.W., Felgner, P.L., Verma, I.M., 1989. Cationic liposome-mediated RNA transfection. Proc. Natl. Acad. Sci. U. S. A. 86, 6077–6081.

Maxfield, F.R., McGraw, T.E., 2004. Endocytic recycling. Nat. Rev. Mol. Cell Biol. 5, 121–132. https://doi.org/10.1038/nrm1315

McDermott, A.B., Cohen, S.B., Zuckerman, J.N., Madrigal, J.A., 1998. Hepatitis B third-generation vaccines: improved response and conventional vaccine non-response--evidence for genetic basis in humans. J. Viral Hepat. 5 Suppl 2, 9–11. https://doi.org/10.1046/j.1365-2893.1998.0050s2009.x

Menéndez-Arias, L., Álvarez, M., Pacheco, B., 2014. Nucleoside/nucleotide analog inhibitors of hepatitis B virus polymerase: mechanism of action and resistance. Curr. Opin. Virol. 8, 1–9. https://doi.org/10.1016/j.coviro.2014.04.005

Micco, L., Peppa, D., Loggi, E., Schurich, A., Jefferson, L., Cursaro, C., Panno, A.M., Bernardi, M., Brander, C., Bihl, F., Andreone, P., Maini, M.K., 2013. Differential boosting of innate and adaptive antiviral responses during pegylated-interferon-alpha therapy of chronic hepatitis B. J. Hepatol. 58, 225–233. https://doi.org/10.1016/j.jhep.2012.09.029

Milligan, J.F., Groebe, D.R., Witherell, G.W., Uhlenbeck, O.C., 1987. Oligoribonucleotide synthesis using T7 RNA polymerase and synthetic DNA templates. Nucleic Acids Res. 15, 8783–8798.

Moolla, N., Kew, M., Arbuthnot, P., 2002. Regulatory elements of hepatitis B virus transcription. J. Viral Hepat. 9, 323–331. https://doi.org/10.1046/j.1365-2893.2002.00381.x

Mowa, M.B., Crowther, C., Ely, A., Arbuthnot, P., 2012. Efficient silencing of hepatitis B virus by helper-dependent adenovirus vector-mediated delivery of artificial antiviral primary micro RNAs. MicroRNA Shariqah United Arab Emir. 1, 19–25. https://doi.org/10.2174/2211536611201010019

Mu, X., Hur, S., 2021. Immunogenicity of In Vitro-Transcribed RNA. Acc. Chem. Res. 54, 4012–4023. https://doi.org/10.1021/acs.accounts.1c00521

Murphy, C.M., Xu, Y., Li, F., Nio, K., Reszka-Blanco, N., Li, X., Wu, Y., Yu, Y., Xiong, Y., Su, L., 2016. Hepatitis B Virus X Protein Promotes Degradation of SMC5/6 to Enhance HBV Replication. Cell Rep. 16, 2846–2854. https://doi.org/10.1016/j.celrep.2016.08.026

Naso, M.F., Tomkowicz, B., Perry, W.L., Strohl, W.R., 2017. Adeno-Associated Virus (AAV) as a Vector for Gene Therapy. BioDrugs Clin. Immunother. Biopharm. Gene Ther. 31, 317–334. https://doi.org/10.1007/s40259-017-0234-5

Nassal, M., 1992. The arginine-rich domain of the hepatitis B virus core protein is required for pregenome encapsidation and productive viral positive-strand DNA synthesis but not for virus assembly. J. Virol. 66, 4107–4116. https://doi.org/10.1128/JVI.66.7.4107-4116.1992

Nassal, M., Junker-Niepmann, M., Schaller, H., 1990. Translational inactivation of RNA function: discrimination against a subset of genomic transcripts during HBV nucleocapsid assembly. Cell 63, 1357–1363. https://doi.org/10.1016/0092-8674(90)90431-d

Nassal, M., Rieger, A., 1996. A bulged region of the hepatitis B virus RNA encapsidation signal contains the replication origin for discontinuous first-strand DNA synthesis. J. Virol. 70, 2764–2773. https://doi.org/10.1128/JVI.70.5.2764-2773.1996

Nelson, J., Sorensen, E.W., Mintri, S., Rabideau, A.E., Zheng, W., Besin, G., Khatwani, N., Su, S.V., Miracco, E.J., Issa, W.J., Hoge, S., Stanton, M.G., Joyal, J.L., 2020. Impact of mRNA chemistry and manufacturing process on innate immune activation. Sci. Adv. 6, eaaz6893. https://doi.org/10.1126/sciadv.aaz6893

Nguyen, T.A., Jo, M.H., Choi, Y.-G., Park, J., Kwon, S.C., Hohng, S., Kim, V.N., Woo, J.-S., 2015. Functional Anatomy of the Human Microprocessor. Cell 161, 1374–1387. https://doi.org/10.1016/j.cell.2015.05.010

Papastergiou, V., Lombardi, R., MacDonald, D., Tsochatzis, E.A., 2015. Global Epidemiology of Hepatitis B Virus (HBV) Infection. Curr. Hepatol. Rep. 14, 171–178. https://doi.org/10.1007/s11901-015-0269-3

Papatheodoridis, G.V., Sypsa, V., Dalekos, G., Yurdaydin, C., van Boemmel, F., Buti, M., Goulis, J., Calleja, J.L., Chi, H., Manolakopoulos, S., Loglio, A., Siakavellas, S., Gatselis, N., Keskın, O., Lehretz, M., Savvidou, S., de la Revilla, J., Hansen, B.E., Kourikou, A., Vlachogiannakos, I., Galanis, K., Idilman, R., Colombo, M., Esteban, R., Janssen, H.L.A., Berg, T., Lampertico, P., 2018. Eight-year survival in chronic

hepatitis B patients under long-term entecavir or tenofovir therapy is similar to the general population. J. Hepatol. 68, 1129–1136. https://doi.org/10.1016/j.jhep.2018.01.031

Passman, M., Weinberg, M., Kew, M., Arbuthnot, P., 2000. In Situ Demonstration of Inhibitory Effects of Hammerhead Ribozymes That Are Targeted to the Hepatitis Bx Sequence in Cultured Cells. Biochem. Biophys. Res. Commun. 268, 728–733. https://doi.org/10.1006/bbrc.2000.2209

Pattyn, J., Hendrickx, G., Vorsters, A., Van Damme, P., 2021. Hepatitis B Vaccines. J. Infect. Dis. 224, S343–S351. https://doi.org/10.1093/infdis/jiaa668

Poland, G.A., Jacobson, R.M., 2004. Prevention of Hepatitis B with the Hepatitis B Vaccine. N. Engl. J. Med. 351, 2832–2838. https://doi.org/10.1056/NEJMcp041507

Poletti, V., Mavilio, F., 2018. Interactions between Retroviruses and the Host Cell Genome. Mol. Ther. Methods Clin. Dev. 8, 31–41. https://doi.org/10.1016/j.omtm.2017.10.001

Prifti, G.-M., Moianos, D., Giannakopoulou, E., Pardali, V., Tavis, J.E., Zoidis, G., 2021. Recent Advances in Hepatitis B Treatment. Pharmaceuticals 14, 417. https://doi.org/10.3390/ph14050417

Rabe, B., Vlachou, A., Panté, N., Helenius, A., Kann, M., 2003. Nuclear import of hepatitis B virus capsids and release of the viral genome. Proc. Natl. Acad. Sci. 100, 9849–9854. https://doi.org/10.1073/pnas.1730940100

Raper, S.E., Chirmule, N., Lee, F.S., Wivel, N.A., Bagg, A., Gao, G., Wilson, J.M., Batshaw, M.L., 2003. Fatal systemic inflammatory response syndrome in a ornithine transcarbamylase deficient patient following adenoviral gene transfer. Mol. Genet. Metab. 80, 148–158. https://doi.org/10.1016/j.ymgme.2003.08.016

Rieger, A., Nassal, M., 1996. Specific hepatitis B virus minus-strand DNA synthesis requires only the 5’ encapsidation signal and the 3’-proximal direct repeat DR1. J. Virol. 70, 585–589. https://doi.org/10.1128/JVI.70.1.585-589.1996

Rijckborst, V., Sonneveld, M.J., Janssen, H.L.A., 2011. Review article: chronic hepatitis B - anti-viral or immunomodulatory therapy? Aliment. Pharmacol. Ther. 33, 501–513. https://doi.org/10.1111/j.1365-2036.2010.04555.x

Robinson, W.S., 1975. DNA and DNA polymerase in the core of the Dane particle of hepatitis B. Am. J. Med. Sci. 270, 151–159. https://doi.org/10.1097/00000441-197507000-00021

Ryczek, M., Pluta, M., Błaszczyk, L., Kiliszek, A., 2022. Overview of Methods for Large-Scale RNA Synthesis. Appl. Sci. 12, 1543. https://doi.org/10.3390/app12031543

Saeed, U., Kim, J., Piracha, Z.Z., Kwon, H., Jung, J., Chwae, Y.-J., Park, S., Shin, H.-J., Kim, K., 2019. Parvulin 14 and Parvulin 17 Bind to HBx and cccDNA and Upregulate Hepatitis B Virus Replication from cccDNA to Virion in an HBx-Dependent Manner. J. Virol. 93, e01840-18. https://doi.org/10.1128/JVI.01840-18

Schoggins, J.W., 2019. Interferon-Stimulated Genes: What Do They All Do? Annu. Rev. Virol. 6, 567–584. https://doi.org/10.1146/annurev-virology-092818-015756

Schulze, A., Gripon, P., Urban, S., 2007. Hepatitis B virus infection initiates with a large surface protein-dependent binding to heparan sulfate proteoglycans. Hepatol. Baltim. Md 46, 1759–1768. https://doi.org/10.1002/hep.21896

Schwarz, D.S., Hutvágner, G., Du, T., Xu, Z., Aronin, N., Zamore, P.D., 2003. Asymmetry in the assembly of the RNAi enzyme complex. Cell 115, 199–208. https://doi.org/10.1016/s0092-8674(03)00759-1

Seeger, C., Mason, W.S., 2000. Hepatitis B virus biology. Microbiol. Mol. Biol. Rev. MMBR 64, 51–68. https://doi.org/10.1128/mmbr.64.1.51-68.2000

Seto, W.-K., Wong, D.K.-H., Fung, J., Huang, F.-Y., Lai, C.-L., Yuen, M.-F., 2013. Reduction of hepatitis B surface antigen levels and hepatitis B surface antigen seroclearance in chronic hepatitis B patients receiving 10 years of nucleoside analogue therapy. Hepatol. Baltim. Md 58, 923–931. https://doi.org/10.1002/hep.26376

Sonveaux, N., Thines, D., Ruysschaert, J.M., 1995. Characterization of the HBsAg particle lipid membrane. Res. Virol. 146, 43–51. https://doi.org/10.1016/0923-2516(96)80588-7

Steinle, H., Behring, A., Schlensak, C., Wendel, H.P., Avci-Adali, M., 2017. Concise Review: Application of In Vitro Transcribed Messenger RNA for Cellular Engineering and Reprogramming: Progress and Challenges. Stem Cells Dayt. Ohio 35, 68–79. https://doi.org/10.1002/stem.2402

Stoorvogel, W., Strous, G.J., Geuze, H.J., Oorschot, V., Schwartz, A.L., 1991. Late endosomes derive from early endosomes by maturation. Cell 65, 417–427. https://doi.org/10.1016/0092-8674(91)90459-c

Subaiya, S., Dumolard, L., Lydon, P., Gacic-Dobo, M., Eggers, R., Conklin, L., 2015. Global Routine Vaccination Coverage, 2014. Morb. Mortal. Wkly. Rep. 64, 1252–1255.

Suk, J.S., Xu, Q., Kim, N., Hanes, J., Ensign, L.M., 2016. PEGylation as a strategy for improving nanoparticle-based drug and gene delivery. Adv. Drug Deliv. Rev., Non-antigenic regulators of targeting for imaging and therapy 99, 28–51. https://doi.org/10.1016/j.addr.2015.09.012

Sunbul, M., 2014. Hepatitis B virus genotypes: Global distribution and clinical importance. World J. Gastroenterol. WJG 20, 5427–5434. https://doi.org/10.3748/wjg.v20.i18.5427

Tenney, D.J., Rose, R.E., Baldick, C.J., Pokornowski, K.A., Eggers, B.J., Fang, J., Wichroski, M.J., Xu, D., Yang, J., Wilber, R.B., Colonno, R.J., 2009. Long-term monitoring shows hepatitis B virus resistance to entecavir in nucleoside-naïve patients is rare through 5 years of therapy. Hepatol. Baltim. Md 49, 1503–1514. https://doi.org/10.1002/hep.22841

Terrault, N.A., Lok, A.S.F., McMahon, B.J., Chang, K.-M., Hwang, J.P., Jonas, M.M., Brown, R.S., Bzowej, N.H., Wong, J.B., 2018. Update on prevention, diagnosis, and treatment of chronic hepatitis B: AASLD 2018 hepatitis B guidance. Hepatol. Baltim. Md 67, 1560–1599. https://doi.org/10.1002/hep.29800

Tong, S., Revill, P., 2016. Overview of hepatitis B viral replication and genetic variability. J. Hepatol. 64, S4–S16. https://doi.org/10.1016/j.jhep.2016.01.027

Treiber, T., Treiber, N., Meister, G., 2019. Regulation of microRNA biogenesis and its crosstalk with other cellular pathways. Nat. Rev. Mol. Cell Biol. 20, 5–20. https://doi.org/10.1038/s41580-018-0059-1

Tsai, E., 2021. Review of Current and Potential Treatments for Chronic Hepatitis B Virus Infection. Gastroenterol. Hepatol. 17, 367–376.

Tsukuda, S., Watashi, K., 2020. Hepatitis B virus biology and life cycle. Antiviral Res. 182, 104925. https://doi.org/10.1016/j.antiviral.2020.104925

Tuttleman, J.S., Pourcel, C., Summers, J., 1986. Formation of the pool of covalently closed circular viral DNA in hepadnavirus-infected cells. Cell 47, 451–460. https://doi.org/10.1016/0092-8674(86)90602-1

Ueda, K., Tsurimoto, T., Matsubara, K., 1991. Three envelope proteins of hepatitis B virus: large S, middle S, and major S proteins needed for the formation of Dane particles. J. Virol. 65, 3521–3529. https://doi.org/10.1128/JVI.65.7.3521-3529.1991

Velkov, S., Ott, J.J., Protzer, U., Michler, T., 2018. The Global Hepatitis B Virus Genotype Distribution Approximated from Available Genotyping Data. Genes 9, 495. https://doi.org/10.3390/genes9100495

Wadhwa, A., Aljabbari, A., Lokras, A., Foged, C., Thakur, A., 2020. Opportunities and Challenges in the Delivery of mRNA-Based Vaccines. Pharmaceutics 12, 102. https://doi.org/10.3390/pharmaceutics12020102

Watanabe, T., Sorensen, E.M., Naito, A., Schott, M., Kim, S., Ahlquist, P., 2007. Involvement of host cellular multivesicular body functions in hepatitis B virus

budding. Proc. Natl. Acad. Sci. U. S. A. 104, 10205–10210. https://doi.org/10.1073/pnas.0704000104

Weinberg, M.S., Ely, A., Barichievy, S., Crowther, C., Mufamadi, S., Carmona, S., Arbuthnot, P., 2007. Specific inhibition of HBV replication in vitro and in vivo with expressed long hairpin RNA. Mol. Ther. J. Am. Soc. Gene Ther. 15, 534–541. https://doi.org/10.1038/sj.mt.6300077

Weng, Y., Huang, Q., Li, C., Yang, Y., Wang, X., Yu, J., Huang, Y., Liang, X.-J., 2020. Improved Nucleic Acid Therapy with Advanced Nanoscale Biotechnology. Mol. Ther. Nucleic Acids 19, 581–601. https://doi.org/10.1016/j.omtn.2019.12.004

Witteveldt, J., Ivens, A., Macias, S., 2018. Inhibition of Microprocessor Function during the Activation of the Type I Interferon Response. Cell Rep. 23, 3275–3285. https://doi.org/10.1016/j.celrep.2018.05.049

World Health Organization, 2017. Global hepatitis report, 2017.

Wu, Z., Yang, H., Colosi, P., 2010. Effect of genome size on AAV vector packaging. Mol. Ther. J. Am. Soc. Gene Ther. 18, 80–86. https://doi.org/10.1038/mt.2009.255

Xia, Y., Guo, H., 2020. Hepatitis B virus cccDNA: Formation, regulation and therapeutic potential. Antiviral Res. 180, 104824. https://doi.org/10.1016/j.antiviral.2020.104824

Xu, C., Guo, H., Pan, X.-B., Mao, R., Yu, W., Xu, X., Wei, L., Chang, J., Block, T.M., Guo, J.-T., 2010. Interferons Accelerate Decay of Replication-Competent Nucleocapsids of Hepatitis B Virus. J. Virol. 84, 9332–9340. https://doi.org/10.1128/JVI.00918-10

Yan, H., Zhong, G., Xu, G., He, W., Jing, Z., Gao, Z., Huang, Y., Qi, Y., Peng, B., Wang, H., Fu, L., Song, M., Chen, P., Gao, W., Ren, B., Sun, Y., Cai, T., Feng, X., Sui, J., Li, W., 2012. Sodium taurocholate cotransporting polypeptide is a functional receptor for human hepatitis B and D virus. eLife 1, e00049. https://doi.org/10.7554/eLife.00049

Yuen, M.-F., Seto, W.-K., Chow, D.H.-F., Tsui, K., Wong, D.K.-H., Ngai, V.W.-S., Wong, B.C.-Y., Fung, J., Yuen, J.C.-H., Lai, C.-L., 2007. Long-term lamivudine therapy reduces the risk of long-term complications of chronic hepatitis B infection even in patients without advanced disease. Antivir. Ther. 12, 1295–1303.

Zhang, F., Cong, L., Lodato, S., Kosuri, S., Church, G.M., Arlotta, P., 2011. Efficient construction of sequence-specific TAL effectors for modulating mammalian transcription. Nat. Biotechnol. 29, 149–153. https://doi.org/10.1038/nbt.1775

Zhang, H., Kolb, F.A., Jaskiewicz, L., Westhof, E., Filipowicz, W., 2004. Single processing center models for human Dicer and bacterial RNase III. Cell 118, 57–68. https://doi.org/10.1016/j.cell.2004.06.017

Zhang, Y., 2018. Cell toxicity mechanism and biomarker. Clin. Transl. Med. 7, 34. https://doi.org/10.1186/s40169-018-0212-7

Zhao, F., Xie, X., Tan, X., Yu, H., Tian, M., Lv, H., Qin, C., Qi, J., Zhu, Q., 2021. The Functions of Hepatitis B Virus Encoding Proteins: Viral Persistence and Liver Pathogenesis. Front. Immunol. 12.

Ziello, J.E., Huang, Y., Jovin, I.S., 2010. Cellular endocytosis and gene delivery. Mol. Med. Camb. Mass 16, 222–229. https://doi.org/10.2119/molmed.2009.00101

Zlotnick, A., Venkatakrishnan, B., Tan, Z., Lewellyn, E., Turner, W., Francis, S., 2015. Core protein: A pleiotropic keystone in the HBV lifecycle. Antiviral Res. 121, 82–93. https://doi.org/10.1016/j.antiviral.2015.06.020